PLOS ONE

RESEARCH ARTICLE

Kinetics and mechanisms of catalyzed dual-E (antithetic) controllers

Qaiser Waheed[☯], **Huimin Zhou**[☯], **Peter Ruoff***

Department of Chemistry, Bioscience, and Environmental Engineering, University of Stavanger, Stavanger, Norway

☯ These authors contributed equally to this work.
* peter.ruoff@uis.no

Citation: Waheed Q, Zhou H, Ruoff P (2022) Kinetics and mechanisms of catalyzed dual-E (antithetic) controllers. PLoS ONE 17(8): e0262371. https://doi.org/10.1371/journal.pone.0262371

Editor: Rafael Vazquez-Duhalt, Universidad Nacional Autonoma de Mexico Centro de Nanociencias y Nanotecnologia, MEXICO

Received: December 16, 2021

Accepted: August 2, 2022

Published: August 18, 2022

Data Availability Statement: All relevant data are within the paper and its Supporting information files.

Funding: The authors received no specific funding for this work.

Competing interests: The authors have declared that no competing interests exist.

Abstract

Homeostasis plays a central role in our understanding how cells and organisms are able to oppose environmental disturbances and thereby maintain an internal stability. During the last two decades there has been an increased interest in using control engineering methods, especially integral control, in the analysis and design of homeostatic networks. Several reaction kinetic mechanisms have been discovered which lead to integral control. In two of them integral control is achieved, either by the removal of a single control species E by zero-order kinetics ("single-E controllers"), or by the removal of two control species by second-order kinetics ("antithetic or dual-E control"). In this paper we show results when the control species E_1 and E_2 in antithetic control are removed enzymatically by ping-pong or ternary-complex mechanisms. Our findings show that enzyme-catalyzed dual-E controllers can work in two control modes. In one mode, one of the two control species is active, but requires zero-order kinetics in its removal. In the other mode, both controller species are active and both are removed enzymatically. Conditions for the two control modes are put forward and biochemical examples with the structure of enzyme-catalyzed dual-E controllers are discussed.

Introduction

During the last twenty years there has been an increasing interest in the design of molecular models that can exhibit integral control and show robust homeostasis/perfect adaptation. [1–11]. Integral control, which is part of many industrial regulation processes works in the following way (Fig 1): the controlled variable A, outlined in blue, is compared with the controller's set-point A_{set} (shown in red). The difference (or error) between A_{set} and the actual value of A, $\epsilon = A_{set} - A$, is calculated and integrated in time. The time integral of ϵ, described as the variable E, is then used to correct for perturbations acting on A. It can be shown that for step-wise perturbations an integral feedback will move A precisely to A_{set} [3].

Mustafa Khammash's group recently suggested an interesting alternative approach, termed antithetic control, where instead of one controller molecule E there are two (E_1 and E_2) [7, 8,

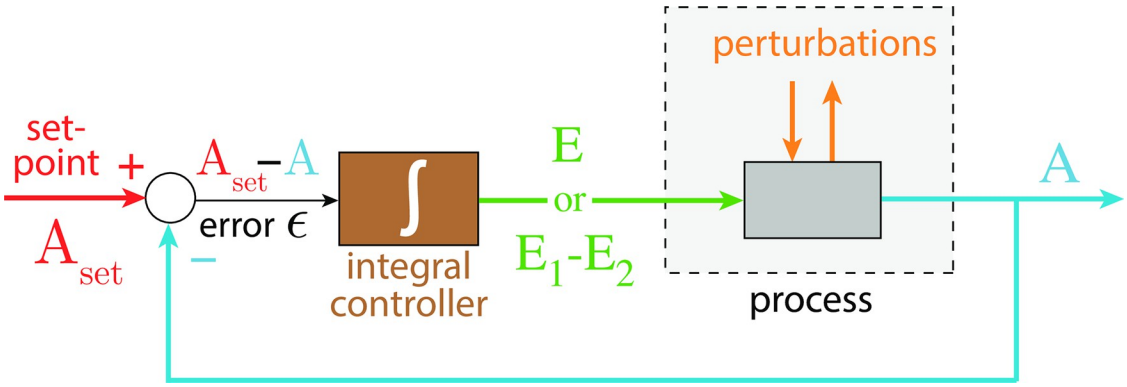

Fig 1. The concept of integral control. In single-E controllers the variable E is proportional to the integrated error ϵ, $\int \epsilon dt$, which is used to correct for perturbations in A. In dual-E (antithetic) controllers the difference between variables E_1 and E_2 is proportional to the integrated error (see S1 Text). In both cases integral control will move A precisely to its set-point A_{set} when A is perturbed by step-wise perturbations [3].

https://doi.org/10.1371/journal.pone.0262371.g001

10, 11]. In the single-E control case the condition of integral control is given by

$$\dot{E} = K(A^E_{set} - A) \tag{1}$$

where K is a constant.

In the antithetic/dual-E case integral control is achieved by

$$\dot{E}_1 - \dot{E}_2 = K'(A^E_{set} - A) \tag{2}$$

with K' being a constant. Fig 2 shows, as an example, how integral control in single- and dual-E controllers can be achieved in a negative feedback structure termed motif 5. Motif 5, an outflow controller, is one of eight basic negative feedback structures, which divide equally into two sets of inflow and outflow controllers [6]. Briefly, in inflow controllers the compensatory flux opposes an uncontrolled removal of the controlled variable (here A), while in outflow controllers an uncontrolled inflow of the controlled variables is compensated.

As indicated in Fig 2, left panel, and by Eq 1 the steady state condition of E ($\dot{E} = 0$) for a single-E controller determines its set-point. Since the antithetic controller is based on a reaction between E_1 and E_2 with speed v and rate constant k_{17} (Fig 2, right panel), i.e.,

$$v = k_{17} \cdot E_1 \cdot E_2 \tag{3}$$

the set-point for this controller is determined by the difference of the steady state conditions between E_1 and E_2 (Eq 2).

Aim of this work

As practically all processes within a cell are catalyzed by enzymes, we asked the question what influence enzymes may have on dual-E controllers, specifically when the reaction between controller species E_1 and E_2 is catalyzed. We here show the behaviors of a set of catalyzed antithetic/dual-E controllers. The enzymatic mechanisms for the removal of E_1 and E_2 include ping-pong, as well as random-order and compulsory order ternary-complex mechanisms [12, 13]. The role of total enzyme concentration is investigated and how the negative feedback structure of the motifs influence controller performance. Fig 3 shows the incorporation of

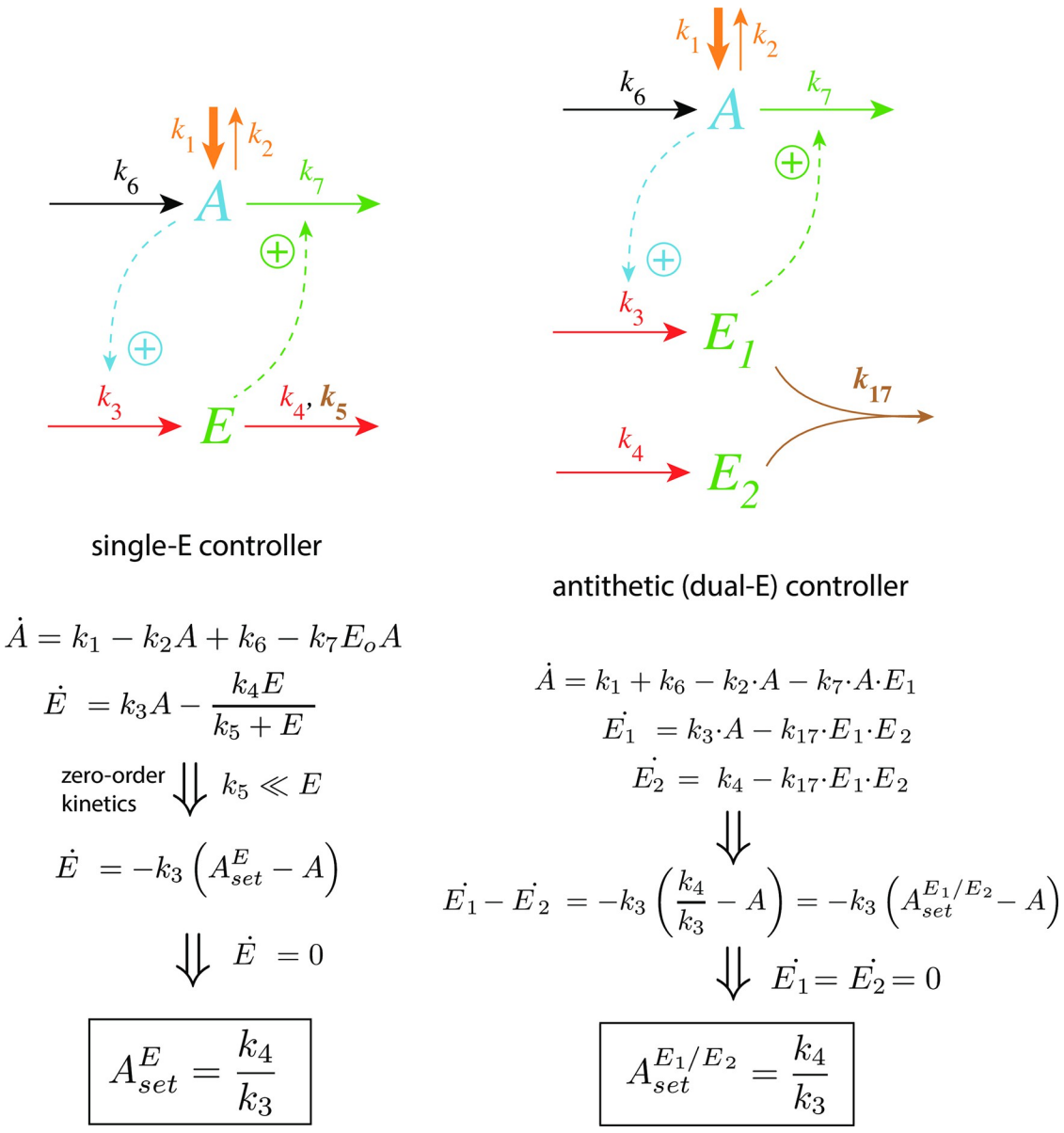

Fig 2. Single-E and dual-E (antithetic) representations of integral control using a motif 5 negative feedback structure. Left panel: Single-E controller where error integration occurs by zero-order kinetics (low k_5) removing E [4, 6]. Right panel: Dual-E controller [7, 8, 10] with controller pairs E_1 and E_2. Error integration occurs by the (here second-order) reaction between E_1 and E_2. In the single-E controller the concentration of E is proportional to the integrated error $A_{set}^{E} - A$. In the antithetic (dual-E) controller, the difference E_1–E_2 is proportional to the integrated error $A_{set}^{E_1/E_2} - A$. The colorings of the reaction schemes relate to the different parts in the general control loop shown in Fig 1.

https://doi.org/10.1371/journal.pone.0262371.g002

dual-E integral control into the eight negative feedback motifs [6] with enzyme Ez catalyzing the reaction between E_1 and E_2.

We will show that the performance of the catalyzed dual-E controllers, like response time, depends to a certain degree on the feedback structure/motif and on the enzymatic processing mechanism of E_1 and E_2. In comparison with single-E control [4, 6] the enzymatic dual-E controllers have the advantage that robust homeostasis is not bound to the requirement of zero-order kinetics, but can also work in its presence.

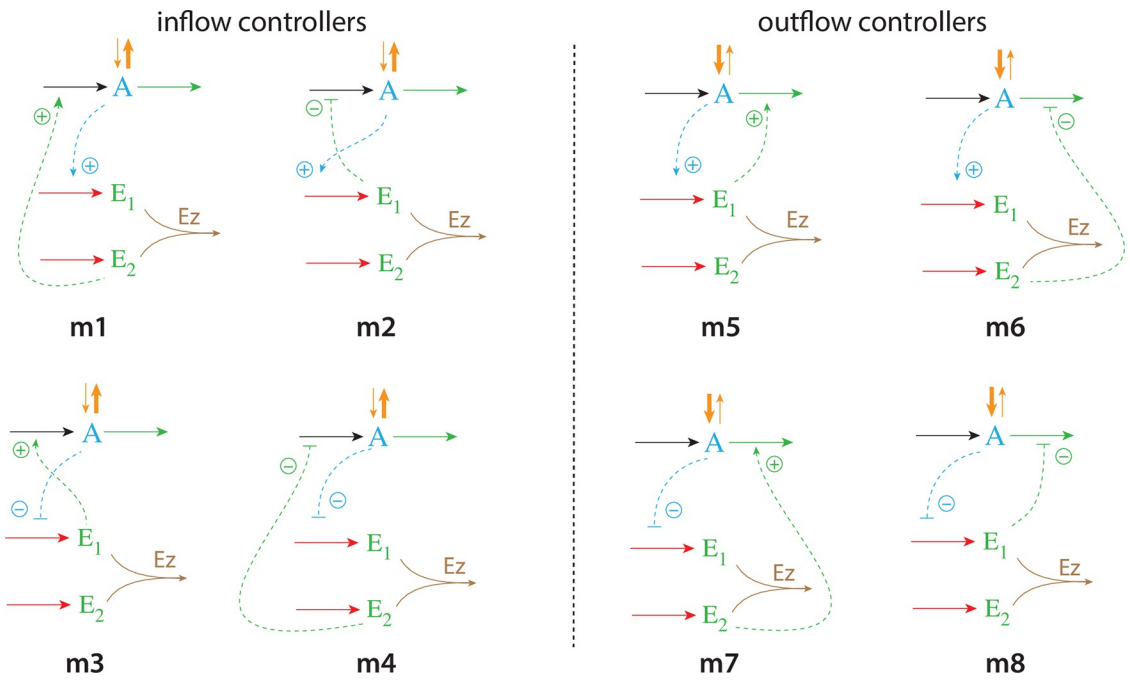

Fig 3. Dual-E (antithetic) integral control in combination with the eight negative feedback structures m1-m8. In the calculations the removal of E_1 and E_2 is catalyzed by enzyme Ez using different mechanisms. The signaling between A and the manipulated variables E_1/E_2 occurs either by an "inner loop" between A and E_1 (motifs m2, m3, m5, and m8), or by an "outer-loop" signaling between A and E_2 (motifs m1, m4, m6, and m7).

https://doi.org/10.1371/journal.pone.0262371.g003

Materials and methods

Computations were performed by using the Fortran subroutine LSODE [14]. Plots were generated with gnuplot (www.gnuplot.info) and edited with Adobe Illustrator (adobe.com). To make notations simpler, concentrations of compounds are generally denoted by compound names without square brackets. Time derivatives are indicated by the 'dot' notation. Concentrations and rate parameter values are given in arbitrary units (au). Set-point values are arbitrarily chosen. For certain feedback structures we observe a switch between dual-E and single-E control when a set-point determining parameter is changed. In these cases the homeostatic properties of the two control modes were studied at different set-points.

Perturbations were applied as single steps without considering (more realistic) time-dependent perturbations [15–17]. The reason for applying steps is that when integral control is operational dual-E (and single-E) controllers will show robust perfect adaptation upon step perturbations, but will principally differ in their speed of resetting.

Enzymatic mechanisms considered

There are two major mechanisms [12, 13] when E_1 and E_2 are processed by an enzyme Ez, i.e.,

$$E_1 + E_2 \xrightarrow{Ez} P \tag{4}$$

In one of them, a ternary complex $E_1{\cdot}Ez{\cdot}E_2$ between enzyme and substrates E_1 and E_2 is formed, either via a random binding order (Fig 4a) or by a compulsory binding order (Fig 4b). The other mechanism, termed "ping-pong", contains two compulsory order binding events. During the first step one of the substrates E_1 or E_2 binds to the enzyme Ez, releases a possible

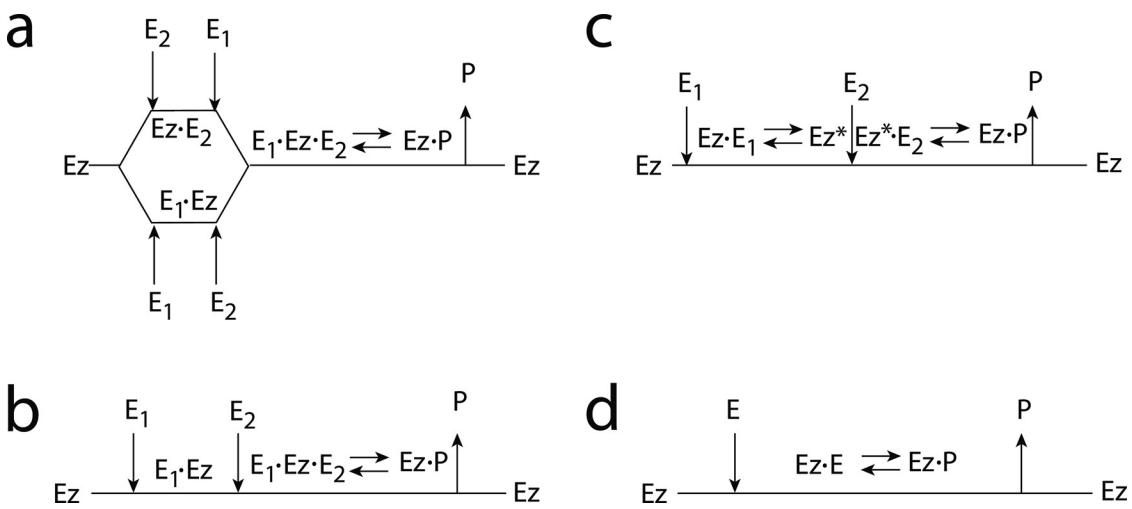

Fig 4. Overview (Cleland notation [19]) of the enzymatic mechanisms removing E_1 and E_2 (Eq 4). (a) Ternary complex mechanism with random binding of E_1 and E_2 to the enzyme. (b) Ternary complex mechanism with compulsory binding order. Here E_1 binds first to free enzyme Ez then E_2 binds to the $E_1{\cdot}Ez$ complex. Alternatively, E_2 can bind first to Ez and then E_1 to form the ternary complex. (c) Ping-pong mechanism. E_1 (or E_2) bind first to Ez leading to the alternate enzyme form Ez^*, which then can bind E_2 (or E_1). (d) Single-substrate Michaelis-Menten mechanism used in single-E controllers.

https://doi.org/10.1371/journal.pone.0262371.g004

first product and creates an alternative enzymatic form Ez^*, which is able to bind the second substrate. In the final step the enzymatic species Ez is regenerated and a possible second product is released. A new enzymatic cycle can start again (Fig 4c).

In the case of single-E controllers E is removed by enzyme Ez

$$\mathrm{E} \xrightarrow{\mathrm{Ez}} \mathrm{P} \tag{5}$$

by using (single-substrate) Michaelis-Menten kinetics (Fig 4d). Although single-E controllers have already been analyzed to a large extent before [4, 6, 18], we will encounter their catalyzed versions also here, because some of the dual-E controllers can switch between single-E and dual-E control mode.

We noted that a necessary condition for robust homeostasis to occur is that the involved negative feedback loops need to be described as irreversible processes. Therefore, the enzymatic reactions in Eqs 4 and 5 need to be irreversible. Already in 1925 Lotka [20] investigated whether certain biological phenomena, such as oscillations and homeostasis, could be based on Le Chatelier's principle, since at that time biologists attempted to apply the principle to biological systems [21]. Lotka concluded in the negative. Today we regard life as an overall irreversible process, a "dissipative structure" being far from chemical equilibrium [22, 23] and which allows for self-maintenance [24].

For each of the three mechanisms in Fig 4a–4c steady state expressions for v of reaction 4 have been found numerically with LSODE and by using the King-Altman method [25] (S1 Text). The King-Altman method has the advantage that v can be expressed as an analytical function of the concentrations of E_1 and E_2 and the other rate parameters. Our calculations showed that the steady state expressions of v were always in excellent agreement with the corresponding numerical results.

Feedback motifs considered

From the eight feedback structures of Fig 3 we have analyzed four of them: two of the four "inner-loop" motifs m2 and m5 and the two "outer-loop" motifs m4 and m7. The remaining four motifs have similar feedback symmetries and we do not expect significant differences to those considered here.

Results

For each of the motifs m2, m4, m5, and m7 we describe how the controllers perform under step-wise perturbations when the above mentioned ternary-complex and ping-pong mechanisms are applied to remove E_1 and E_2.

Controllers based on motif 2

This motif's performance has been found to be remarkably good, especially with respect to perturbations which increase their strength with time [15, 16]. Motif 2 is an inflow type of controller which opposes outflow perturbations in the controlled variable.

Motif 2 dual-E controller removing E_1 and E_2 by an enzymatic random-order ternary-complez mechanism. Fig 5 shows the reaction scheme when E_1 and E_2 are removed enzymatically by using a ternary-complex mechanism with random binding order and E_1 as the derepressing agent.

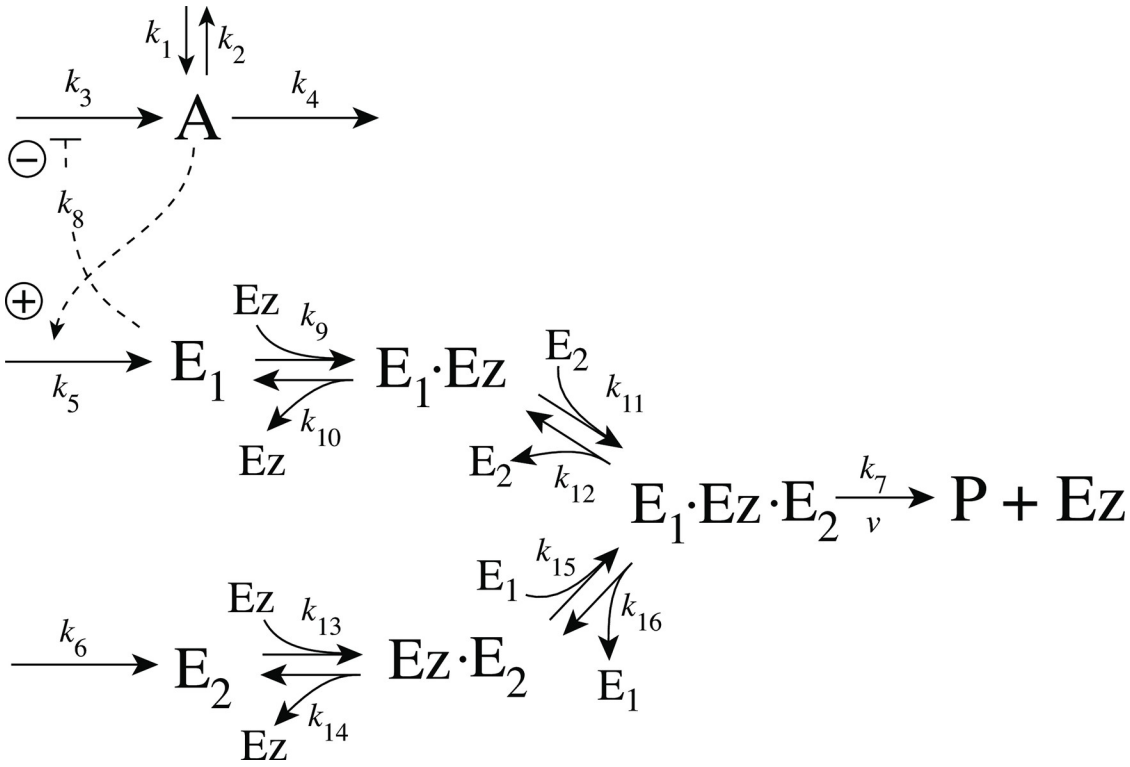

Fig 5. Motif 2 antithetic controller: Removal of E_1 and E_2 by enzyme Ez using a ternary-complex mechanism with random binding order.

https://doi.org/10.1371/journal.pone.0262371.g005

The rate equations are:

$$\dot{A} = k_1 - k_2 \cdot A - k_4 \cdot A + \frac{k_3 k_8}{k_8 + E_1} \tag{6}$$

$$\dot{E_1} = k_5 \cdot A - k_9(E_1)(Ez) + k_{10}(E_1 \cdot Ez) - k_{15}(Ez \cdot E_2)(E_1) + k_{16}(E_1 \cdot Ez \cdot E_2) \tag{7}$$

$$\dot{E_2} = k_6 - k_{11}(E_1 \cdot Ez)(E_2) + k_{12}(E_1 \cdot Ez \cdot E_2) - k_{13}(E_2)(Ez) + k_{14}(Ez \cdot E_2) \tag{8}$$

$$\dot{Ez} = -k_9(E_1)(Ez) + k_{10}(E_1 \cdot Ez) - k_{13}(E_2)(Ez) + k_{14}(Ez \cdot E_2) + k_7(E_1 \cdot Ez \cdot E_2) \tag{9}$$

$$\frac{d(E_1 \cdot Ez)}{dt} = k_9(E_1)(Ez) - k_{10}(E_1 \cdot Ez) - k_{11}(E_1 \cdot Ez)(E_2) + k_{12}(E_1 \cdot Ez \cdot E_2) \tag{10}$$

$$\frac{d(E_1 \cdot Ez \cdot E_2)}{dt} = k_{11}(E_1 \cdot Ez)(E_2) + k_{15}(Ez \cdot E_2)(E_1) - (k_7 + k_{12} + k_{16})(E_1 \cdot Ez \cdot E_2) \tag{11}$$

$$\frac{d(Ez \cdot E_2)}{dt} = k_{13}(E_2)(Ez) - k_{14}(Ez \cdot E_2) - k_{15}(Ez \cdot E_2)(E_1) + k_{16}(E_1 \cdot Ez \cdot E_2) \tag{12}$$

An analytical expression for the reaction velocity

$$v = \dot{P} = k_7(E_1 \cdot Ez \cdot E_2) \tag{13}$$

can be obtained by the steady state approximation (S1 Text), which has been found (see below) to be in excellent agreement with the numerical results.

We observed that the enzymatic controller in Fig 5 can show two set-points of A. One is given by

$$A_{set} = \frac{k_6}{k_5} \tag{14}$$

when both E_1 and E_2 participate in the regulation of A (dual-E control).

The other set-point is given by

$$A_{set} = \frac{k_7 \mathrm{Ez}_{\mathrm{tot}}}{k_5} \tag{15}$$

In this case only E_1 participates in the control of A. (single-E control). The switching between the two control modes is described in more detail below.

Motif 2 single-E controller with Michaelis-Menten removal of E. Due to the above indicated switch between catalyzed dual-E and single-E control mode we here show the catalyzed single-E m2 controller (Fig 6), which will also be compared with the catalyzed m2 dual-E controller.

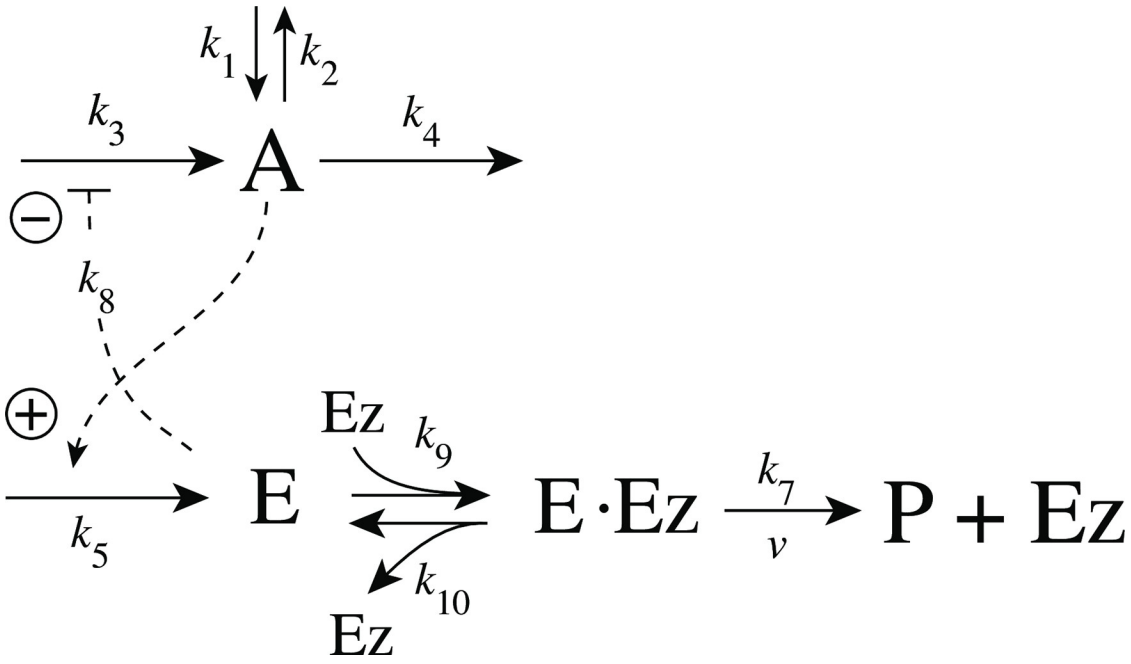

Fig 6. Motif 2 single-E controller: Removal of E by enzyme Ez using a Michaelis-Menten mechanism.

https://doi.org/10.1371/journal.pone.0262371.g006

The rate equations for the scheme in Fig 6 are:

$$\dot{A} = k_1 - k_2 \cdot A - k_4 \cdot A + \frac{k_3 k_8}{k_8 + E} \tag{16}$$

$$\dot{E} = k_5 \cdot A - k_9(E)(Ez) + k_{10}(E \cdot Ez) \tag{17}$$

$$\dot{Ez} = -k_9(E)(Ez) + k_{10}(E \cdot Ez) + k_7(E \cdot Ez) \tag{18}$$

$$\frac{d(E \cdot Ez)}{dt} = k_9(E)(Ez) - k_{10}(E \cdot Ez) - k_7(E \cdot Ez) \tag{19}$$

In this case the set-point of the controller is described by Eq 15.

The catalyzed m2-controllers: Failure at larger perturbation strengths and enzyme limitation. Fig 7 shows a comparison of the single-E controller of Fig 5 and the dual-E controller of Fig 6 for step-wise perturbations in k_2. While rate constants have been more or less arbitrarily set, for comparison reasons the set-points of the controllers are both put at 2.0. Due to the two different set-point expressions for the dual-E and the single-E controllers (Eqs 14 and 15) k_5 and k_7 values differ slightly as indicated in the legend of Fig 7. Perturbations are applied as follows: During phase 1 (0–10 time units) A is at the controllers' set-points (2.0) with a k_2-value of 10.0. During phase 2 k_2 is increased step-wise using the three perturbations: 1, $k_2 = 1{\times}10^2$; 2, $k_2 = 1{\times}10^3$; 3, $k_2 = 2{\times}10^4$. By comparing the left panels of Fig 7 it is seen that one of the advantages of the dual-E controller is that it can maintain irs set-point even under enzymatic non-zero conditions, which means that Ez is not saturated by its substrates E_1 and E_2. The single-E controller, however, has problems to defend its set-point as with increasing k_2

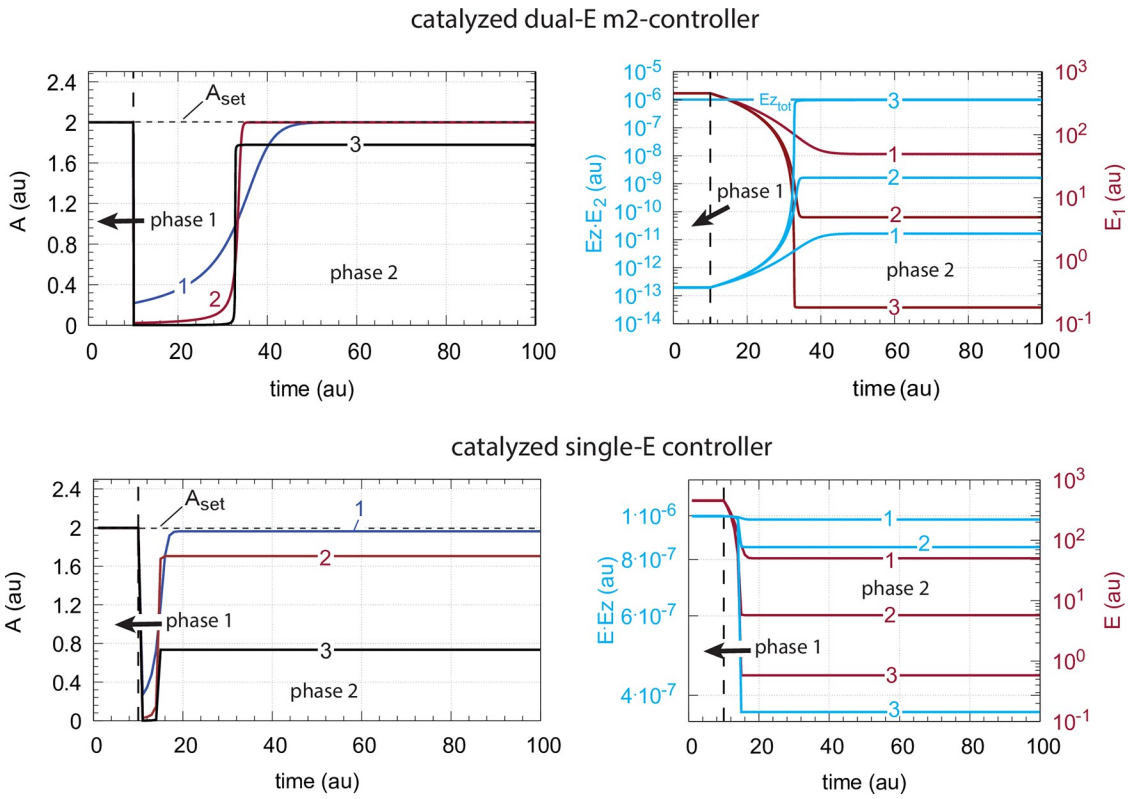

Fig 7. Behavior of the catalyzed dual-E controller (Fig 5) and the single-E controller (Fig 6) towards step-wise perturbations in k_2. Total enzyme concentration $Ez_{tot}=1\times10^{-6}$. Upper left panel: Behavior of controlled variable A of the dual-E controller. Phase 1: $k_2=10.0$; phase 2: **1**, $k_2 = 1\times10^2$; **2**, $k_2 = 1\times10^3$; **3**, $k_2 = 2\times10^4$, note the offset in A from A_{set}. Upper right panel: Behavior of E_1 and $Ez{\cdot}E_2$ as a function of k_2-perturbations 1–3. Note that for perturbation 3 the enzyme is saturated with E_2. Rate constants: $k_1=0.0$, $k_3=1\times10^5$, $k_4=1.0$, $k_5=10.0$, $k_6=20.0$, $k_7=1\times10^9$, $k_8=0.1$, $k_9=1\times10^8$, $k_{10}=1\times10^3$, $k_{11}=1\times10^8$, $k_{12}=1\times10^3$, $k_{13}=1\times10^8$, $k_{14}=1\times10^3$, $k_{15}=1\times10^8$, $k_{16}=1\times10^3$. Initial concentrations: $A_0=2.0$, $E_{1,0}=454.4$, $E_{2,0}=0.204$, $Ez_0=4.4\times10^{-10}$, $(E_1{\cdot}Ez)_0=9.796\times10^{-7}$, $(E_1{\cdot}Ez{\cdot}E_2)_0=2.0\times10^{-8}$, $(Ez{\cdot}E_2)_0=1.98\times10^{-13}$. Lower left panel: Behavior of controlled variable A for the single-E controller. Same step-wise k_2 perturbations 1–3 as for the dual-E controller. Lower right panel: Behavior of E as a function of k_2-perturbations. Rate constant values are the same as for the dual-E controller, except that $k_5=50.0$, and $k_7=1\times10^8$. Initial concentrations: $A_0=1.995$, $E_0=455.5$, $Ez_0=2.19\times10^{-9}$, $(Ez{\cdot}E)_0=9.976\times10^{-7}$.

https://doi.org/10.1371/journal.pone.0262371.g007

values the E·Ez complex shows increased dissociation (Fig 7, lower right panel) leading to an increasingly poorer performance and thereby increased offsets in A from A_{set}.

However, with perturbation 3 also the enzyme-catalyzed dual-E controller starts to break down. The reason for the breakdown is related to the total amount of enzyme, Ez_{tot}, and the values of k_5 and k_6. In the present settings k_5 and k_6 are relatively high, which leads in the dual-E controller to a saturation of Ez by E_2, i.e. the concentration of EzE_2 approaches that of the total enzyme concentration Ez_{tot}. Under these conditions, however, the relationship

$$k_5 A_{ss} = k_7(E_1 EzE_2) \tag{20}$$

is still obeyed leading to the A steady state

$$A_{ss} = \frac{k_7(E_1 EzE_2)}{k_5} \tag{21}$$

Thus, E_1 still exerts control over A in the dual-E controller, but now in form of a *single-E (i.e. E_1) control mode*. In case Ez works under zero-order conditions ($(E_1EzE_2)\approx Ez_{tot}$), Eq 21

becomes Eq 15. In this mode E_2 shows wind-up: E_2 increases linearly in time with slope $\dot{E}_2$ increasing with increasing k_2 values. It is the increase of E_2 which leads to the saturation (poisoning) of Ez by E_2 (see Fig 7, upper right panel).

The above described limitation of the the dual-E controller can still be circumvented by either decreasing k_5 and k_6, or by increasing Ez_{tot} (see next section). It should however be pointed out that there is another way of a (dual-E) controller breakdown which cannot be opposed by either increasing Ez_{tot}) or by decreasing k_5 and k_6. This type of breakdown occurs when E_1 is driven by k_2 to such a low concentration that the compensatory flux j_{comp} approaches its maximum value k_3, i.e.

$$j_{comp} = \frac{k_3 k_8}{k_8 + E_1} \xrightarrow{\text{low } E_1} k_3 \tag{22}$$

By setting in Eq 6 the term $k_3k_8/(k_8+ E_1)$ to k_3 and A to A_{set} we can calculate the upper limit of k_2, k_2^{ul},

$$k_2^{ul} = \frac{k_1 + k_3 - k_4 A_{set}}{A_{set}} \tag{23}$$

Whenever $k_2 > k_2^{ul}$ the controller breaks down irrespective of the values of k_5, k_6, and Ez_{tot}. Note, that in curve 3 of the upper right panel of Fig 7 we have that

$$k_2 = 2 \times 10^4 < k_2^{ul} = k_2 = 2 \times 10^4 \tag{24}$$

which is the reason why the dual-E's homeostatic behavior can be restored as described in the next section.

A more detailed description of this type of breakdown is given in the section *Dual-E controllers based on motif 4*.

Avoiding enzyme limitations. Enzyme overload can be avoided by two means, either by increasing the total amount of enzyme, or by decreasing the reaction rates k_5 and k_6 by which E, E_1, and E_2 are formed.

Fig 8 illustrates the behavior of the controlled variable A for the antithetic controller (A_{cat}^{antith}, outlined in orange) in Fig 7 when perturbation 3 is applied. In panel a the total amount of enzyme has been increased from 10^{-6} to 10^{-5}. In panel b the enzyme concentration is kept at 10^{-6}, but k_5 and k_6 are in phase 2 decreased by one order of magnitude to respectively 1.0 and 2.0. In comparison, the behavior of the controlled variable A for the zero-order controller (A_{zo}, outlined in black) is also shown. For the higher total enzyme concentrations both controllers behave identical, while for the decreased values of k_5 and k_6 the antithetic controller is less aggressive, but eventually moves A to the controller's set-point.

Switching between dual-E and single-E control mode at zero-order conditions. We found that a change in the control mode of the dual-E controller (Fig 5) occurs in dependence to the relative values of k_5 and k_6. When k_6 is lower than the rate k_7Ez_{tot} the controller works in an antithetic/dual-E mode. We assume here that the dual-E controller works under zero-order conditions with large values of k_9 and k_{11} relative to k_{10} and k_{12} (Fig 5) leading that v is at its maximum velocity, i.e.

$$v = k_7 E1 \cdot Ez.E2 \simeq k_7 Ez_{tot} = V_{max} \tag{25}$$

In dual-E mode both E_1 and E_2 participate in the regulation of A and A_{set} is given by Eq 14. However, when k_6 is larger than k_7Ez_{tot} the system switches to a single-E control mode where only E_1 takes part in the regulation of A. A_{set} is now described by Eq 15. Fig 9 illustrates the behavior. Panel a shows the steady state values of A (A_{ss}, gray solid circles) as a function of k_6

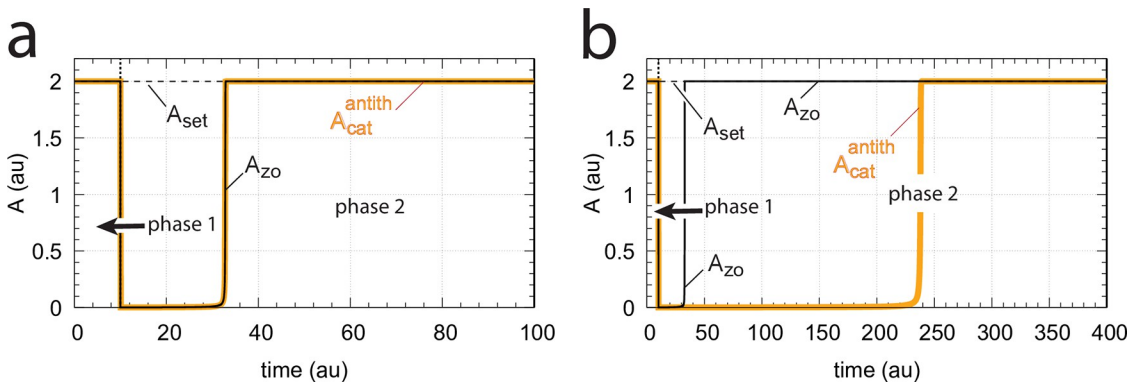

Fig 8. Avoiding enzyme overload. Same system as in Fig 7 with perturbation 3 applied, i.e., during phase 1 (0–10 time units) k_2=10.0, while during phase 2 $k_2 = 2\times10^4$. All other rate constants are as in Fig 7, except that in panel (a) the total amount of enzyme Ez has been increased by one order of magnitude to $Ez_0=10^{-5}$, while in panel (b) $Ez_0=10^{-6}$, but k_5 and k_6 have been decreased in phase 2 by one order of magnitude to 1.0 and 2.0, respectively. Initial concentrations: (a) A_0=2.0, $E_{1,0}$=454.4, $E_{2,0}$=0.0204, $Ez_0=4.4\times10^{-10}$, $(E_1{\cdot}Ez)_0=9.98\times10^{-6}$, $(E_1{\cdot}Ez{\cdot}E_2)_0=2.0\times10^{-8}$, $(Ez{\cdot}E_2)_0=1.98\times10^{-14}$; (b) as in Fig 7.

https://doi.org/10.1371/journal.pone.0262371.g008

when k_5=0.4, $k_7=1\times10^6$ and $Ez_{tot}=1\times10^{-6}$. For k_6 values lower than k_7Ez_{tot} (=1.0) the system shows dual-E control with a set-point of k_6/k_5, while when k_6 is larger than k_7Ez_{tot}=1 single-E control is observed with A_{set} being k_7Ez_{tot}/k_5 (=2.5). In such a setting the system behaves precisely as a single-E controller (Fig 6) where E is replaced by E_1 and Ez is replaced by $Ez{\cdot}E_2$. Under single-E mode conditions E_2 does not participate in the control of A and its concentration rises continuously (showing wind-up).

Fig 9b shows numerical and steady state values of v (Eq 13); they are in excellent agreement.

As illustrations, Fig 9c and 9d show that the set-points of single- and dual-E control are indeed defended. The two panels show the homeostatic responses when k_6=10 (vertical downward red arrow in Fig 9a) and when k_6=0.4 (vertical upright blue arrow in Fig 9a).

Fig 9e shows the part of the network (outlined in red) when single-E control is active. At the steady state in A, the rate k_5A_{set} becomes equal to the degradation rate $v=k_7(E1{\cdot}Ez{\cdot}E2)= k_7 Ez_{tot}$. Typical for the dual-E control (Fig 9f) is that k_5A_{set} and k_6 are equal to $v=k_7(E1{\cdot}Ez{\cdot}E2)$.

Switching between dual-E and single-E control mode at nonzero-order conditions. In this section we compare the dual-E and single-E control modes when $v = k_7(E_1{\cdot}Ez{\cdot}E_2)$ is not zero-order with respect to $(E_1{\cdot}Ez{\cdot}E_2)$.

For single-E control (Fig 9e) nonzero-order conditions imply that

$$A_{ss} = \frac{k_7(E_1 \cdot Ez \cdot E_2)}{k_5} < \frac{k_7 Ez_{tot}}{k_5} \tag{26}$$

For the dual-*E* control (Fig 9f) A_{ss} is given by Eq 14 *independent* whether the removal of the ternary complex is zero-order or not. However, dual-*E* mode will switch to single-*E* mode when

$$k_6 > k_7(E_1 \cdot Ez \cdot E_2) \tag{27}$$

In this case E_2 will show wind-up (i.e., continuously increase unless there is a removal of E_2)

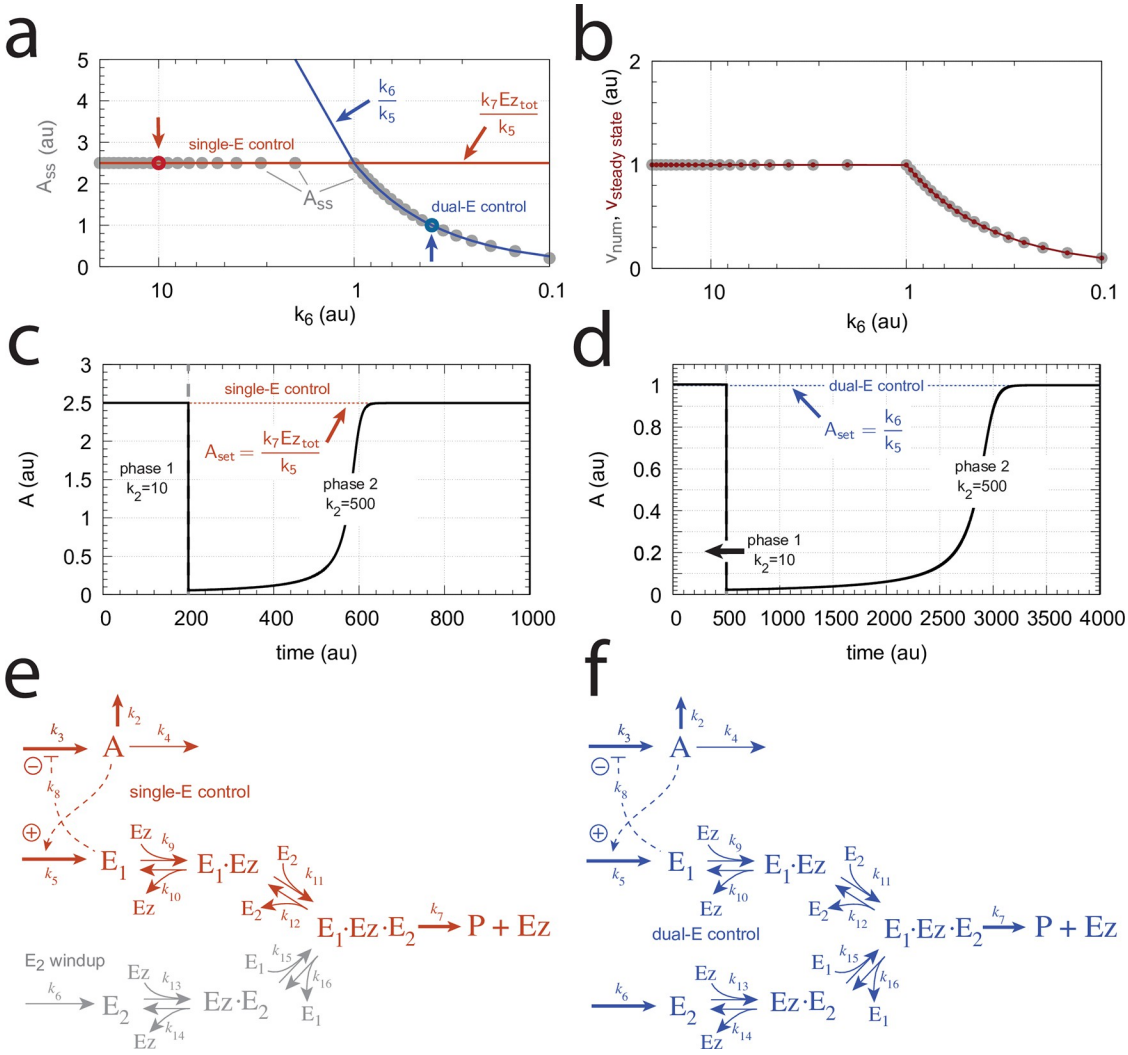

Fig 9. Switch between dual-E and single-E control in the motif 2 antithetic controller with a random-order ternary-complex mechanism removing E_1 and E_2 (Fig 5). (a) A_{ss} (steady state in A) as a function of k_6. Red and blue lines indicate the respective set-point values for single-E and dual-E control. Gray solid points show the numerically calculated steady state levels. The outlined red and blue circles (indicated by the vertical arrows) show the k_6 values (10.0 and 0.4) used in panels c and d when changes in k_2 are applied. (b) Steady state values of v (Eq 13) obtained by the King-Altman method (inner red dots, S1 Text) and numerically calculated velocities (gray dots). (c) and (d) Single-E and dual-E control when k_6 values are respectively 10.0 and 0.4, and k_2 changes step-wise from 10.0 to 500. Other rate constants: k_3=1×10^5, k_4=1.0, k_5=0.4, k_7=1×10^6, k_8=0.1, k_9=1×10^8, k_{10}=1×10^3, k_{11}=1×10^8, k_{12}=1×10^3, k_{13}=1×10^8, k_{14}=1×10^3, k_{15}=1×10^8, k_{16}=1×10^3. Initial concentrations, panel c: A_0=2.5, $E_{1,0}$=363.5, $E_{2,0}$=4.5×10^4, Ez_0=3.04×10^{-13}, $(E_1{\cdot}Ez)_0$=4.3×10^{-13}, $(E_1{\cdot}Ez{\cdot}E_2)_0$=1.0×10^{-6}, $(Ez{\cdot}E_2)_0$=2.7×10^{-11}. Initial concentrations, panel d: A_0=1.0, $E_{1,0}$=905.3, $E_{2,0}$=6.7×10^{-3}, Ez_0=4.4×10^{-12}, $(E_1{\cdot}Ez)_0$=6.0×10^{-7}, $(E_1{\cdot}Ez{\cdot}E_2)_0$=4.0×10^{-7}, $(Ez{\cdot}E_2)_0$=4.5×10^{-15}. (e) Outlined in red: the active part of the network during single-E control. E_2 is continuously increasing (wind-up). (f) In dual-E control the entire network participates in the control of A (outlined in blue).

https://doi.org/10.1371/journal.pone.0262371.g009

and A_{ss} is determined by the relationship:

$$\begin{aligned} A_{ss} &= \frac{k_7(E_1 \cdot Ez \cdot E_2)}{k_5} \\ &= V_{max}\left(\frac{k_{14}k_9E_1k_{11}E_2 + k_9E_1k_{11}E_2k_{15}E_1 + k_{10}k_{13}E_2k_{15}E_1 + k_{13}E_2k_{15}E_1k_{11}E_2}{k_5 D}\right) \end{aligned} \tag{28}$$

where V_{max}=$k_7(Ez_{tot})$. D is the sum of all King-Altman numerator terms described in S1 Text.

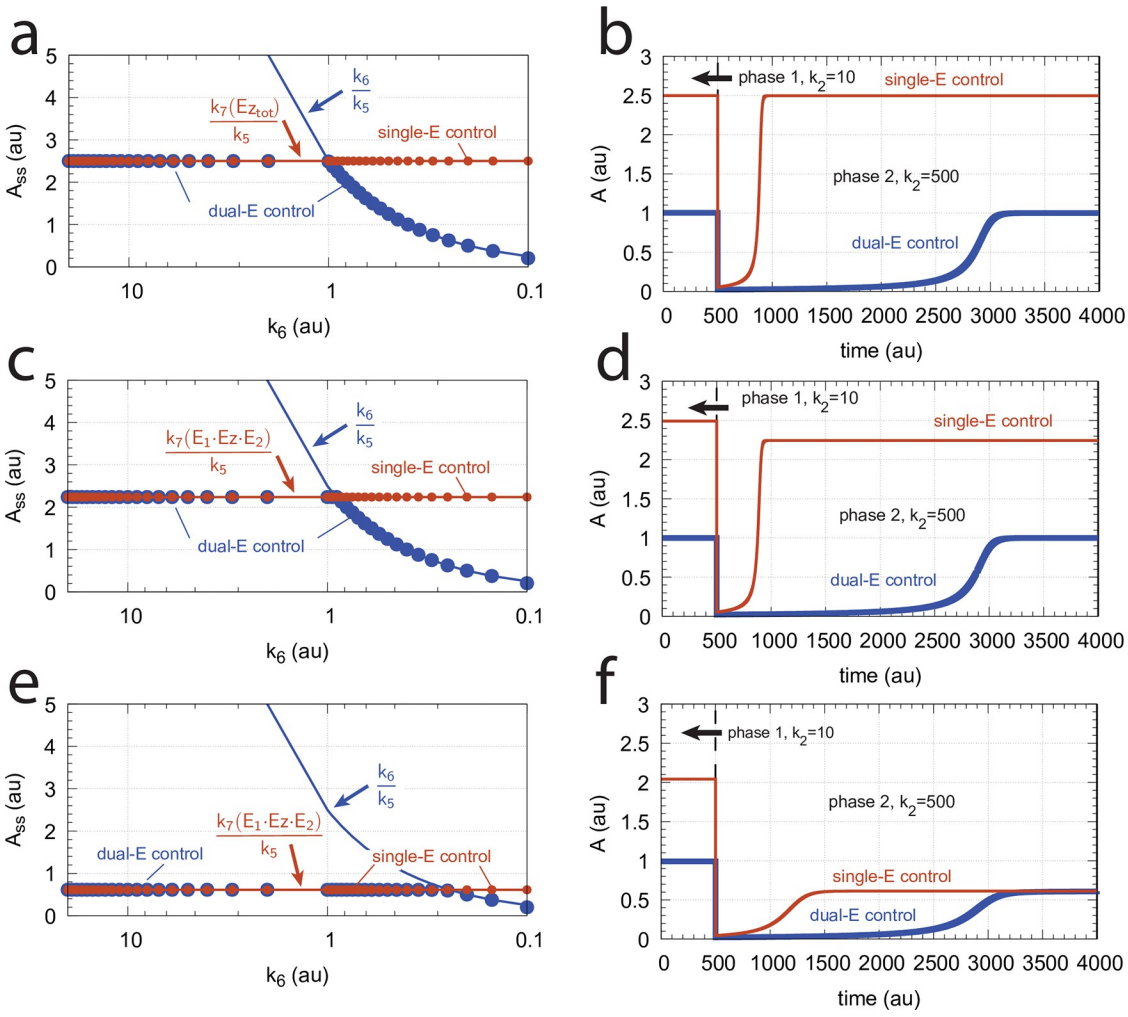

Fig 10. Behaviors of single-E control and dual-E control for the schemes in Fig 9e and 9f when going from zero-order to nonzero-order conditions. In panels (a) and (b), $k_9=k_{11}=k_{13}=k_{15}=1\times10^8$ (zero-order condition); in panels (c) and (d), $k_9=k_{11}=k_{13}=k_{15}=1\times10^6$ (weak nonzero-order); in panels (e) and (f), $k_9=k_{11}=k_{13}=k_{15}=1\times10^4$ (strong nonzero-order). Panels b, d, and f to the right show the time-dependent kinetics of A for a step-wise perturbation in k_2 from 10 (phase 1) to 500 (phase 2) applied at t = 500. The k_6 values in these calculations were 0.4. Other rate constants as in Fig 9. Initial concentrations for panels (a), (c), and (e), dual-E controller: $A_0=2.0$, $E_{1,0}=4.5\times10^2$, $E_{2,0}=2.0\times10^{-1}$, $Ez_0=4.4\times10^{-10}$, $(E_1{\cdot}Ez)_0=9.7\times10^{-7}$, $(E_1{\cdot}Ez{\cdot}E_2)_0=2.0\times10^{-8}$, $(Ez{\cdot}E_2)_0=2.0\times10^{-13}$; single-$E$ controller: $A_0=2.5$, $E_0=3.6\times10^2$, $Ez_0=2.8\times10^{-11}$, $(E{\cdot}Ez)_0=1.0\times10^{-8}$; steady state concentrations were obtained after 2000 time units. Initial concentrations panels (b) and (d): dual-E controller: $A_0=1.0$, $E_{1,0}=9.1\times10^2$, $E_{2,0}=6.7\times10^{-1}$, $Ez_0=4.4\times10^{-10}$, $(E_1{\cdot}Ez)_0=6.0\times10^{-7}$, $(E_1{\cdot}Ez{\cdot}E_2)_0=4.0\times10^{-7}$, $(Ez{\cdot}E_2)_0=7.6\times10^{-13}$; single-$E$ controller: $A_0=2.5$, $E_0=3.6\times10^2$, $Ez_0=2.7\times10^{-9}$, $(E{\cdot}Ez)_0=1.0\times10^{-8}$. Initial concentrations panels panel (f): dual-E controller: $A_0=1.0$, $E_{1,0}=9.1\times10^2$, $E_{2,0}=6.7\times10^{-1}$, $Ez_0=4.4\times10^{-10}$, $(E_1{\cdot}Ez)_0=6.0\times10^{-7}$, $(E_1{\cdot}Ez{\cdot}E_2)_0=4.0\times10^{-7}$, $(Ez{\cdot}E_2)_0=7.6\times10^{-13}$; single-$E$ controller: $A_0=2.04$, $E_0=4.5\times10^2$, $Ez_0=1.8\times10^{-7}$, $(E{\cdot}Ez)_0=8.1\times10^{-7}$.

https://doi.org/10.1371/journal.pone.0262371.g010

Fig 10 illustrates the behavior going from zero-order to nonzero-order conditions. To impose nonzero-order conditions we have for the sake of simplicity, changed the values of k_9, k_{11}, k_{13}, and k_{15} from 1×10^8 (practical zero-order, panels a and b) to 1×10^6 (panels c and d) and 1×10^4 (panels e and f), while other rate constants are kept unchanged. In all panels single-E control responses are outlined in red, while dual-E control is outlined in blue. Fig 10 clearly shows that when the system moves into a nonzero-order kinetics regime (by lowering k_9, k_{11}, k_{13}, and k_{15}) the performance by single-E control gets successively worse. However, although dual-E control can maintain/defend its set-point (Eq 14) the range of the dual-E

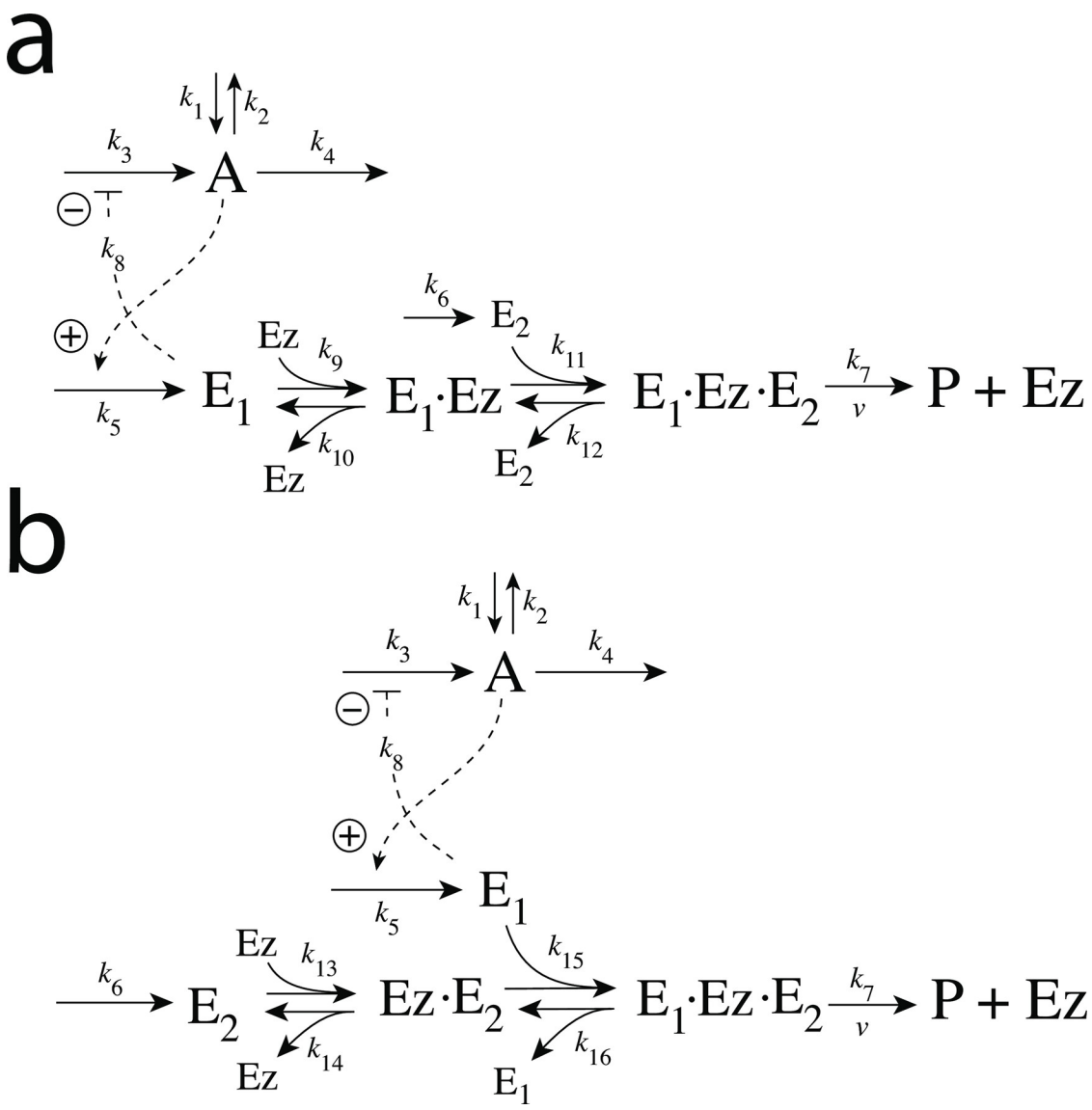

Fig 11. Motif 2 dual-E controller when E_1 and E_2 are removed enzymatically by compulsory-order ternary-complex mechanisms. Panel a: E_1 binds first to free enzyme Ez. Panel b: E_2 binding first to Ez.

https://doi.org/10.1371/journal.pone.0262371.g011

working mode shrinks with increasing nonzero-order kinetics (i.e., with decreasing values of k_9, k_{11}, k_{13}, and k_{15}).

Motif 2 dual-E controller removing E_1 and E_2 by enzymes using compulsory-order ternary complex mechanisms. In the compulsory-order ternary-complex mechanisms E_1 and E_2 bind in an ordered manner to enzyme *Ez*, either E_1 first (Fig 11a), or E_2 first (Fig 11b).

Both mechanisms in Fig 11 can show single-E (E_1) or dual-E control dependent on the value of k_6.

We found that the mechanism when E_1 binds first (Fig 11a) behaves analogous to the random-order ternary complex mechanism of Fig 5. Fig 12a shows the identical responses of the compulsory-order (E_1 binds first) and the random-order ternary complex mechanisms when both controllers work in dual-E mode and both are subject to the same step-wise changes in k_2

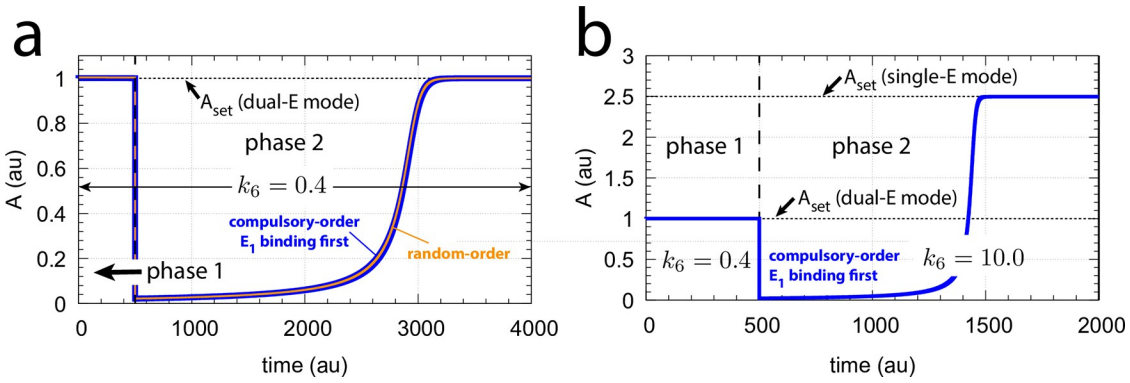

Fig 12. Dual- and single-E control mode of the m2 feedback loop when E_1 and E_2 are removed by a compulsory-order ternary complex mechanism and when E_1 binds first to Ez (Fig 11a). Panel a, outlined in blue, shows the concentration of A for the mechanism of Fig 11a with a step-wise change of k_2 from 10.0 (phase 1) to 500.0 (phase 2). For comparison, outlined in orange, the results of Fig 10b for the random-order ternary complex mechanism working in dual-E mode are shown. Rate constant k_6=0.4 for both phases. Other rate constants and initial concentrations are the same as for Fig 10b. Panel b shows the concentration of A for the compulsory-order ternary complex mechanism from panel a, but k_6 is changed in phase 2 from 0.4 to 10.0. The controller switches in phase 2 from dual-E mode to single-E mode with the associated change of A_{set} from 1.0 (Eq 14) to 2.5 (Eq 15). Initial concentrations and rate constants as in panel a.

https://doi.org/10.1371/journal.pone.0262371.g012

from 10.0 to 500.0. The switch of the compulsory-order (E_1 binds first) controller (Fig 11a) from dual-E to single-E mode is shown in Fig 12b when in phase 2, besides the step-wise increase of k_2, k_6 is increased from 0.4 to 10.0.

Fig 13 shows the single-E and dual-E control mode when E_1 and E_2 are removed by a compulsory-order ternary complex mechanism, but E_2 binds first to Ez (Fig 11b). Panel a shows A_{ss} as a function of k_6 while panel b shows the numerical and the King-Altman steady state values of the degradation rate v of the ternary complex (S1 Text). In single-E mode the controller of Fig 11b behaves precisely as the single-E controller of Fig 6.

Also for this compulsory-order ternary-complex mechanism (Fig 11b) single-E control is observed when k_6 is getting larger than $k_7(E_1 \cdot Ez \cdot E_2)$ or, as in Fig 13, k_6 is larger than $k_7(Ez_{tot})$

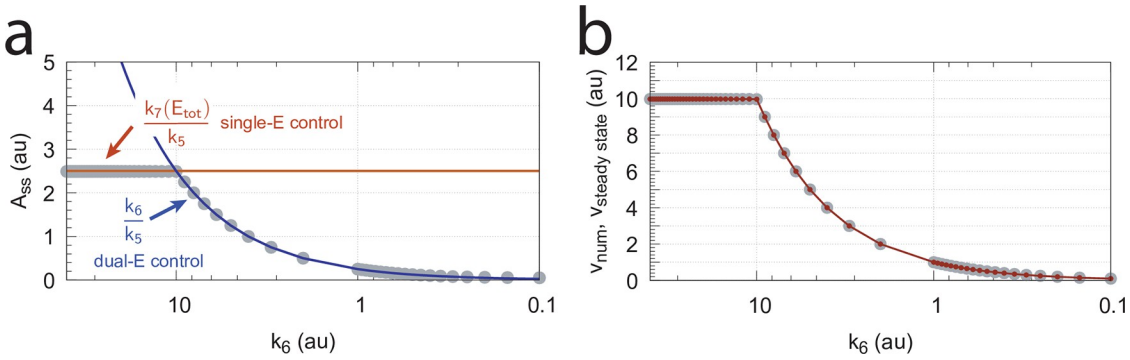

Fig 13. Switch between single-E and dual-E control for the m2 controller when E_1 and E_2 are removed by a compulsory-order ternary-complex mechanism with E_2 binding first to Ez (Fig 11b). Panel a: steady state values of A (A_{ss}) as a function of k_6. Gray dots show numerical results. The line outlined in red describes the set-point of A ($k_7 Ez_{tot}/k_5$) at single-E control. The blue line shows the set-point of A (k_6/k_5) when the system is in dual-E control mode. Panel b: corresponding numerical (gray dots) and steady state values (red small dots, calculated by King-Altman method, S1 Text) of the degradation rate v of the ternary-complex (Eq 13). Rate constants: k_1=0.0, k_2=100.0, k_3=1 × 10^5, k_4=1.0, k_5=4.0, k_6 varies between 40.0 and 0.05, k_7=1 × 10^7, k_8=0.1, k_{13}=k_{15}=1 × 10^8, k_{14}=k_{16}=1 × 10^3. Initial concentrations: A_0=1.0, $E_{1,0}$=9.1 × 10^2, $E_{2,0}$=6.7 × 10^{-2}, Ez_0=6.0 × 10^{-7}, $(E_1 \cdot Ez \cdot E_2)_0$=4.0 × 10^{-7}, $(Ez \cdot E_2)_0$=4.4 × 10^{-11}. Ez_{tot}=1.0 × 10^{-6}. Steady state values were obtained after 10000 time units.

https://doi.org/10.1371/journal.pone.0262371.g013

in the case v is zero-order with respect to $(E_1 \cdot Ez \cdot E_2)$. When k_6 is smaller than $k_7(E_1 \cdot Ez \cdot E_2)$ (or $k_7(Ez_{tot})$) the controller of Fig 11b will work in dual-E mode.

Critical slowing down at spontaneous single-E to dual-E mode transitions. We have seen above that when E_1 and E_2 are removed by an enzymatic ternary-complex mechanism then, dependent on k_6, the m2-controller can work either in a single-E or in a dual-E mode, where each of the control modes can have separate set-points. However, even when the condition for dual-E control mode is fulfilled, i.e. when

$$k_6 < k_7(E1 \cdot Ez \cdot E2) \tag{29}$$

the system can still stay in single-E mode whenever E_2 is kept at a high value. In this situation the single-E control mode is "*metastable*", i.e., A will be kept at the set-point of the single-E control mode until E_2 has reached its steady state. Then A changes abruptly to the set-point of the dual-E controller. This "metastability" of the single-E control mode, with the condition of Eq 29 fulfilled, is illustrated in Fig 14a with two values of k_6. For this purpose we have chosen the controller described by Fig 11b, but the other mechanism (Fig 11a) also shows this phenomenon. Outlined in red are the traces of A, while blue lines indicate the concentrations of E_2. Continuous lines have a k_6 of 4.0 while the dotted lines relate to a k_6 value of 8.0. Calculations start with a high initial values of E_2 (see legend of Fig 14). While E_2 gradually decreases A remains at the set-point of the single-E control mode until it ubruptly changes to the set-point of the dual-E control mode. Also note that even when the single-E controller is metastable, it can still defend its set-point (see the m5 motif below for an explicit example).

The *transition time* T (Fig 14a) denotes the time span A is kept at the set-point of the single-E controller until its transition to dual-E control. With increasing k_6 the system shows the behavior of critical slowing down [26], i.e. T increases and approaches infinity when

$$k_6 \rightarrow k_7(E1 \cdot Ez \cdot E2) \tag{30}$$

and the set-point for the dual-E control mode vanishes (Fig 14b).

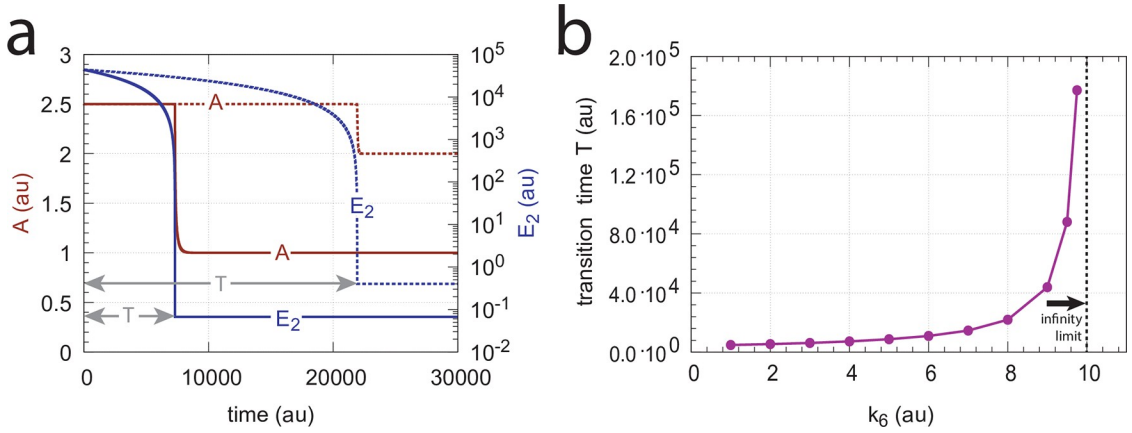

Fig 14. Critical slowing down in the transition from single-E to dual-E control in the negative feedback loop of Fig 11b. The set-point of A during single-E control is 2.5, but 1.0 during dual-E control. Panel a: Time profiles of A and E_2 for k_6=4.0 (solid lines) and k_6=8.0 (dotted lines). T, the transition time, is the time difference from t = 0 until E_2 has reached steady state. Panel b: T as a function of k_6. When $k_6 \rightarrow 10.0$ the steady state of the dual-E control mode vanishes and $T \rightarrow \infty$. Rate constants (for each data point): k_1=0.0, k_2=10.0, $k_3=1 \times 10^5$, k_4=1.0, k_5=4.0, k_6 takes the values 1.0, 2.0, . . ., 9.0, 9.5 and 9.75, $k_7=1 \times 10^7$, k_8=0.1, $k_{13}=k_{15}=1 \times 10^8$, $k_{14}=k_{16}=1 \times 10^3$. Initial concentrations: A_0=2.5, $E_{1,0}=3.635 \times 10^2$, $E_{2,0}=4.38 \times 10^4$, $Ez_0=2.28 \times 10^{-13}$, $(E_1 \cdot Ez \cdot E_2)_0=1.0 \times 10^{-6}$, $(Ez \cdot E_2)_0=2.75 \times 10^{-11}$.

https://doi.org/10.1371/journal.pone.0262371.g014

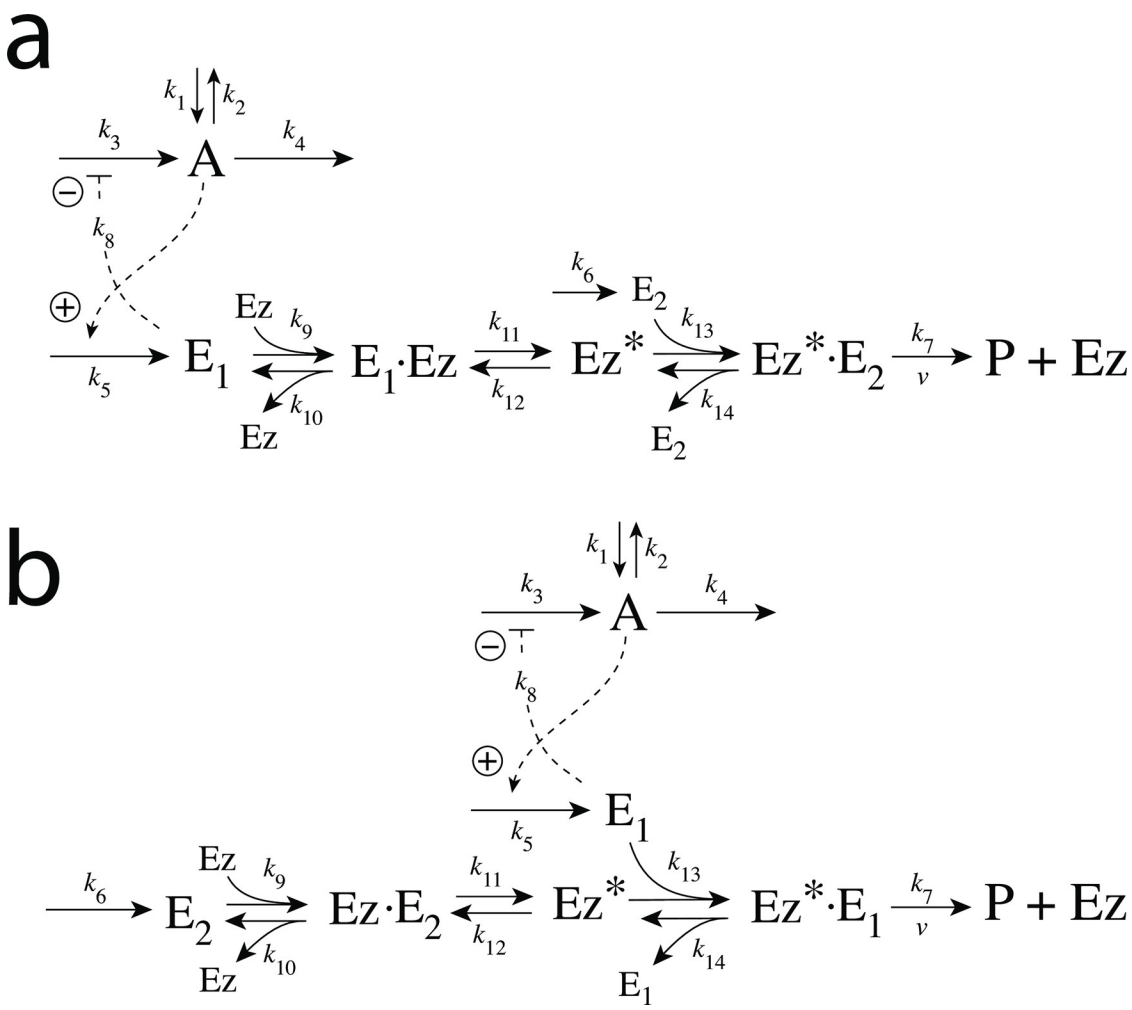

Fig 15. Enzymatic ping-pong mechanisms removing E_1 and E_2 in m2 dual-E controller. (a) E_1 binds first to Ez. (b) E_2 binds first to Ez.

https://doi.org/10.1371/journal.pone.0262371.g015

Ping-pong mechanism: Influence of total enzyme concentration on single-E and dual-E control mode. In this section we turn, for completeness, to the ping-pong type of mechanisms (Fig 15). However, we should mention that no significant differences between the behaviors of ternary-complex mechanisms and ping-pong mechanisms have been observed. Although we could have used one of the ternary-complex mechanisms to illustrate how total enzyme concentration influences m2-controller dynamics and the transitions between single-E and dual-E control modes, we use here the ping-pong mechanism of Fig 15a. While in ternary-complex mechanisms E_1 and E_2 need both to bind to enzyme Ez to undergo catalysis, in ping-pong mechanisms one of the substrates (E_1 or E_2) binds first and creates an alternative enzyme form Ez^* after forming a first product (for the sake of simplicity we have omitted it). Then Ez^* can bind the second substrate which leads to the final product, and regenerates Ez (Fig 4a and 4b). The two mechanisms in Fig 15 differ in the binding order of E_1 and E_2. When

E_1 binds first to Ez (Fig 15a) the rate equations become:

$$\dot{A} = k_1 - k_2 \cdot A - k_4 \cdot A + \frac{k_3 k_8}{k_8 + E_1} \tag{31}$$

$$\dot{E_1} = k_5 \cdot A - k_9(E_1)(Ez) + k_{10}(E_1 Ez) \tag{32}$$

$$\dot{E_2} = k_6 - k_{13}(E_2)(Ez^*) + k_{14}(Ez^* E_2) \tag{33}$$

$$\dot{Ez} = -k_9(E_1)(Ez) + k_{10}(E_1 Ez) + k_7(Ez^* E_2) \tag{34}$$

$$\frac{d(E_1 Ez)}{dt} = k_9(E_1)(Ez) - k_{10}(E_1 Ez) - k_{11}(E_1 Ez) + k_{12}(Ez^*) \tag{35}$$

$$\frac{d(Ez^*)}{dt} = k_{11}(E_1 Ez) + k_{14}(Ez^* E_2) - k_{12}(Ez^*) - k_{13}(Ez^*)(E_2) \tag{36}$$

$$\frac{d(Ez^* E_2)}{dt} = k_{13}(E_2)(Ez^*) - (k_7 + k_{14})(Ez^* E_2) \tag{37}$$

Fig 16 shows the effect of total enzyme concentration (Ez_{tot}) when in Fig 15a k_9, k_{11}, and k_{13} values are such high that the removal rate of E_1 and E_2, given by

$$v = k_7(Ez^* E_2) \tag{38}$$

becomes zero order with respect to E_1 and E_2, i.e., $v \approx V_{max} = k_7 Ez_{tot}$.

Panels a-d of Fig 16 show the steady state of A (A_{ss}, gray dots) as a function of k_6 when Ez_{tot} increases from 1×10^{-6} (panel a) up to 1×10^{-4}. One sees clearly the increase of the operational range for the dual-E control mode to higher k_6 values, while the set-point corresponding to the single-E control mode increases with increasing Ez_{tot} concentration.

Ping-pong mechanism: Influence of nonzero-order conditions on single-E and dual-E control mode. In this section we show how nonzero-order conditions of $v = k_7(Ez^* E_1)$ with respect to E_1 and E_2 influence the ping-pong mechanism. For this purpose we show the results for the mechanism of Fig 15b when E_2 binds first to Ez.

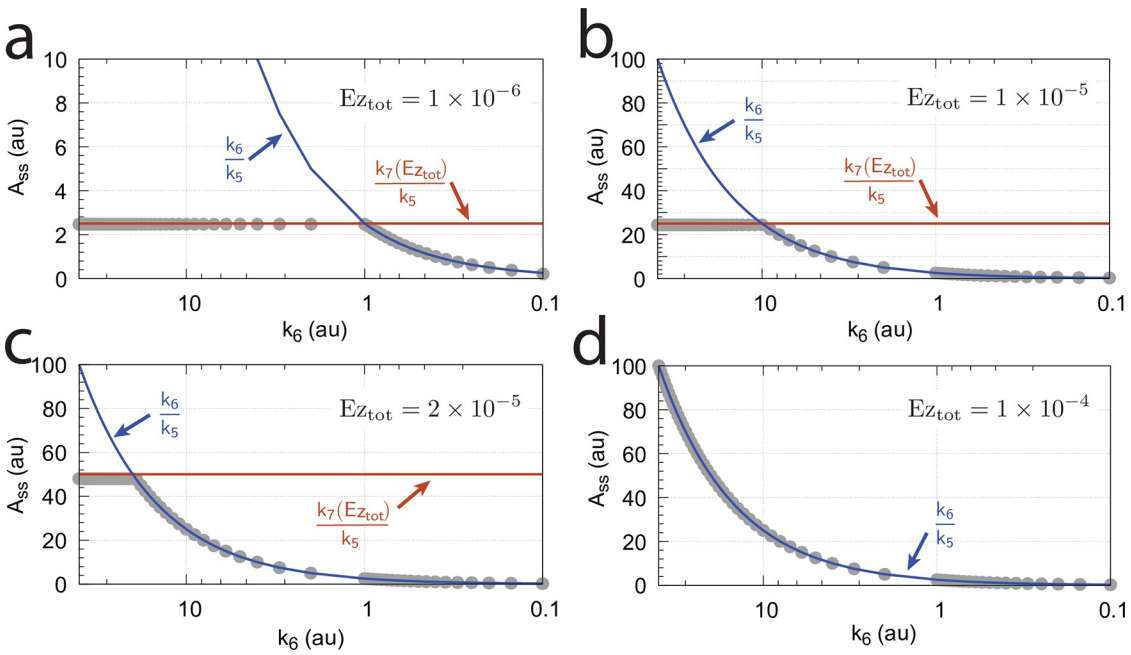

Fig 16. Influence of total enzyme concentration Ez_{tot} on the switch between dual-E and single-E control in the m2 controller with ping-pong mechanism of Fig 15a. (a) $Ez_{tot}=1 \times 10^{-6}$, (b) $Ez_{tot}=1 \times 10^{-5}$, (c) $Ez_{tot}=2 \times 10^{-5}$, (d) $Ez_{tot}=1 \times 10^{-4}$. Rate constants: k_1=0.0, k_2=500.0, $k_3=1 \times 10^5$, k_4=1.0, k_5=0.4, k_6 varies between 40.0 and 0.05, $k_7=1 \times 10^6$, k_8=0.1, $k_9=k_{11}=k_{13}=1 \times 10^8$, $k_{10}=k_{12}=k_{14}=1 \times 10^3$. Initial concentrations: A_0=2.0, $E_{1,0}=4.5 \times 10^2$, $E_{2,0}=2.0 \times 10^{-1}$, $Ez_0=Ez_{tot}$, $(E_1 \cdot Ez \cdot)_0$=0.0, $(Ez^* E_2)_0$=0.0. Steady state values were obtained after 4000 time units.

https://doi.org/10.1371/journal.pone.0262371.g016

The rate equations are:

$$\dot{A} = k_1 - k_2 \cdot A - k_4 \cdot A + \frac{k_3 k_8}{k_8 + E_1} \tag{39}$$

$$\dot{E_1} = k_5 \cdot A - k_{13}(E_1)(Ez^*) + k_{14}(Ez^* E_1) \tag{40}$$

$$\dot{E_2} = k_6 - k_9(Ez)(E_2) + k_{10}(EzE_2) \tag{41}$$

$$\dot{Ez} = -k_9(Ez)(E_2) + k_{10}(EzE_2) + k_7(Ez^* E_1) \tag{42}$$

$$\frac{d(EzE_2)}{dt} = k_9(Ez)(E_2) - k_{10}(EzE_2) - k_{11}(EzE_2) + k_{12}(Ez^*) \tag{43}$$

$$\frac{d(Ez^*)}{dt} = k_{11}(EzE_2) + k_{14}(Ez^* E_1) - k_{12}(Ez^*) - k_{13}(Ez^*)(E_1) \tag{44}$$

$$\frac{d(Ez^* E_1)}{dt} = k_{13}(E_1)(Ez^*) - (k_7 + k_{14})(Ez^* E_1) \tag{45}$$

Fig 17 shows the switching behavior from dual-E control, gray dots on blue lines) to single-E control (horizontal gray dots) with changing k_6 as a function of the rate constants k_9, k_{11}, and k_{13}. The red lines indicate the steady state of A when single-E control mode works under

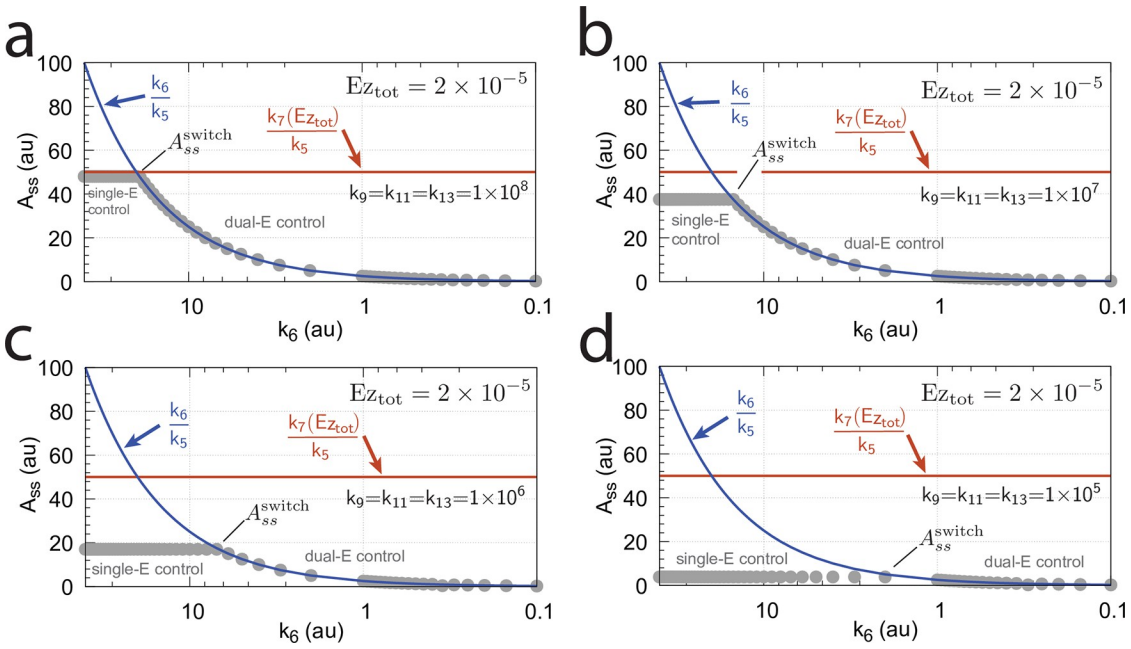

Fig 17. Change of the switch point between dual-E and single-E control with decreasing values of k_9, k_{11}, and k_{13}. (a) $k_9=k_{11}=k_{13}=1\times10^8$; (b) $k_9=k_{11}=k_{13}=1\times10^7$; (c) $k_9=k_{11}=k_{13}=1\times10^6$; (d) $k_9=k_{11}=k_{13}=1\times10^5$. Other rate constants: k_1=0.0, k_2=500.0, $k_3=1\times10^5$, k_4=1.0, k_5=0.4, k_6 takes values between 0.1 and 40.0 (indicated by the gray dots), $k_7=1\times10^6$, and k_8=0.1. Initial concentrations: A_0=2.0, $E_{1,0}=4.5\times10^2$, $E_{2,0}=2.0\times10^{-1}$, $Ez_0=Ez_{tot}=2.0\times10^{-5}$, $(EzE_2)_0$=0.0, $(Ez^*)_0$=0.0, $(Ez^*E_1)_0$=0.0. Steady state values were obtained after 4000 time units.

https://doi.org/10.1371/journal.pone.0262371.g017

zero-order conditions, i.e. at high values of k_9, k_{11}, and k_{13}. In this case we have that

$$A_{ss} = \frac{k_7(Ez^*E_1)_{ss}}{k_5} \quad \text{with} \quad (Ez^*E_1)_{ss} \approx Ez_{tot} \tag{46}$$

In the calculations of Fig 17 the total enzyme concentration Ez_{tot} is 2×10^{-5}. With decreasing values of k_9, k_{11}, and k_{13} (from panel a to d), the system moves towards nonzero-order kinetics (with respect to E_1 and E_2) and the steady state value of (Ez^*E_1) decreases. The switch-point in A_{ss} (A_{ss}^{switch}) from dual-E control to single-E control occurs now at lower A_{ss} values, described by the equation

$$A_{ss}^{switch} = \frac{k_7(Ez^*E_1)_{ss}}{k_5} \quad \text{with} \quad (Ez^*E_1)_{ss} < Ez_{tot} \tag{47}$$

showing that nonzero-order conditions diminish the operational range of dual-E control.

Also increased values of the perturbation k_2 reduces the operational range and moves A_{ss}^{switch} to lower values (Fig 18).

Summary of the catalyzed m2 controllers. The catalyzed m2 controller works for all the four basic enzymatic mechanisms shown in Fig 4. Zero-order conditions for v (=dP/dt) with respect to E_1 and E_2 provide optimum controller performance, which, however, becomes limited at low enzyme concentrations and high perturbation (k_2) values. Catalyzed antithetic controllers (i.e. controllers working in dual-E mode) become more aggressive by increased turnover numbers (k_7 values). Switch to single-E control mode is observed when the rate forming E_2 by k_6 exceeds the degradation rate of the controller species E_1 and E_2. For nonzero-

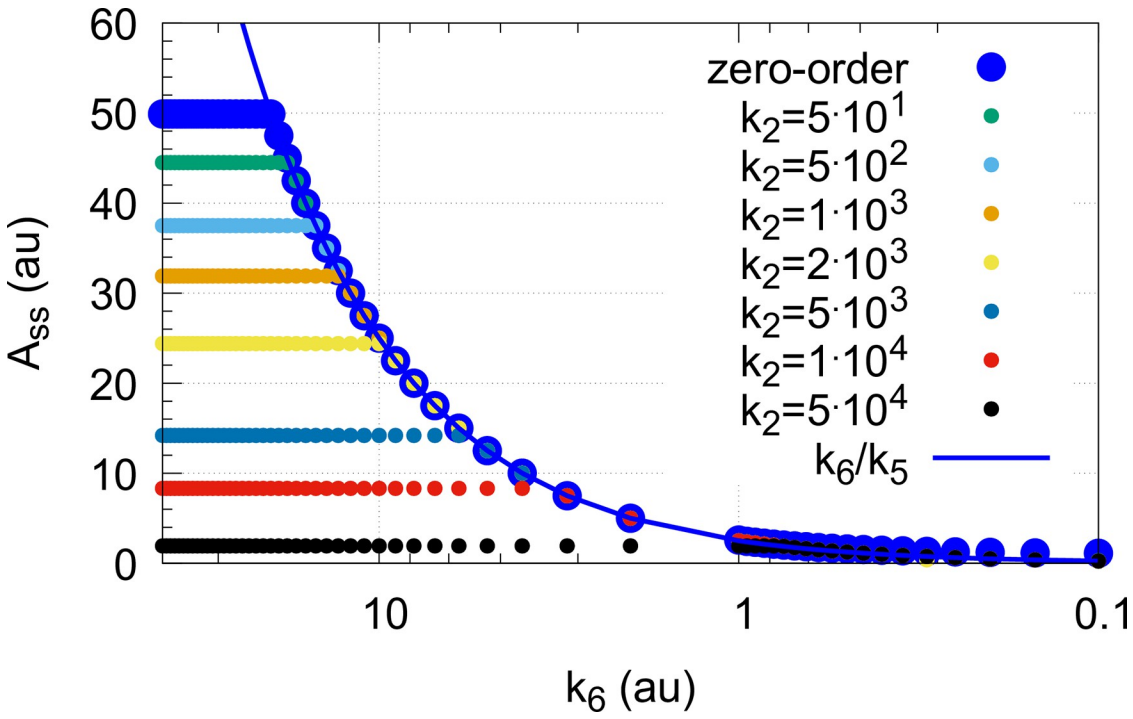

Fig 18. Influence of step-wise k_2 for catalyzed m2 controller under nonzero-order conditions. The mechanism considered in that of Fig 15b. Small colored dots indicate A_{ss} levels for different k_2 values when k_9=k_{11}=k_{13}=1 × 10^7 and Ez$_{tot}$=2.0 × 10^{-5}. For comparison, large blue dots show the A_{ss} values under zero-order conditions when k_9=k_{11}=k_{13}=1 × 10^9 and k_2=1.0. Other rate constant values and initial concentrations are as in Fig 17.

https://doi.org/10.1371/journal.pone.0262371.g018

order conditions A_{ss} in single-E control mode decreases with increasing k_2 values. While this is also true for the dual-E control mode, in dual-E mode A_{ss} is still determined by the ratio k_6/k_5 and thereby, unlike a single-E controller, shows robust control even for nonzero-order conditions.

Controllers based on motif 4

Motif 4 is based on double inhibition. In the antithetic/dual-E setting (Fig 3), A is inhibiting the synthesis of E_1, while E_2 is now activating the compensatory flux by derepression.

Motif 4 dual-E controller removing E_1 and E_2 by a random-order ternary-complex mechanism. Fig 19 shows the dual-E m4-controller removing E_1 and E_2 by a random-order ternary-complex mechanism. It is, like the corresponding m2-controller, also an inflow type of controller, where the compensatory flux, j_{comp}^{m4} is based on derepression, now by E_2, i.e

$$j_{comp}^{m4} = \frac{k_3 k_8}{k_8 + E_2} \tag{48}$$

The rate equations for the m4-controller are:

$$\dot{A} = k_1 - k_2 \cdot A - k_4 \cdot A + \frac{k_3 k_8}{k_8 + E_2} \tag{49}$$

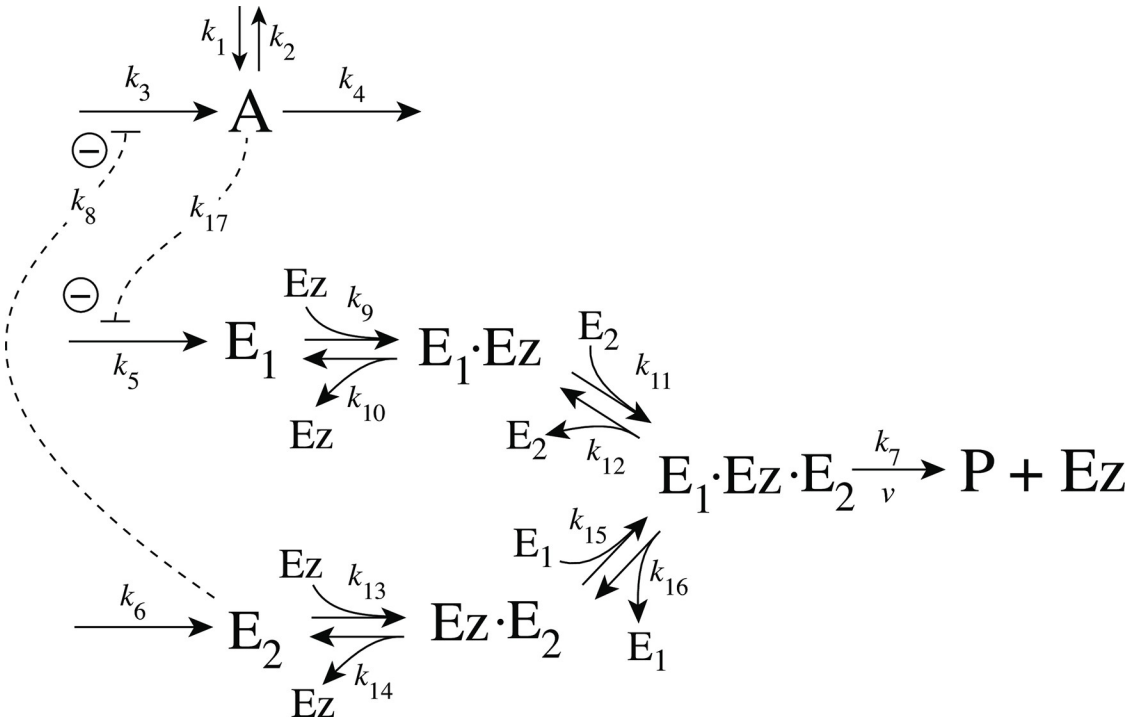

Fig 19. Motif 4 dual-E/antithetic controller using an enzymatic random-order ternary-complex mechanism for the removal of E_1 and E_2.

https://doi.org/10.1371/journal.pone.0262371.g019

$$\dot{E_1} = \frac{k_5 k_{17}}{k_{17} + A} - k_9(E_1)(Ez) + k_{10}(E_1 \cdot Ez) - k_{15}(Ez \cdot E_2)(E_1) + k_{16}(E_1 \cdot Ez \cdot E_2) \tag{50}$$

$$\dot{E_2} = k_6 - k_{11}(E_1 \cdot Ez)(E_2) + k_{12}(E_1 \cdot Ez \cdot E_2) - k_{13}(E_2)(Ez) + k_{14}(Ez \cdot E_2) \tag{51}$$

$$\dot{Ez} = -k_9(E_1)(Ez) + k_{10}(E_1 \cdot Ez) - k_{13}(E_2)(Ez) + k_{14}(Ez \cdot E_2) + k_7(E_1 \cdot Ez \cdot E_2) \tag{52}$$

$$\frac{d(E_1 \cdot Ez)}{dt} = k_9(E_1)(Ez) - k_{10}(E_1 \cdot Ez) - k_{11}(E_1 \cdot Ez)(E_2) + k_{12}(E_1 \cdot Ez \cdot E_2) \tag{53}$$

$$\frac{d(E_1 \cdot Ez \cdot E_2)}{dt} = k_{11}(E_1 \cdot Ez)(E_2) + k_{15}(Ez \cdot E_2)(E_1) - (k_7 + k_{12} + k_{16})(E_1 \cdot Ez \cdot E_2) \tag{54}$$

$$\frac{d(Ez \cdot E_2)}{dt} = k_{13}(E_2)(Ez) - k_{14}(Ez \cdot E_2) - k_{15}(Ez \cdot E_2)(E_1) + k_{16}(E_1 \cdot Ez \cdot E_2) \tag{55}$$

When the controller works in dual-E mode, its set-point is calculated from the following relationship

$$j_5 = \frac{k_5 k_{17}}{k_{17} + A_{set}} = k_7(\mathrm{E_1} \cdot \mathrm{Ez} \cdot \mathrm{E_2}) = k_{16} \quad \Rightarrow \quad A_{set} = \frac{k_{17}(k_5 - k_6)}{k_6} \tag{56}$$

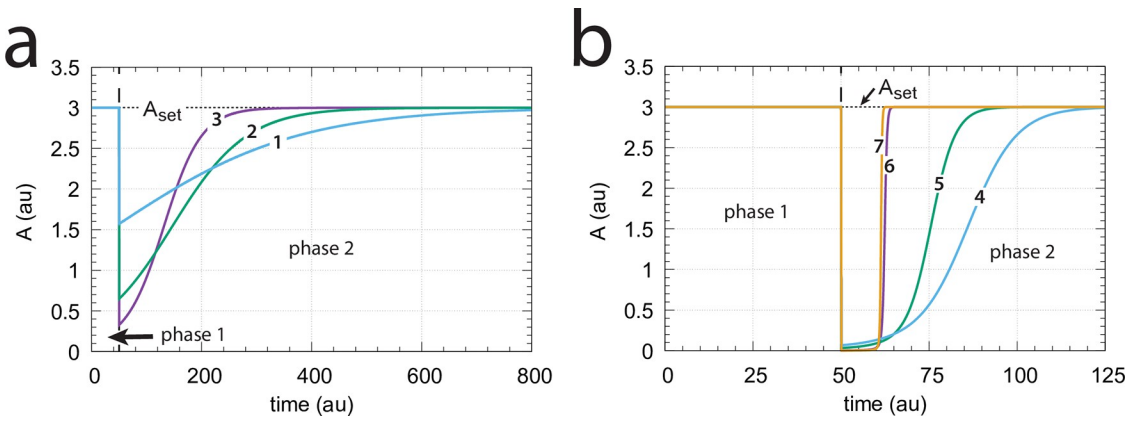

Fig 20. Response of the m4 random-order ternary-complex controller (Fig 19) with respect to step-wise changes in k_2. (a) Phase 1: k_2=10. At time t = 50 phase 2 starts with the following changes in k_2: (1) k_2=20, (2) k_2=50, (3) k_2=100. (b) Phase 1: k_2=10. At time t = 50 phase 2 starts with the following changes in k_2: (4) k_2=500, (5) $k_2=1\times10^3$, (6) $k_2=1\times10^4$, (7) $k_2=2\times10^4$. Other rate constants: k_1=0.0, $k_3=1\times10^5$, k_4=1.0, k_5=31.0, k_6=1.0, $k_7=1\times10^8$, k_8=0.1, $k_9=k_{11}=k_{13}=k_{15}=1\times10^8$, $k_{10}=k_{12}=k_{14}=k_{16}=1\times10^3$, k_{17}=0.1. Initial concentrations: A_0=3.0, $E_{1,0}=1.0\times10^{-2}$, $E_{2,0}=3.0\times10^2$, $Ez_0=3.3\times10^{-11}$, $(E_1{\cdot}Ez)_0=1.4\times10^{-15}$, $(E_1{\cdot}Ez{\cdot}E_2)_0=1.0\times10^{-8}$, $(EzE_2)_0=9.9\times10^{-7}$. Total enzyme concentration $Ez_{tot}=1.0\times10^{-6}$.

https://doi.org/10.1371/journal.pone.0262371.g020

In comparison with the corresponding m2 dual-E controller (Fig 7) also for the m4 feedback arrangement the response time decreases with increased levels of step-wise perturbations in k_2. Fig 20 shows the controller's homeostatic behavior upon step-wise perturbations in k_2 (curves 1–7) applied at time t = 50 from k_2=10 (phase 1) up to $k_2=2\times10^4$ (curve 7, phase 2).

For a given set-point A_{set} the steady state condition of Eq 49 determines the range of k_2 perturbations the controller can defend. By setting in Eq 49 E_2=0 and $A = A_{set}$ the upper limit of k_2, k_2^{ul}, can be determined, i.e.,

$$k_2^{ul} = \frac{k_1 + k_3 - k_4 A_{set}}{A_{set}} \tag{57}$$

For $k_2 < k_2^{ul}$ the m4 controller will defend the set-point described by Eq 56, i.e., $A_{ss} = A_{set}$. This is indicated by the the blue area in Fig 21a. The red area in Fig 21 shows the k_2 values when $k_2 > k_2^{ul}$ for a given set-point A_{set}. In this case $A_{ss} < A_{set}$ and an offset in A concentration from A_{set} will be observed. Fig 21b illustrates this. During phase 1 (time between 0 and 50) k_2=10.0 and the value of A is at its set-point A_{set} = 3.0. At time t = 50.0 (indicated by the blue downward arrow 1) k_2 is increased to 2×10^4. The controller is able to defend the perturbation and is still within the blue area as indicated in Fig 21a by point 1. At time t = 250.0 phase 3 starts with a k_2 of 5×10^4 (red downward arrow 2). Now $k_2 > k_2^{ul}$ and the controller shows an offset in the controlled variable, i.e. the steady state value of A is below A_{set}. With increasing k_2 values the offset will increase.

Another influence on the operational range of the m4 controller is the reaction-order by which the enzyme Ez removes E_1 and E_2. The reaction order is closely related to the ratios of k_{10}/k_9, k_{12}/k_{11}, k_{14}/k_{13}, and k_{16}/k_{15}. The ratios can be interpreted as K_M values (in a rapid-equilibrium approach). For example, in the single-E m2 controller (Fig 6), an offset from A_{set}=-$k_7(Ez_{tot})/k_5$ (Eq 15) is observed when k_{10}/k_9 is relatively large, i.e. not small enough for the degradation of E to become zero-order (see Ref [4, 6] for more details). For the m4 controller (Fig 19) increasing values of the ratios k_{10}/k_9, k_{12}/k_{11}, k_{14}/k_{13}, and k_{16}/k_{15} will lead to a reduction of the controller's operational range. Fig 22 illustrates this. For the sake of simplicity, all odd-numbered rate constants k_9,. . .k_{15} and all equal-numbered rate constants k_{10},. . .k_{16} have

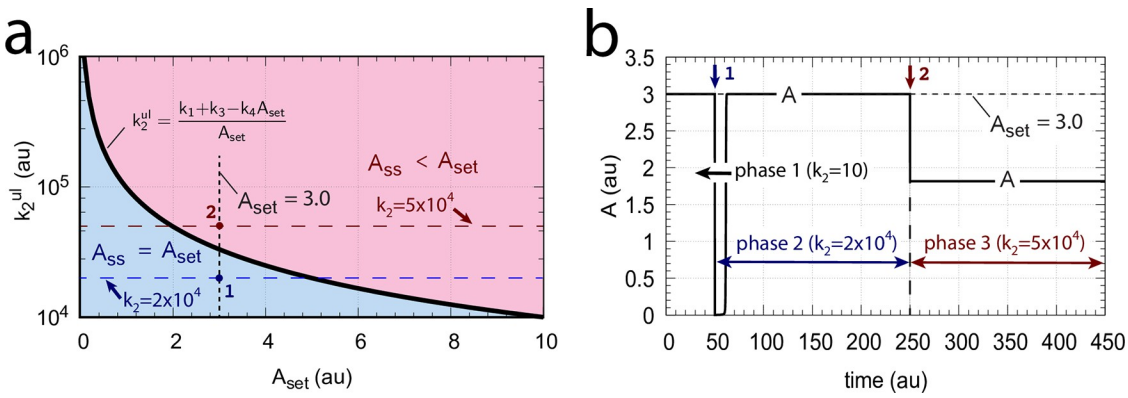

Fig 21. Operational range of m4 controller with upper defendable limit of k_2 ($k_2^{ul}=k_1+k_3-k_4A_{set}/A_{set}$). (a) Blue area indicates the $k_2 < k_2^{ul}$ range as a function of A_{set} in which the controller can defend A_{set}. Black solid curve: k_2^{ul} as a function of A_{set} when k_1=0.0, k_3=1 × 10^5, and k_4=1.0. Red area: $k_2 > k_2^{ul}$ where A_{ss} is lower than A_{set}. (b) Computation showing the partial loss of homeostasis when k_2 becomes larger than k_2^{ul}. Phase 1 (0–50 time units): k_2=10; phase 2 (50–250 time units): k_2=2 × 10^4; phase 3 (250–450 time units): k_2=5 × 10^4. Other rate constants and initial conditions as in Fig 20. For further descriptions, see S1 Text.

https://doi.org/10.1371/journal.pone.0262371.g021

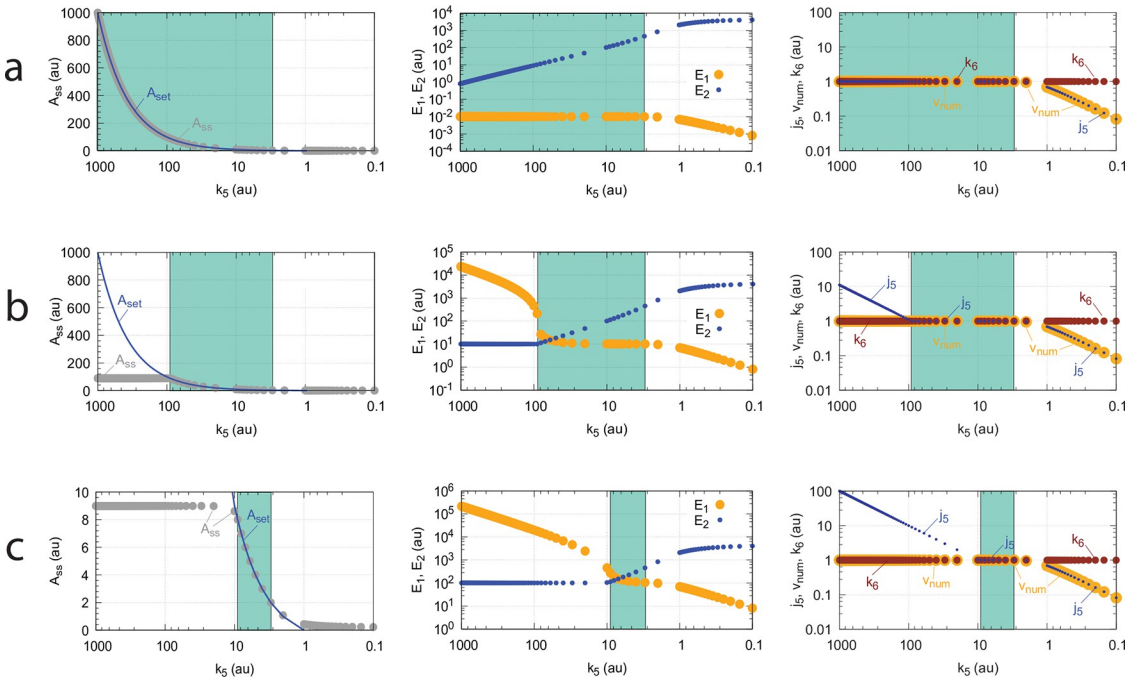

Fig 22. Operational range of the controller from Fig 19 as a function of k_5 and the ratios (k_{10}/k_9)=(k_{12}/k_{11})=(k_{14}/k_{13})=(k_{16}/k_{15}). A_{set} in the left panels is the theoretical set-point described by Eq 56. A_{ss} (gray dots) are the numerically calculated steady state values of A. Middle panels show the concentrations of E_1 and E_2 indicated by blue and orange dots, respectively. Panels to the right show the flux j_5 (small blue dots) which generates E_1 by A-repression (Eq 56). v_{num} (yellow dots) is the numerically calculated degradation velocity of the ternary-complex. Dark red dots show k_6. Turquoise areas indicate the controllers operational range when Eq 56 is satisfied. (a) k_9=k_{11}=k_{13}=k_{15}=1 × 10^8. (b) k_9=k_{11}=k_{13}=k_{15}=1 × 10^5. (c) k_9=k_{11}=k_{13}=k_{15}=1 × 10^4. Remaining rate constants and initial concentrations are as in Fig 20.

https://doi.org/10.1371/journal.pone.0262371.g022

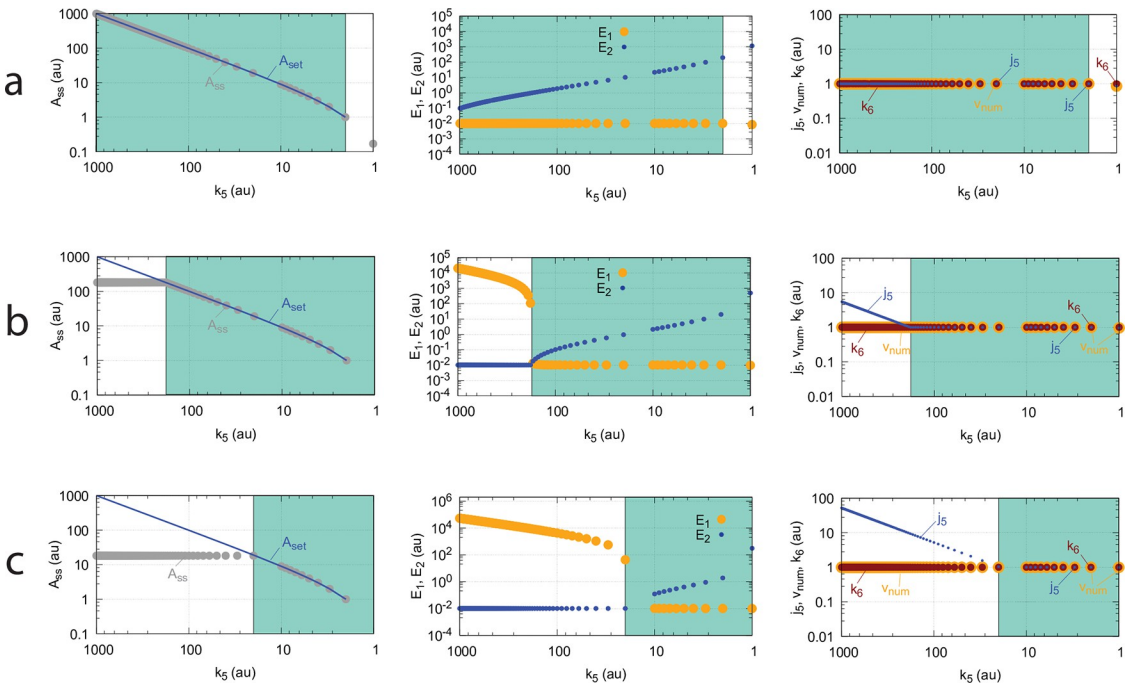

Fig 23. Influence of k_2 on the operational range of the m4 controller Fig 19. See Fig 22 for explanation of symbols. (a) k_2 = 50.0, (b) k_2 = 500.0, (c) k_2 = 5000.0. Other rate constants and initial concentrations are as in Fig 20.

https://doi.org/10.1371/journal.pone.0262371.g023

among themselves the same values, respectively. The turquoise areas in Fig 22 show the fully functional range of the controller as a function of k_5, i.e. when the condition of Eq 56 is fulfilled and the controller works in dual-E mode. With increasing values of $(k_{10}/k_9)=(k_{12}/k_{11})=(k_{14}/k_{13})=(k_{16}/k_{15})$ the operational range of the controller is clearly reduced.

Interestingly, also in these calculations critical slowing down is observed, similar as in Fig 14b, when the border between dual-E control (turquoise area) and constant A_{ss} values is approached with increasing k_5 values.

Importantly, unlike the corresponding m2-controller which goes into a regime of defended single-E control under zero-order conditions (Fig 9), the constant A_{ss} regime of the m4 controller *is not defended*, but A_{ss} decreases with increasing k_2 (perturbation) values. This is shown in Fig 23, where the $(k_{10}/k_9)=(k_{12}/k_{11})=(k_{14}/k_{13})=(k_{16}/k_{15})$ ratios are kept constant at 1×10^{-4}, while k_2 is changed from 50 (panel a) to 500 (panel b). Finally, in panel c k_2=5000. With increasing k_2 values a reduction in A_{ss} and the controller's operational range is observed.

Motif 4 dual-E controller removing E_1 and E_2 by compulsory-order ternary-complex mechanisms. Fig 24 shows the two mechanisms when the removal of E_1 and E_2 goes through a compulsory-order ternary-complex. In panel a E_1 binds first to the free enzyme Ez, while in panel b E_2 binds first.

In case E_1 binds first to Ez (Fig 24a), the rate equations are:

$$\dot{A} = k_1 - k_2 \cdot A - k_4 \cdot A + \frac{k_3 k_8}{k_8 + E_2} \tag{58}$$

$$\dot{E_1} = \frac{k_5 k_{17}}{k_{17} + A} - k_9(E_1)(Ez) + k_{10}(E_1 \cdot Ez) \tag{59}$$

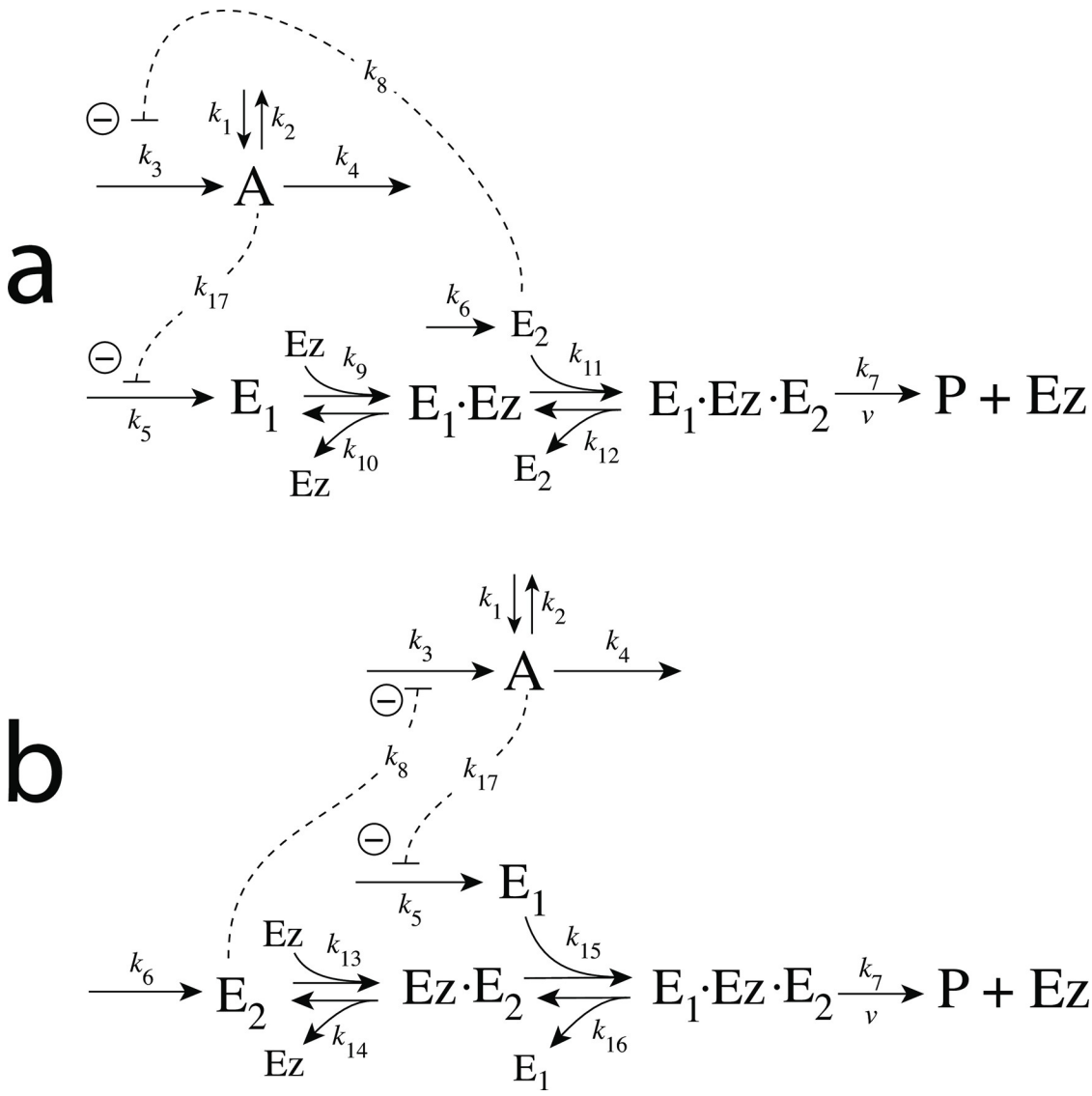

Fig 24. Reaction schemes when E_1 and E_2 in a m4-type of control structure (Fig 3) are removed by enzyme *Ez* with two compulsory-order ternary-complex mechanism. In (a) E_1 binds first to *Ez*, while in (b) E_2 binds first.

https://doi.org/10.1371/journal.pone.0262371.g024

$$\dot{E_2} = k_6 - k_{11}(E_1 \cdot Ez)(E_2) + k_{12}(E_1 \cdot Ez \cdot E_2) \tag{60}$$

$$\dot{Ez} = -k_9(E_1)(Ez) + k_{10}(E_1 \cdot Ez) + k_7(E_1 \cdot Ez \cdot E_2) \tag{61}$$

$$\frac{d(E_1 \cdot Ez)}{dt} = k_9(E_1)(Ez) - k_{10}(E_1 \cdot Ez) - k_{11}(E_1 \cdot Ez)(E_2) + k_{12}(E_1 \cdot Ez \cdot E_2) \tag{62}$$

$$\frac{d(E_1 \cdot Ez \cdot E_2)}{dt} = k_{11}(E_1 \cdot Ez)(E_2) - (k_7 + k_{12})(E_1 \cdot Ez \cdot E_2) \tag{63}$$

When E_2 is binding first to free Ez (Fig 24b), the rate equations are:

$$\dot{A} = k_1 - k_2 \cdot A - k_4 \cdot A + \frac{k_3 k_8}{k_8 + E_2} \tag{64}$$

$$\dot{E_1} = \frac{k_5 k_{17}}{k_{17} + A} - k_{15}(Ez \cdot E_2)(E_1) + k_{16}(E_1 \cdot Ez \cdot E_2) \tag{65}$$

$$\dot{E_2} = k_6 - k_{13}(E_2)(Ez) + k_{14}(Ez \cdot E_2) \tag{66}$$

$$\dot{Ez} = -k_{13}(E_2)(Ez) + k_{14}(Ez \cdot E_2) + k_7(E_1 \cdot Ez \cdot E_2) \tag{67}$$

$$\frac{d(Ez \cdot E_2)}{dt} = k_{13}(E_2)(Ez) - k_{14}(Ez \cdot E_2) - k_{15}(Ez \cdot E_2)(E_1) + k_{16}(E_1 \cdot Ez \cdot E_2) \tag{68}$$

$$\frac{d(E_1 \cdot Ez \cdot E_2)}{dt} = k_{15}(Ez \cdot E_2)(E_1) - (k_7 + k_{16})(E_1 \cdot Ez \cdot E_2) \tag{69}$$

For both reaction schemes the set-point for the dual-E controller

$$A_{set} = \frac{k_{15}(k_5 - k_6)}{k_6} \tag{70}$$

is given by the same balance conditions as for the m4 random-order ternary-complex mechanism, i.e., we have a balance between the two inflow rates $j_5 = k_5 k_{17}/(k_{17} + A) = k_6$, and the outflow rate $k_7(E_1 \cdot Ez \cdot E_2)$ (see Eq 56).

As already seen for the m2-controller (Fig 12) when working in dual-E mode, the random-order and compulsory-order ternary-complex mechanisms show for the m4-feedback schemes the same kinetic behavior on step-wise changes in k_2. Fig 25 illustrates this for the three m4-controllers removing E_1 and E_2 by enzymatic ternary-complex mechanisms (Figs 19 and 24). Even the breakdown at large k_2 values show identical kinetics in A (Fig 25d).

Fig 26 shows the concentration profiles of E_1, E_2 and the different enzyme species for the three m4 controller arrangements in case of their breakdown described in Fig 25d.

Although the concentration profiles of A, E_1, E_2, and the ternary-complex ($E_1 \cdot Ez \cdot E_2$) are identical for the three controller configurations the other enzyme species replace each other in their functions. For example, when E_1 binds first in the compulsory-order mechanisms of Fig 24a the complex ($E_1 \cdot Ez$) is low during phase 1 but becomes close to the total enzyme concentration Ez_{tot} during the breakdown in phase 2 (Fig 26b). In the compulsory-order mechanism when E_2 binds first (Fig 24b) the role of ($E_1 \cdot Ez$) is now taken over by the free enzyme Ez (Fig 26c). In the random-order mechanism the role of the enzyme species is slightly more complex: during phase 1 Ez and ($Ez \cdot E_2$) have the same concentration profiles as in the compulsory-order mechanism where E_2 binds first to Ez (Fig 24b). However, in phase 2 the Ez profile of the random-order mechanism is that of the other compulsory-order mechanism (Fig 26b)!

Motif 4 dual-E enzymatic controller in which E_1 and E_2 are removed by ping-pong mechanisms. Fig 27 shows the two possibilities when enzyme Ez removes E_1 and E_2 by a ping-pong mechanism. In panel a E_1 binds to the free enzyme and creates the alternative enzymatic form Ez^*, which then bind the derepressing controller species E_2. In panel b this is reversed. Here E_2 binds first and forms Ez^*, which can bind E_1. As for the m2 controller case we have, for the sake of simplicity, omitted the release of a product prior to the formation of Ez^*.

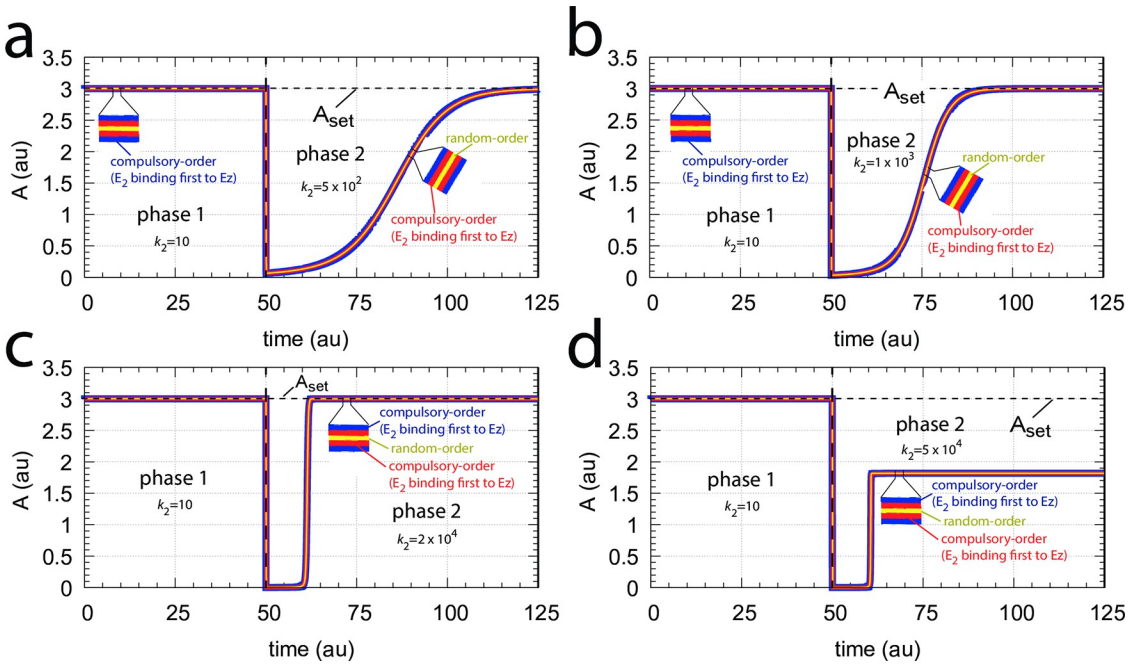

Fig 25. Comparison between the three m4-controllers when E_1 and E_2 are removed by enzymatic ternary-complex mechanisms (Figs 19 and 24) upon step-wise changes at time $t = 50$ from k_2=10 to (a) k_2=500, (b) k_2=1 × 10^3, (c) k_2=2 × 10^4, (d) k_2=5 × 10^4. Color coding: Thick blue line, compulsory-order mechanism with E_2 binding first to Ez; overlaid red line, compulsory-order mechanism with E_1 binding first to Ez; top overlaid yellow line, random-order mechanism. Rate constants and initial concentrations as for the random-order ternary-complex mechanism (Fig 20).

https://doi.org/10.1371/journal.pone.0262371.g025

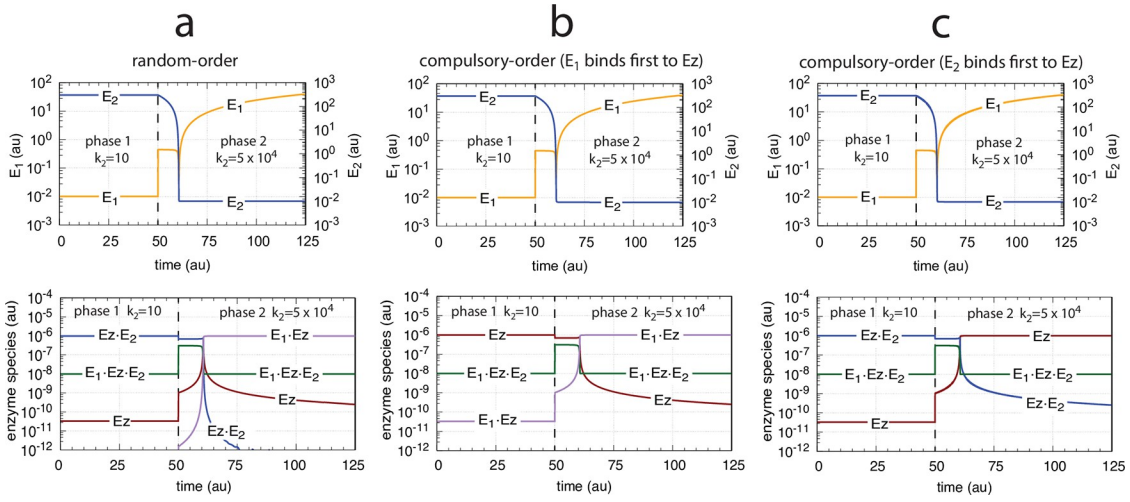

Fig 26. Concentration profiles of E_1, E_2, and enzyme species with respect to the controllers' breakdown shown in Fig 25d. Column a: Random-order mechanism (Fig 19). Column b: Compulsory-order mechanism (Fig 24a). Column c: Compulsory-order mechanism (Fig 24b). Rate constants and initial concentrations as in Fig 25.

https://doi.org/10.1371/journal.pone.0262371.g026

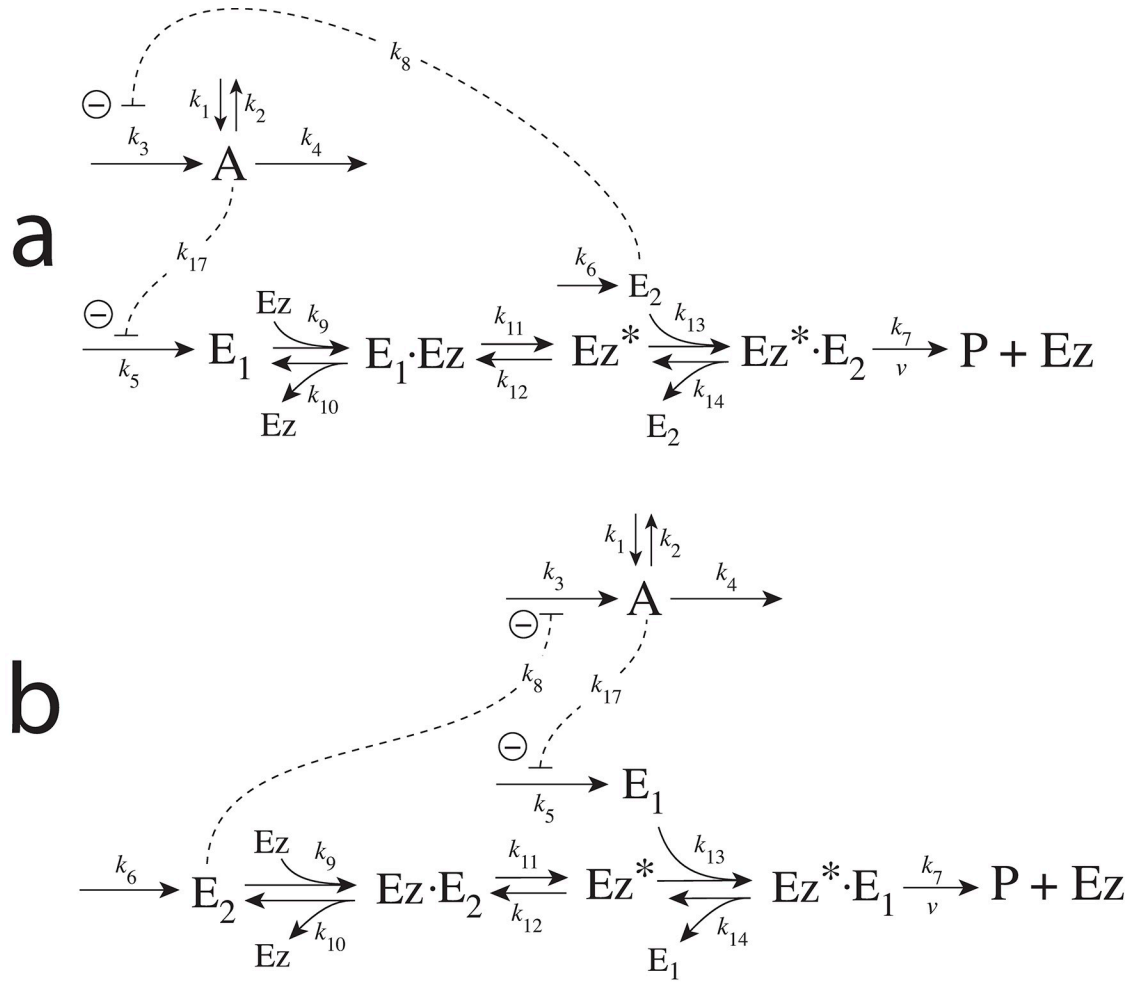

Fig 27. Reaction schemes when E_1 and E_2 in a m4-type of control structure (Fig 3) are removed by enzyme Ez following two ping-pong mechanisms. In (a) E_1 binds first to the free enzyme Ez, while in (b) E_2 binds first.

https://doi.org/10.1371/journal.pone.0262371.g027

For the scheme of Fig 27a the rate equations are:

$$\dot{A} = k_1 - k_2 \cdot A - k_4 \cdot A + \frac{k_3 k_8}{k_8 + E_2} \tag{71}$$

$$\dot{E_1} = \frac{k_5 k_{17}}{k_{17} + A} - k_9(E_1)(Ez) + k_{10}(E_1 Ez) \tag{72}$$

$$\dot{E_2} = k_6 - k_{13}(E_2)(Ez^*) + k_{14}(Ez^* E_2) \tag{73}$$

$$\dot{Ez} = -k_9(E_1)(Ez) + k_{10}(E_1 Ez) + k_7(Ez^* E_2) \tag{74}$$

$$\frac{d(E_1Ez)}{dt} = k_9(E_1)(Ez) - k_{10}(E_1Ez) - k_{11}(E_1Ez) + k_{12}(Ez^*) \tag{75}$$

$$\frac{d(Ez^*)}{dt} = k_{11}(E_1Ez) + k_{14}(Ez^*E_2) - k_{12}(Ez^*) - k_{13}(Ez^*)(E_2) \tag{76}$$

$$\frac{d(Ez^*E_2)}{dt} = k_{13}(E_2)(Ez^*) - (k_7 + k_{14})(Ez^*E_2) \tag{77}$$

In case E_2 binds first to Ez (Fig 27b), the rate equations are:

$$\dot{A} = k_1 - k_2 \cdot A - k_4 \cdot A + \frac{k_3 k_8}{k_8 + E_2} \tag{78}$$

$$\dot{E_1} = \frac{k_5 k_{17}}{k_{17} + A} - k_{13}(E_1)(Ez^*) + k_{14}(Ez^*E_1) \tag{79}$$

$$\dot{E_2} = k_6 - k_9(Ez)(E_2) + k_{10}(EzE_2) \tag{80}$$

$$\dot{Ez} = -k_9(Ez)(E_2) + k_{10}(EzE_2) + k_7(Ez^*E_1) \tag{81}$$

$$\frac{d(EzE_2)}{dt} = k_9(Ez)(E_2) - k_{10}(EzE_2) - k_{11}(EzE_2) + k_{12}(Ez^*) \tag{82}$$

$$\frac{d(Ez^*)}{dt} = k_{11}(EzE_2) + k_{14}(Ez^*E_1) - k_{12}(Ez^*) - k_{13}(Ez^*)(E_1) \tag{83}$$

$$\frac{d(Ez^*E_1)}{dt} = k_{13}(E_1)(Ez^*) - (k_7 + k_{14})(Ez^*E_1) \tag{84}$$

We have compared the two m4 ping-pong mechanisms (Fig 27) with the three m4 ternary-complex mechanisms (Figs 19 and 24) and found that their homeostatic behavior in A as well as the concentration profiles in E_1 and E_2 have identical dynamics with those shown in Fig 25 and the upper row in Fig 26, respectively (data not shown). However, despite their identical dynamical behaviors in the controlled variable A as well as in the controller variables E_1 and E_2 the different enzyme species show, like in the lower row of Fig 26, a mechanism-dependent restructuring of the enzyme species' concentration profiles. This indicates that in the different mechanisms different enzyme species take over the tasks to decrease E_2 (causing an increase in the compensatory flux when k_2 is increased) and to increase E_1, thereby leading to homeostasis in A. Specifically, for the intact m4 dual-E *ternary-complex controllers* (i.e. no breakdown occurs) the condition of Eq 56 defines the profiles of the enzyme species, while for the m4 ping-pong controllers the conditions

$$j_5 = \frac{k_5 k_{17}}{k_{17} + A_{set}} = k_7(Ez^*E_2) = k_6 \tag{85}$$

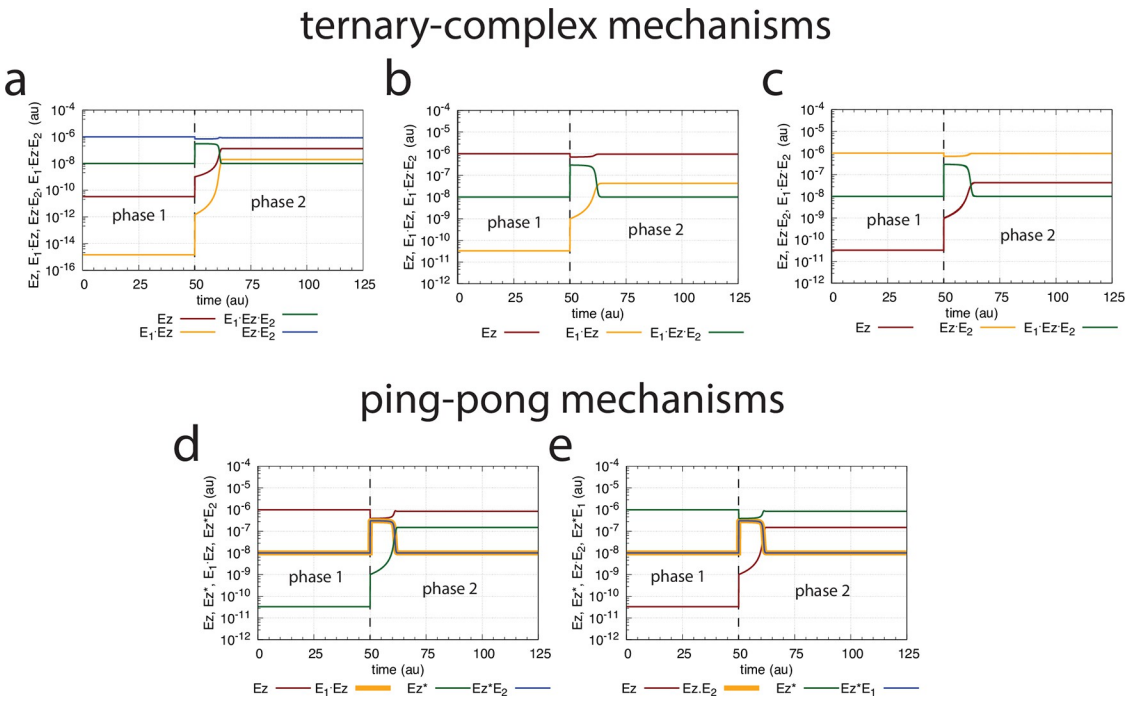

Fig 28. Enzyme species profiles of the m4 ternary-complex (Figs 19 and 24) and ping-pong mechanisms (Fig 27) when k_2=10 in phase 1, and k_2=2 × 10^4 in phase 2. (a) random-order ternary-complex mechanism, (b) compulsory-order ternary-complex mechanism with E_1 binding first to *Ez*, (c) compulsory-order ternary-complex mechanism with E_2 binding first to *Ez*, (d) ping-pong mechanism with E_1 binding first to *Ez*, (e) ping-pong mechanism with E_2 binding first to *Ez*. Rate constants (if applicable) are as in Fig 20. Initial concentrations: (a) A_0=3.0, $E_{1,0}$=1.0 × 10^{-2}, $E_{2,0}$=3.0 × 10^2, Ez_0=3.3 × 10^{-11}, $(E_1{\cdot}Ez)_0$=1.4 × 10^{-15}, $(E_1{\cdot}Ez{\cdot}E_2)_0$=1.0 × 10^{-8}, $(EzE_2)_0$=9.9 × 10^{-7}. (b) A_0=3.0, $E_{1,0}$=1.0 × 10^{-2}, $E_{2,0}$=3.0 × 10^2, Ez_0=9.9 × 10^{-7}, $(E_1{\cdot}Ez)_0$=3.3 × 10^{-11}, $(E_1{\cdot}Ez{\cdot}E_2)_0$=1.0 × 10^{-8}. (c) A_0=3.0, $E_{1,0}$=1.0 × 10^{-2}, $E_{2,0}$=3.0 × 10^2, Ez_0=3.3 × 10^{-11}, $(EzE_2)_0$=9.9 × 10^{-7}, $(E_1{\cdot}Ez{\cdot}E_2)_0$=1.0 × 10^{-8}. (d) A_0=3.0, $E_{1,0}$=1.0 × 10^{-2}, $E_{2,0}$=3.0 × 10^2, Ez_0=9.8 × 10^{-7}, $(E_1{\cdot}Ez)_0$=1.0 × 10^{-8}, Ez^*_0=3.3 × 10^{-11}, $(Ez^*E_2)_0$=1.0 × 10^{-8}. (e) A_0=3.0, $E_{1,0}$=1.0 × 10^{-2}, $E_{2,0}$=3.0 × 10^2, Ez_0=3.3 × 10^{-11}, $(Ez^*E_1)_0$=1.0 × 10^{-8}, Ez^*_0 = 9.8 × 10^{-7}, $(EzE_2)_0$=1.0 × 10^{-8}.

https://doi.org/10.1371/journal.pone.0262371.g028

or

$$j_5 = \frac{k_5 k_{17}}{k_{17} + A_{set}} = k_7(Ez^*E_1) = k_6 \tag{86}$$

determine the enzyme species concentration profiles when E_1 or E_2 bind first to *Ez*, respectively (see Fig 27). In both cases the set-point is

$$k_6 = \frac{k_5 k_{17}}{(k_{17} + A_{ss})} \quad \Rightarrow \quad A_{ss} = A_{set} = \frac{k_{17}(k_5 - k_6)}{k_6} \tag{87}$$

Fig 28 illustrates the concentration profiles of the enzyme species when all five mechanisms show the same homeostatic behavior in *A* as in Fig 25c with identical changes in E_1 and E_2.

As an example, in the ping-pong mechanisms the role of the ternary-complex $E_1{\cdot}Ez{\cdot}E_2$ (Fig 28a–28c, outlined in green) is replaced by Ez^*E_2 (Fig 28d, E_1 binding first to *Ez*) or by Ez^*E_1 (Fig 28e, E_2 binding first to *Ez*) as implied by Eqs 56, 85 and 86. Likewise, the steady state concentrations of the other enzyme species can be derived from the above rate equations (see the King-Altman expressions in the S1 Text), but are not further elaborated here.

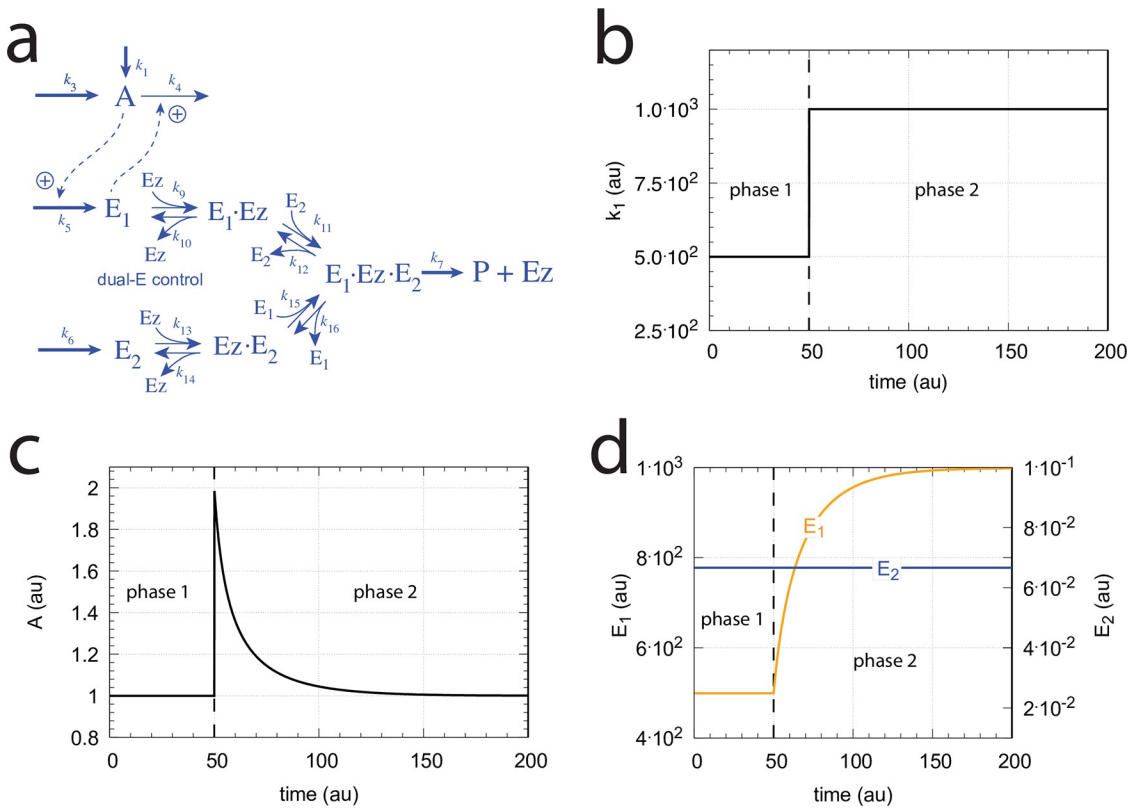

Fig 29. Example of m5 feedback loop where E_1 and E_2 are removed by a random-order ternary-complex mechanism which works under dual-E control. (a) Reaction scheme. (b) Step-wise change of k_1 from 500.0 to 1000.0 at time $t = 50$. (c) In dual-E mode the set-point is $A_{set}=k_6/k_5$ (= 1.0) which is defended. The panel shows the response of A with respect to the step-wise change of k_1 in panel (a). (d) Change of E_1 and E_2 in response to the step-wise change of k_1 in panel (a). Rate constants: k_1=500.0 (phase 1), k_1=1000.0 (phase 2), k_2=1.0, k_3=0.0, k_4=1.0, k_5=40.0, k_6=40.0 $k_7=1\times10^8$, $k_9=k_{11}=k_{13}=k_{15}=1\times10^9$, $k_{10}=k_{12}=k_{14}=k_{16}=1\times10^3$. Initial concentrations: A_0=1.0, $E_{1,0}$=499.0, $E_{2,0}=6.67\times10^{-2}$, $Ez_0=8.02\times10^{-11}$, $(E_1{\cdot}Ez)_0=5.99\times10^{-7}$, $(E_1{\cdot}Ez{\cdot}E_2)_0=4.0\times10^{-7}$, $(EzE_2)_0=1.15\times10^{-14}$.

https://doi.org/10.1371/journal.pone.0262371.g029

Controllers based on motif 5

As indicated in Fig 2, motif m5 is an outflow controller [6] and opposes inflow perturbations on the controlled variable A. Like the m2 controller the dual-E (antithetic) version of m5 has an "inner-loop" signaling (Fig 3).

Motif 5 dual-E controller removing E_1 and E_2 by a random-order ternary-complex mechanism. Fig 29a shows the reaction scheme when in a m5 controller configuration E_1 and E_2 are removed by an enzymatic random-order ternary-complex mechanism.

The rate equations are:

$$\dot{A} = k_1 - k_4 \cdot E_1 \cdot A + k_3 \tag{88}$$

$$\dot{E_1} = k_5 \cdot A - k_9(E_1)(Ez) + k_{10}(E_1 \cdot Ez) - k_{15}(Ez \cdot E_2)(E_1) + k_{16}(E_1 \cdot Ez \cdot E_2) \tag{89}$$

$$\dot{E_2} = k_6 - k_{11}(E_1 \cdot Ez)(E_2) + k_{12}(E_1 \cdot Ez \cdot E_2) - k_{13}(E_2)(Ez) + k_{14}(Ez \cdot E_2) \tag{90}$$

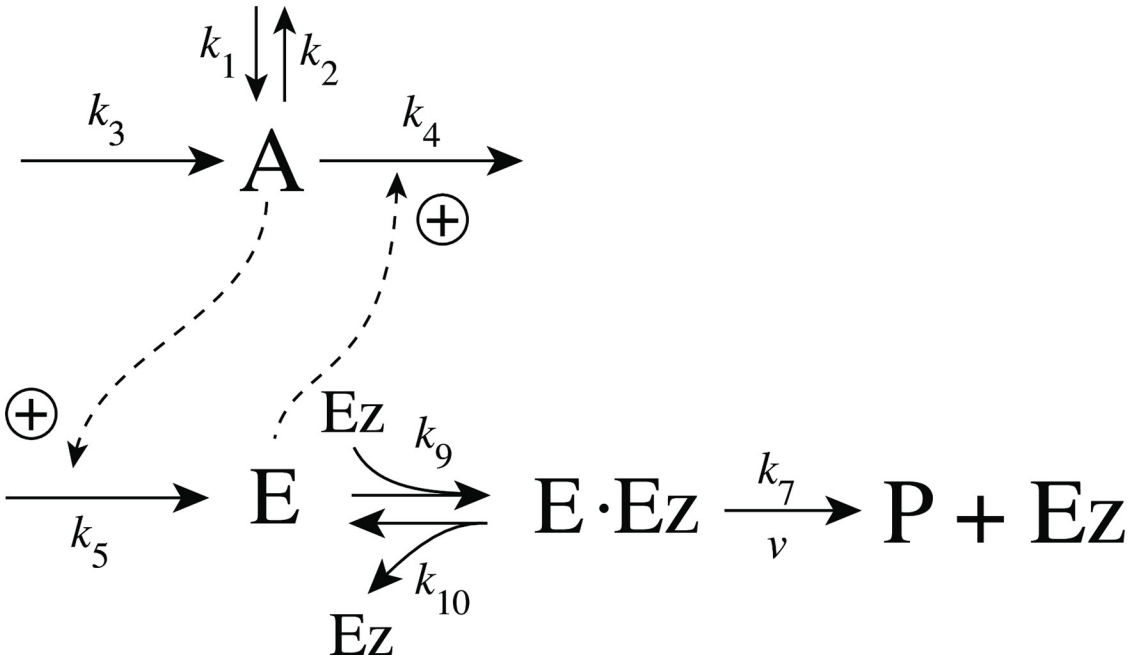

Fig 30. Reaction scheme of the catalyzed single-E m5-type of controller.

https://doi.org/10.1371/journal.pone.0262371.g030

$$\dot{Ez} = -k_9(E_1)(Ez) + k_{10}(E_1 \cdot Ez) - k_{13}(E_2)(Ez) + k_{14}(Ez \cdot E_2) + k_7(E_1 \cdot Ez \cdot E_2) \tag{91}$$

$$\frac{d(E_1 \cdot Ez)}{dt} = k_9(E_1)(Ez) - k_{10}(E_1 \cdot Ez) - k_{11}(E_1 \cdot Ez)(E_2) + k_{12}(E_1 \cdot Ez \cdot E_2) \tag{92}$$

$$\frac{d(E_1 \cdot Ez \cdot E_2)}{dt} = k_{11}(E_1 \cdot Ez)(E_2) + k_{15}(Ez \cdot E_2)(E_1) - (k_7 + k_{12} + k_{16})(E_1 \cdot Ez \cdot E_2) \tag{93}$$

$$\frac{d(Ez \cdot E_2)}{dt} = k_{13}(E_2)(Ez) - k_{14}(Ez \cdot E_2) - k_{15}(Ez \cdot E_2)(E_1) + k_{16}(E_1 \cdot Ez \cdot E_2) \tag{94}$$

The corresponding single-E controller is shown in Fig 30
with the corresponding rate equations:

$$\dot{A} = k_1 + k_3 - k_2 \cdot A - k_4 \cdot E \tag{95}$$

$$\dot{E} = k_5 \cdot A - k_9(E)(Ez) + k_{10}(E \cdot Ez) \tag{96}$$

$$\dot{Ez} = -k_9(E)(Ez) + k_{10}(E \cdot Ez) + k_7(E \cdot Ez) \tag{97}$$

$$\frac{d(E \cdot Ez)}{dt} = k_9(E)(Ez) - k_{10}(E \cdot Ez) - k_7(E \cdot Ez) \tag{98}$$

The single-E feedback loop in Fig 30 shows robust homeostatic control when enzyme Ez works under zero-order conditions, i.e., $K_M=(k_{10} + k_7)/k_9$ is low and $k_9 \gg k_{10} + k_7$. In this case

the set-point for A is given by the condition

$$k_5 \cdot A_{set} = k_7 \cdot Ez_{tot} \quad \Rightarrow \quad A_{set} = \frac{k_7 \cdot Ez_{tot}}{k_5} \tag{99}$$

For the dual-E m5 controller (Fig 29a) robust homeostasis in A is obtained by the condition

$$k_5 \cdot A_{set} = k_7(E_1 \cdot Ez \cdot E_2) = k_6 \quad \Rightarrow \quad A_{set} = \frac{k_6}{k_5} \tag{100}$$

Fig 29b–29d show the controller's behavior upon a step-wise change in k_1 when working in dual-E mode, i.e., when the homeostatic set-point for A is given by Eq 100.

A switch from dual-E to single-E control mode occurs when k_6 becomes larger than $k_7 Ez_{tot}$. For large k_9/k_{10}, k_{11}/k_{12}, k_{13}/k_{14}, and k_{15}/k_{16} ratios A_{set} of the single-E controller is given by the condition

$$k_5 \cdot A_{ss} = k_5 \cdot A_{set} = k_7(E_1 \cdot Ez \cdot E_2) = k_7 \cdot Ez_{tot} \tag{101}$$

Fig 31 gives an example, where k_6 has been increased to 200.0, while the other rate constant values are as in Fig 29. Fig 31a shows the operative part of the single-E controller outlined in red. The grayed part does not participate in the control of A, but shows a steady increase of E_2

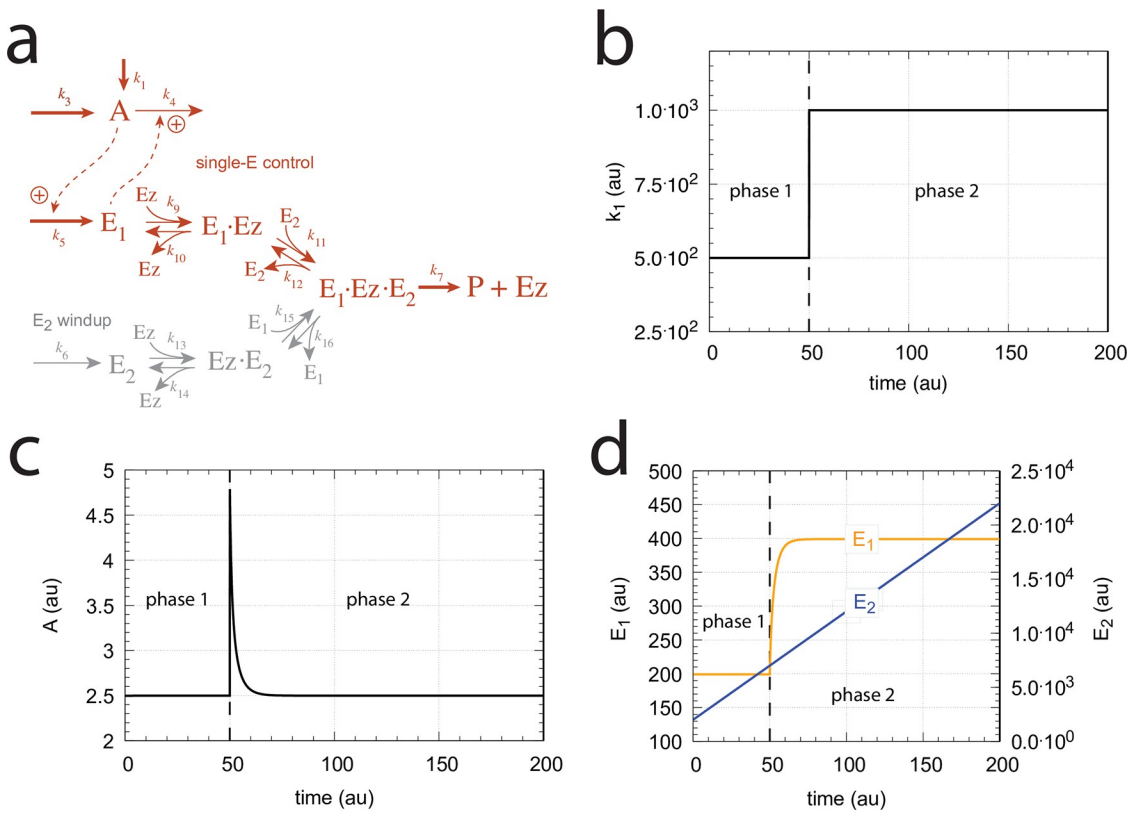

Fig 31. Example of the m5 feedback loop with E_1 and E_2 being removed by a random-order ternary-complex mechanism working in single-E control mode. (a) Scheme outlined in red shows part of the network participating in the control of A. (b) Step-wise change of k_1 from 500.0 to 1000.0 at time $t = 50.0$. (c) Homeostatic response of A, i.e. the controller defends its set-point (=2.5) defined by Eq 99. (d) Change of E_1 and wind-up of E_2. Rate constants as in Fig 29, except that k_6=200. Initial concentrations: A_0=2.5, $E_{1,0}$=199.2, $E_{2,0}$=2.0 × 10^3, Ez_0=4.54 × 10^{-11}, $(E_1 \cdot Ez)_0$=4.51 × 10^{-12}, $(E_1 \cdot Ez \cdot E_2)_0$=9.995 × 10^{-7}, $(EzE_2)_0$=4.56 × 10^{-10}.

https://doi.org/10.1371/journal.pone.0262371.g031

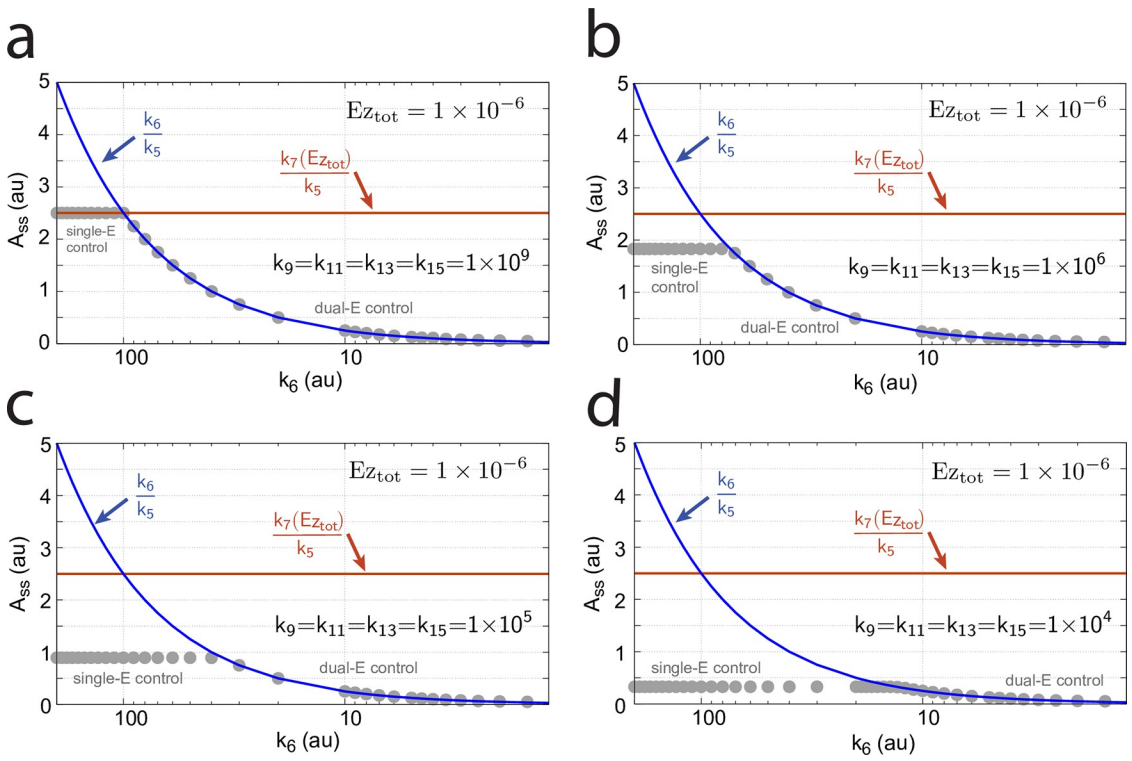

Fig 32. Switching between single-E control (Fig 31) and dual-E control (Fig 29) as a function of k_6 for different values of k_9, k_{11}, k_{13}, and k_{15}. Panel (a): high value (1×10^9) of k_9, k_{11}, k_{13}, and k_{15}. The dual-E controller shows its maximum operational range. In this case the switch occurs when $k_6 > k_7 Ez_{tot}$. Panels (b)-(d): for the lower values of k_9, k_{11}, k_{13}, and k_{15} (indicated inside the figure) the ternary-complex concentration ($E_1 \cdot Ez \cdot E_2$) is lower than Ez_{tot} and the switch occurs at lower k_6 values, which leads to a decreased operational range of the dual-E controller. Due to the lower ($E_1 \cdot Ez \cdot E_2$) concentration the single-E control mode (which occurs analogous to the red-outlined part in Fig 9e) shows an offset below $k_7 Ez_{tot}/k_5$. Note however, that A_{ss} will depend on the perturbation k_1 and move towards A_{set} with increasing k_1, thereby reducing the single-E controller's offset. Other rate constants: k_1=500.0, k_2=1.0, k_3=0.0, k_4=1.0, k_5=40.0, $k_7 = 1 \times 10^8$, $k_{10}=k_{12}=k_{14}=k_{16}=1 \times 10^3$. Initial concentrations: A_0=2.0, $E_{1,0}=5.49 \times 10^{-2}$, $E_{2,0}=5.21 \times 10^3$, $Ez_0=7.4 \times 10^{-14}$, $(E_1 \cdot Ez)_0=9.09 \times 10^{-8}$, $(E_1 \cdot Ez \cdot E_2)_0=9.09 \times 10^{-7}$, $(EzE_2)_0=1.66 \times 10^{-10}$.

https://doi.org/10.1371/journal.pone.0262371.g032

(wind-up). The controller is subject to the same step-wise increase as in k_1 (panel b) as in Fig 29, but has now changed its set-point to 2.5 as described by Eq 99 (panel c). Fig 31d shows the wind-up behavior of E_2 along with the change of E_1, which activates the compensatory flux removing A and compensating for the increasing inflow of A by k_1.

At low k_9/k_{10}, k_{11}/k_{12}, k_{13}/k_{14}, and, k_{15}/k_{16} ratios the operational range of the dual-E controller decreases and the single-E controller's steady state in A drops below A_{set}. Under these conditions the dual-E controller will defend its set-point $A_{set} = k_6/k_5$ exactly, while the single-E controller shows an offset, i.e. $A_{ss} < A_{set} = k_7 \cdot Ez_{tot}/k_5$. Fig 32 illustrates this behavior when the total enzyme concentration is kept constant at 1×10^{-6}.

When Ez_{tot} increases the operational range of the dual-E controller increases as a function of k_6. This is shown in Fig 33 when $k_9=k_{11}=k_{13}=k_{15}=1 \times 10^9$ and Ez_{tot} varies from 1×10^{-6} to 4×10^{-5}. In agreement with Eq 99 we observe that with changing Ez_{tot} the set-point of the single-E controller changes accordingly.

Transition from single-E to dual-E control and critical slowing down. In the previous section we saw that dual-E control occurs in the m5 random-order ternary-complex mechanism when the condition $k_6 < k_7 Ez_{tot}$ is met. In this case, both E_1 and E_2 are engaged in the control of A. On the other hand, single-E control is observed when $k_6 > k_7 Ez_{tot}$. Here, only E_1

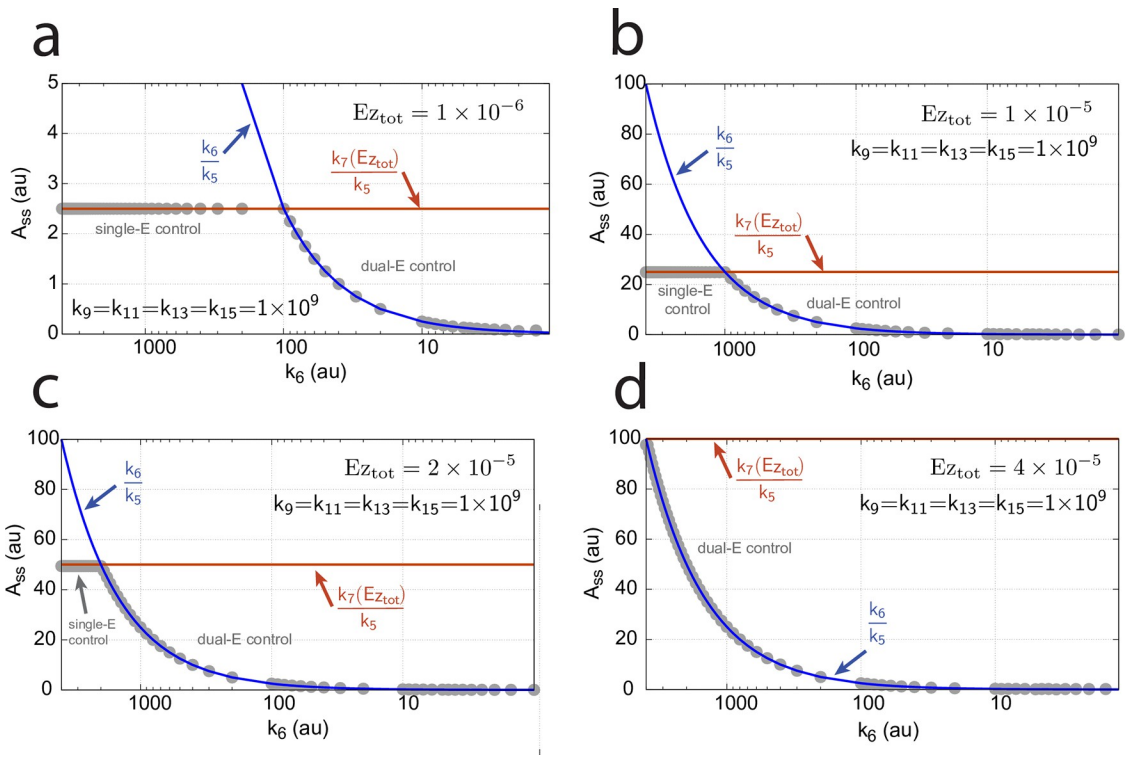

Fig 33. Switching between dual-E and single-E control in the random-order ternary-complex m5 controller at different Ez_{tot} concentrations. Rate constants are as in Fig 32a with Ez_{tot} values as indicated in the four panels. With increasing Ez_{tot} values (from panel (a) to panel (d)) the operational range of the dual-E controller increases together with increasing set-point values of the single-E controller (Eq 99). Initial concentrations, panel (a): A_0=2.0, $E_{1,0}$=5.49 × 10^{-2}, $E_{2,0}$=5.21 × 10^3, Ez_0=7.4 × 10^{-14}, $(E_1{\cdot}Ez)_0$=9.09 × 10^{-8}, $(E_1{\cdot}Ez{\cdot}E_2)_0$=9.09 × 10^{-7}, $(EzE_2)_0$=1.66 × 10^{-10}. Initial concentrations panel (b): A_0=2.5, $E_{1,0}$=5.49, $E_{2,0}$=5.21 × 10^1, Ez_0=1.18 × 10^{-12}, $(E_1{\cdot}Ez)_0$=9.96 × 10^{-6}, $(E_1{\cdot}Ez{\cdot}E_2)_0$=4.5 × 10^{-8}, $(EzE_2)_0$=1.19 × 10^{-17}. Initial concentrations panel (c): A_0=2.5, $E_{1,0}$=5.49, $E_{2,0}$=5.21 × 10^1, Ez_0=1.21 × 10^{-12}, $(E_1{\cdot}Ez)_0$=1.995 × 10^{-5}, $(E_1{\cdot}Ez{\cdot}E_2)_0$=4.5 × 10^{-8}, $(EzE_2)_0$=1.21 × 10^{-17}. Initial concentrations panel (d): A_0=97.63, $E_{1,0}$=4.12, $E_{2,0}$=9.87 × 10^3, Ez_0=3.95 × 10^{-10}, $(E_1{\cdot}Ez)_0$=1.66 × 10^{-13}, $(E_1{\cdot}Ez{\cdot}E_2)_0$=3.905 × 10^{-5}, $(EzE_2)_0$=9.47 × 10^{-7}.

https://doi.org/10.1371/journal.pone.0262371.g033

acts as the controller variable while E_2 shows wind-up. i.e., increases continuously. However, even when the condition for dual-E control is fulfilled, i.e., $k_6 < k_7 Ez_{tot}$, single-E control can be temporarily present, as observed for the m2 controller (Fig 14), when the initial concentration of E_2 is above its steady state value for a given perturbation value of k_1. In this case, the single-E controller is *metastable*: E_2 will decrease and approach its steady state, but during this period the set-point of the single-E controller will be defended when working under zero-order conditions. Fig 34a–34c illustrates the behavior. In this example E_2 concentration starts out high at 9.5 × 10^4, while its steady state value is 6.7 × 10^{-2}. At time t = 100 k_1 is changed from 500.0 to 1000.0 (Fig 34a) and the set-point of A for the single-E controller (=2.5) is defended as long as $E_2 > E_{2,ss}$ (Fig 34b). Note that during single-E control the E_1 value is responsible for keeping A at its set-point, but the E_1 level changes once E_2 is at its steady state and the controller has reached dual-E control mode (Fig 34b and 34c).

We have further tested how the transition time T depends on k_6 for this controller at constant k_1 (for a definition of T see Fig 14a). As for the m2 controller (Fig 14b) T increases with increasing k_6 values. For each value of k_6 it takes T time units until A settles at the set-point of the dual-E controller (=k_6/k_5). $T \rightarrow \infty$ as k_6 approaches 100.0, the value at which the set-point of the dual-E controller approaches the set-point of the single-E controller.

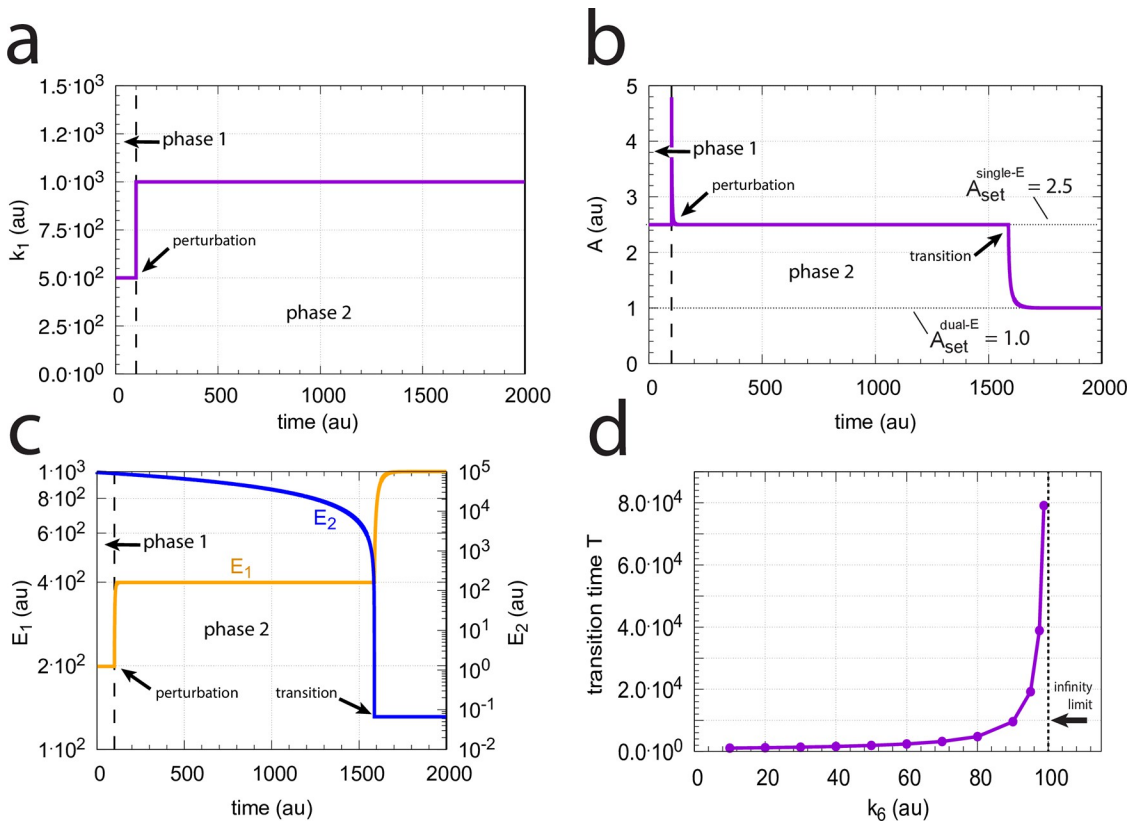

Fig 34. Metastable single-E controller and critical slowing down in the autonomous transition from single-E to dual-E control mode. (a) Step-wise change of k_1 at t = 100.0 from 500.0 (phase 1) to 1000.0 (phase 2). (b) Metastable single-E control mode. The single-E controller defends its set-point (=2.5), but transition to dual-E control mode (indicated by arrow) occurs at approximately 1600 time units when E_2 reaches its steady state. (c) The metastable single-E control mode is operative as long as E_2 is above its steady state value. The transition from single-E to dual-E control mode occurs when E_2 has reached its steady state (indicated by arrow). Rate constants: k_1=500.0 (phase 1), k_1=1000.0 (phase 2), k_2=1.0, k_3=0.0, k_4=1.0, k_5=40.0, k_6=40.0 k_7=1 × 10^8, k_9=k_{11}=k_{13}=k_{15}=1 × 10^9, k_{10}=k_{12}=k_{14}=k_{16}=1 × 10^3. Initial concentrations: A_0=2.5, $E_{1,0}$=199.1, $E_{2,0}$=9.52 × 10^4, Ez_0=1.08 × 10^{-12}, $(E_1{\cdot}Ez)_0$=2.37 × 10^{-15}, $(E_1{\cdot}Ez{\cdot}E_2)_0$=9.995 × 10^{-7}, $(EzE_2)_0$=5.01 × 10^{-10}. (d) Transition time T as a function of k_6. k_1=500.0; all other rate constants and initial concentrations as for (a)-(c).

https://doi.org/10.1371/journal.pone.0262371.g034

Motif 5 dual-E controller removing E_1 and E_2 by a compulsory-order ternary-complex mechanism with E_1 binding first to *Ez*. The scheme of this mechanism is shown in Fig 35.

The rate equations are:

$$\dot{A} = k_1 + k_3 - k_4 \cdot (E_1) \cdot (A) - k_2 A \tag{102}$$

$$\dot{E_1} = k_5 A - k_9 (E_1)(Ez) + k_{10} (E_1 \cdot Ez) \tag{103}$$

$$\dot{E_2} = k_6 - k_{11} (E_1 \cdot Ez)(E_2) + k_{12} (E_1 \cdot Ez \cdot E_2) \tag{104}$$

$$\dot{Ez} = -k_9 (E_1)(Ez) + k_{10} (E_1 \cdot Ez) + k_7 (E_1 \cdot Ez \cdot E_2) \tag{105}$$

$$\frac{d(E_1 \cdot Ez)}{dt} = k_9 (E_1)(Ez) - k_{10} (E_1 \cdot Ez) - k_{11} (E_1 \cdot Ez)(E_2) + k_{12} (E_1 \cdot Ez \cdot E_2) \tag{106}$$

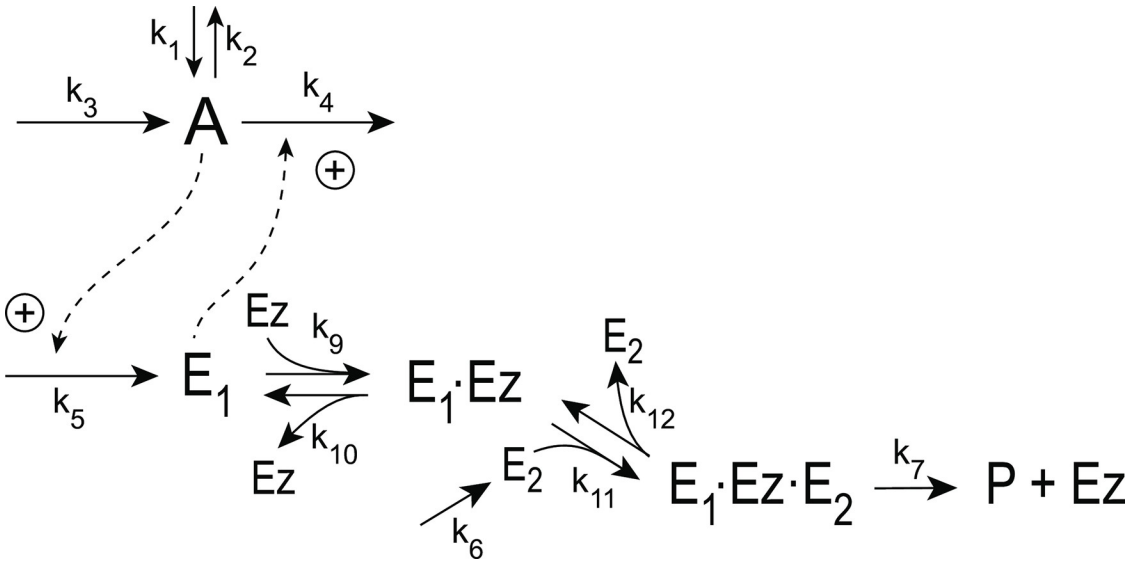

Fig 35. Scheme of the m5 controller when E_1 and E_2 are removed by a compulsory ternary-complex mechanism with E_1 binding first to the free enzyme *Ez*.

https://doi.org/10.1371/journal.pone.0262371.g035

$$\frac{d(E_1 \cdot Ez \cdot E_2)}{dt} = k_{11}(E_1 \cdot Ez)(E_2) - (k_7 + k_{12})(E_1 \cdot Ez \cdot E_2) \tag{107}$$

The reaction velocity producing P and recycling Ez is:

$$\dot{P} = v = k_7(E_1 \cdot Ez \cdot E_2) \tag{108}$$

The conditions for the set-point of the dual-E controller for this mechanism are the same as for the random-order ternary-complex case (Eq 100), i.e.

$$k_5 \cdot A_{set} = k_7(E_1 \cdot Ez \cdot E_2) = k_6 \quad \Rightarrow \quad A_{set} = \frac{k_6}{k_5} \tag{109}$$

As shown for the random-order ternary-complex case (Eq 100), also for this compulsory ternary-complex mechanism dual-E control requires that

$$k_6 \leq k_7 \cdot Ez_{tot} \tag{110}$$

In case $k_6 > k_7 \cdot Ez_{tot}$ the feedback switches to single-E control, with E_2 showing wind-up. The set-point switching and E_2 wind-up is illustrated in Fig 36. There, during phase 1, A is under dual-E control with set-point of 1.0, where k_5=k_6=40.0 at perturbation k_1=1000.0 (Fig 36a). At the beginning of phase 2 k_6 is increased to 200.0, which leads to a change in the set-point of A to 2.5 (=$k_7 \cdot Ez_{tot}/k_5$, analogous to Eq 99, Fig 36b) and to wind-up of E_2 (Fig 36c). In phase 3 k_1 is increased to 2000.0 showing that the single-E controller defends its set-point. During single-E control the E_1Ez enzyme species rapidly depletes (Fig 36d) and the concentration of the ternary-complex $E_1 \cdot Ez \cdot E_2$ becomes practically equal to the total enzyme concentration Ez_{tot}.

Fig 37 shows the switching between dual-E and single-E control as a function of k_6 at four different total enzyme concentrations. Clearly, as previously observed for the other

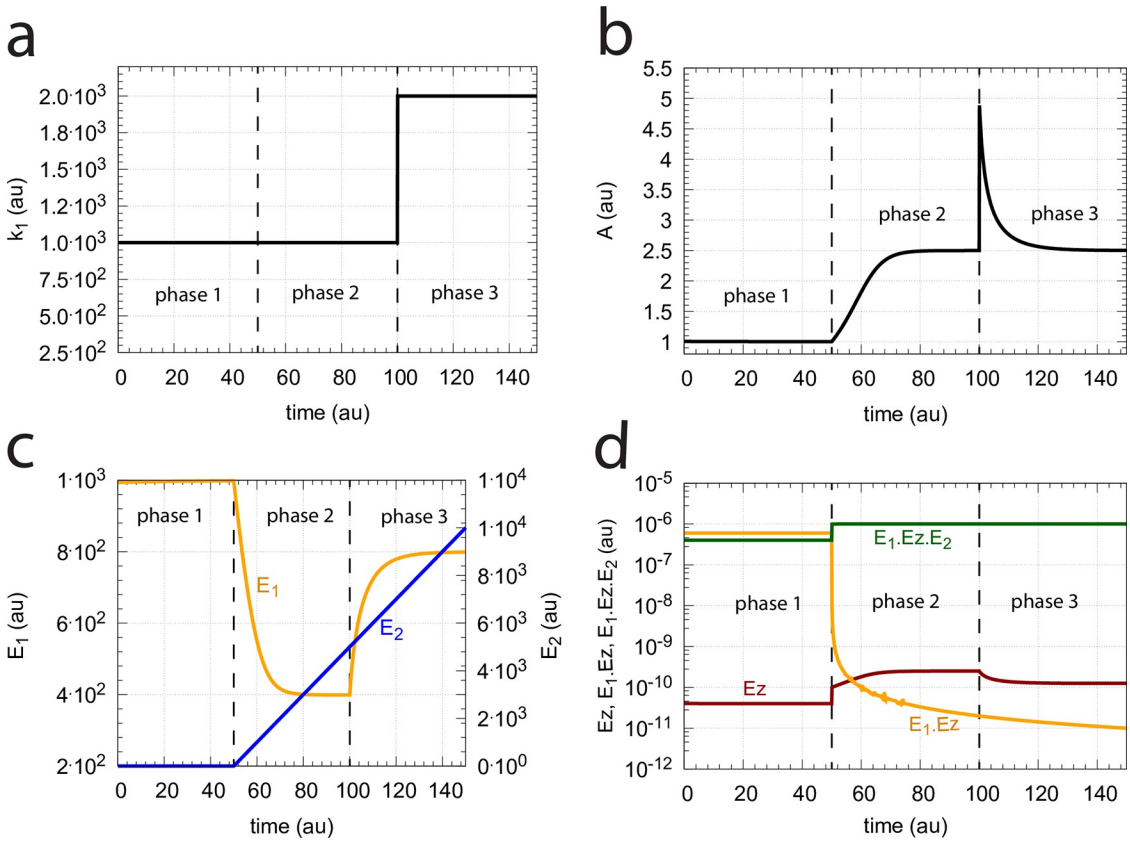

Fig 36. Switch from dual-E control to single-E in the compulsory ternary-complex mechanism of motif 5 when E_1 binds first to free *Ez* (Fig 35). (a) Perturbation k_1 as a function of time. (b) Change of the controlled variable A's concentration as a function of time. Phase 1: dual-E control; phases 2 and 3: single-E control. (c) Concentration of E_1 and E_2 as a function of time. (d) Concentration of the enzymatic species Ez, $E_1{\cdot}Ez$, and $E_1{\cdot}Ez{\cdot}E_2$ as a function of time. Rate constants: k_1=1000.0 (phases 1 and 2), k_1=2000.0 (phase 3), k_2=1.0, k_3=0.0, k_4=1.0, k_5=40.0, k_6=40.0 (phase 1), k_6=200.0 (phases 2 and 3) $k_7=1\times10^8$, $k_9=k_{11}=1\times10^9$, $k_{10}=k_{12}=1\times10^3$. Initial concentrations: A_0=1.0, $E_{1,0}$=993.4, $E_{2,0}=6.67\times10^{-2}$, $Ez_0=4.02\times10^{-11}$, $(E_1{\cdot}Ez)_0=5.999\times10^{-7}$, and $(E_1{\cdot}Ez{\cdot}E_2)_0=4.00\times10^{-7}$.

https://doi.org/10.1371/journal.pone.0262371.g036

mechanisms, an increase in the enzyme concentration leads to an extended range upon which the dual-E controller is able to act. In addition, the k_6 switch-point for the transition to dual-E control occurs at higher values as total enzyme concentration increases. The set-point for the single-E controller increases accordingly.

The velocity how fast P is produced by this mechanism can be expressed analytically using the King-Altman method [25]. The King-Altman treatment leads to

$$v = \dot{P} = \frac{k_7 \cdot Ez_{tot}}{1 + \frac{k_7}{k_{11}E_2} + \frac{k_{12}}{k_{11}E_2} + \frac{k_7}{k_9E_1} + \frac{k_{10}(k_{12}+k_7)}{k_9k_{11}} \cdot \frac{1}{(E_1)(E_2)}} \tag{111}$$

Eq 111 shows that when k_9 and k_{11} are much larger than k_7, k_{10}, and k_{12} the velocity becomes zero-order with respect to E_1 and E_2 such that $v = k_7Ez_{tot}$.

However, when k_9 and k_{11} become equal or lower than k_7, k_{10}, and k_{12} the zero-order condition with respect to E_1 and E_2 does no longer hold. In such a case, and when the mechanism shows single-E control, the wind-up of E_2 makes the E_2 terms in Eq 111 disappear, such that at

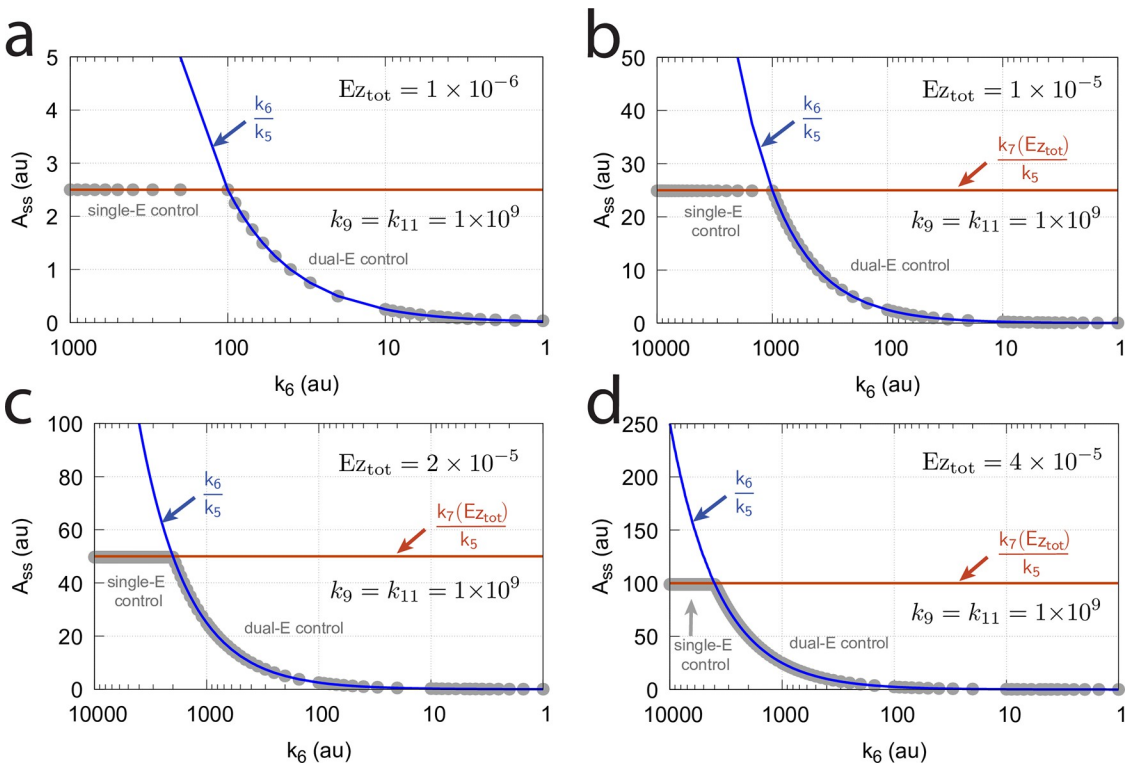

Fig 37. Switch between dual-E and single-E control in the m5 compulsory-order ternary-complex mechanisms (E_1 binding first to Ez) as a function of k_6 and total enzyme concentration Ez_{tot}. (a) $Ez_{tot}=1 \times 10^{-6}$. (b) $Ez_{tot}=1 \times 10^{-5}$; (c) $Ez_{tot}=2 \times 10^{-5}$; (d) $Ez_{tot}=4 \times 10^{-5}$. Set-points for dual-E and single-E control are indicated in blue and red, respectively. Numerical values are shown as gray filled dots. Rate constants: k_1=1000.0, k_2=1.0, k_3=0.0, k_4=1.0, k_5=40.0, k_6 variable, $k_7=1 \times 10^8$, $k_9=k_{11}=1 \times 10^9$, $k_{10}=k_{12}=1 \times 10^3$. Initial concentrations: A_0=1.0, $E_{1,0}$=993.4, $E_{2,0}=6.67 \times 10^{-2}$ Panel (a): $Ez_0=1 \times 10^{-6}$, $(E_1{\cdot}Ez)_0$=0, and $(E_1{\cdot}Ez{\cdot}E_2)_0$=0. Panel (b): $Ez_0=1 \times 10^{-5}$, $(E_1{\cdot}Ez)_0$=0, and $(E_1{\cdot}Ez{\cdot}E_2)_0$=0. Panel (c): $Ez_0=2 \times 10^{-5}$, $(E_1{\cdot}Ez)_0$=0, and $(E_1{\cdot}Ez{\cdot}E_2)_0$=0. Panel (d): $Ez_0=4 \times 10^{-5}$, $(E_1{\cdot}Ez)_0$=0, and $(E_1{\cdot}Ez{\cdot}E_2)_0$=0. A_{ss} values were taken after a simulation time of 20000 time units.

https://doi.org/10.1371/journal.pone.0262371.g037

steady state, we have

$$v = \frac{k_7 \cdot Ez_{tot}}{1 + \frac{k_7}{k_9 E_1}} \tag{112}$$

The condition $k_5{\cdot}A_{ss} = v$ defines the steady-state of A at single-E (single-E) control, i.e.

$$A_{ss}^{single-E} = \frac{k_7 \cdot Ez_{tot}}{k_5} \cdot \frac{E_1}{\left(\frac{k_7}{k_9}\right) + E_1} \tag{113}$$

The influence of decreased k_9 and k_{11} values in this mechanism is shown in Fig 38. At single-E control, Eq 113 shows excellent agreement with the numerical steady-state values of A.

Note, however, that A_{ss} will depend on the perturbation k_1. With increasing k_1 values (at single-E control) E_1 will increase such that

$$\frac{E_1}{\left(\frac{k_7}{k_9}\right) + E_1} \rightarrow 1 \tag{114}$$

and $A_{ss}^{single-E}$ (Eq 113) will move towards the A_{set} value at zero-order conditions.

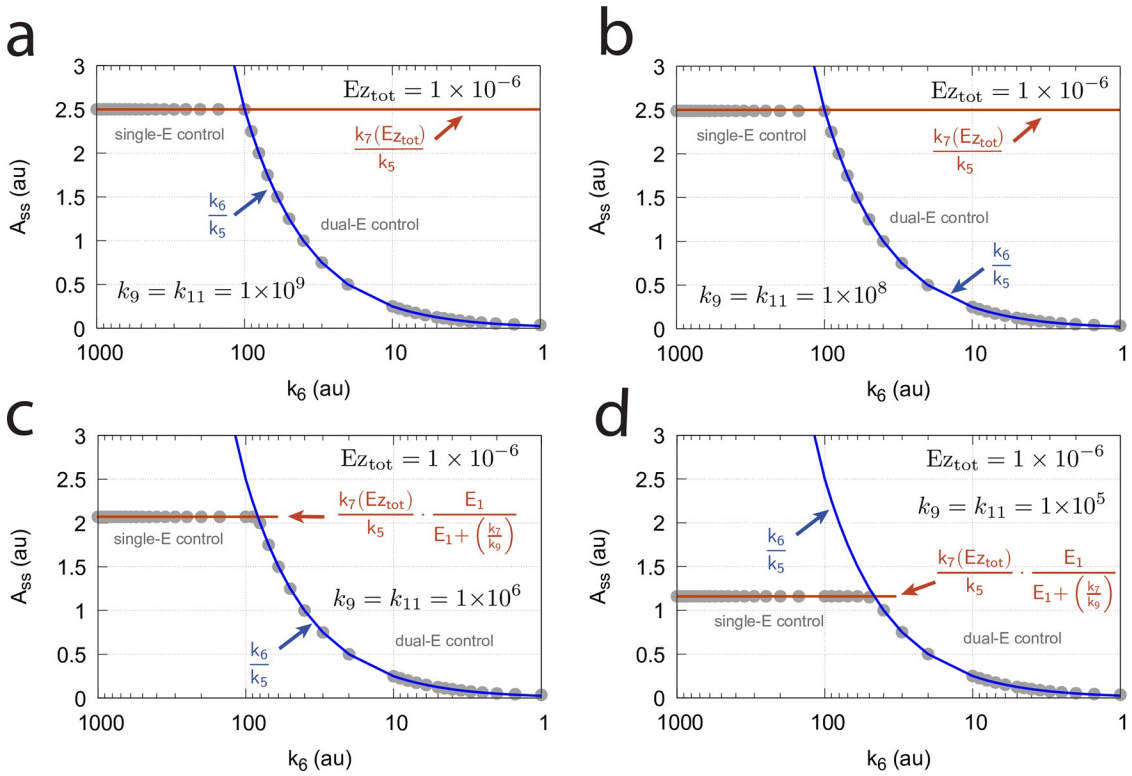

Fig 38. Switch between dual-E and single-E control in the m5 compulsory-order ternary-complex mechanisms (E_1 binding first to Ez) as a function of k_6, k_9, and k_{11}. The total enzyme concentration is 1×10^{-6} and constant. (a) k_9=k_{11}=1×10^9. A_{set} of the single-E controller is 2.5=$k_7 \cdot Ez_{tot}/k_5$. (b) k_9=k_{11}=1×10^8. Also in this case A_{set} of the single-E controller is still close to 2.5. (c) k_9=k_{11}=1×10^6. v ($\dot{P}$) is no longer zero-order but is described by Eq 112, and A_{ss} of the single-E controller is described by Eq 113 with E_1=4.82×10^2 and $A_{ss}^{single-E}$=2.07. (d) k_9=k_{11}=1×10^5. At single-E control conditions we have E_1=4.82×10^2 and $A_{ss}^{single-E}$=1.16 (Eq 113). Other rate constant values and initial concentrations as for Fig 37a.

https://doi.org/10.1371/journal.pone.0262371.g038

Fig 39 shows that increasing k_1 perturbations move A_{ss} towards the set-point of the single-E controller, as with perturbation-induced increases of the controller variable E_1 the factor $E1/((k_7/k_9)+E_1)$ in Eq 114 is getting close to 1.

Motif 5 dual-E controller removing E_1 and E_2 by a compulsory-order ternary-complex mechanism with E_2 binding first to Ez. The scheme of this mechanism is shown in Fig 40.

The rate equations are:

$$\dot{A} = k_1 - k_4 \cdot E_1 \cdot A + k_3 - k_2 \cdot A \tag{115}$$

$$\dot{E_1} = k_5 \cdot A - k_{15}(Ez \cdot E_2)(E_1) + k_{16}(E_1 \cdot Ez \cdot E_2) \tag{116}$$

$$\dot{E_2} = k_6 - k_{13}(E_2)(Ez) + k_{14}(Ez \cdot E_2) \tag{117}$$

$$\dot{Ez} = -k_{13}(E_2)(Ez) + k_{14}(Ez \cdot E_2) + k_7(E_1 \cdot Ez \cdot E_2) \tag{118}$$

$$\frac{d(E_1 \cdot Ez \cdot E_2)}{dt} = k_{15}(Ez \cdot E_2)(E_1) - (k_7 + k_{16})(E_1 \cdot Ez \cdot E_2) \tag{119}$$

$$\frac{d(Ez \cdot E_2)}{dt} = k_{13}(E_2)(Ez) - k_{14}(Ez \cdot E_2) - k_{15}(Ez \cdot E_2)(E_1) + k_{16}(E_1 \cdot Ez \cdot E_2) \tag{120}$$

The set-points for dual-E and single-E control are as described in the previous section for the m5-compulsory-order ternary-complex mechanism when E_1 binds first (Eq 41), i.e., $A_{set}^{dual-E}=k_6/k_5$ and $A_{set}^{single-E}=k_7Ez_{tot}/k_5$.

The velocity v how fast P is produced by this mechanism can be expressed analytically using the King-Altman steady-state method

$$v = \dot{P} = \frac{k_7 \cdot Ez_{tot}}{1 + \frac{k_7}{k_{13}E_2} + \frac{k_{16}}{k_{15}E_1} + \frac{k_7}{k_{15}E_1} + \frac{k_{14}(k_{16}+k_7)}{k_{13}k_{15}} \cdot \frac{1}{(E_1)(E_2)}} \tag{121}$$

Comparison with numerical results show that Eq 121 gives an excellent description of v as a function of E_1 and E_2. Eq 121 also shows that when k_{13} and k_{15} are much larger than k_7, k_{14}, and k_{16} v becomes zero-order with respect to E_1 and E_2 such that $v = k_7Ez_{tot}$.

This mechanism's behavior is in many respects identical to the other compulsory-order ternary-complex mechanism of Fig 35. Fig 41 shows as an example a calculation when the change from dual-E to single-E control occurs in an analogous way to that of the other m5 compulsory-order ternary-complex controller shown in Fig 36. For the same rate constant values and the same perturbation profile (Fig 41a) the behaviors of A, E_1, and E_2 are precisely the same when Fig 41b and 41c are compared with Fig 36b and 36c. Interestingly, Ez in this controller (Fig 41d) has now taken the role of $E_1 \cdot Ez$ in the other controller (Fig 36d), while the function/concentration profile of Ez in Fig 36d is identical to that of $Ez \cdot E_2$ in Fig 41d.

Fig 42 shows another example of identical behaviors between the two (compulsory-order ternary-complex) m5 controllers when the switching between dual-E and single-E control is investigated as a function of k_6 and when zero-order conditions of v with respect to E_1 and E_2 are relaxed. Under single-E control wind-up of E_2 is observed (Fig 41c) such that the

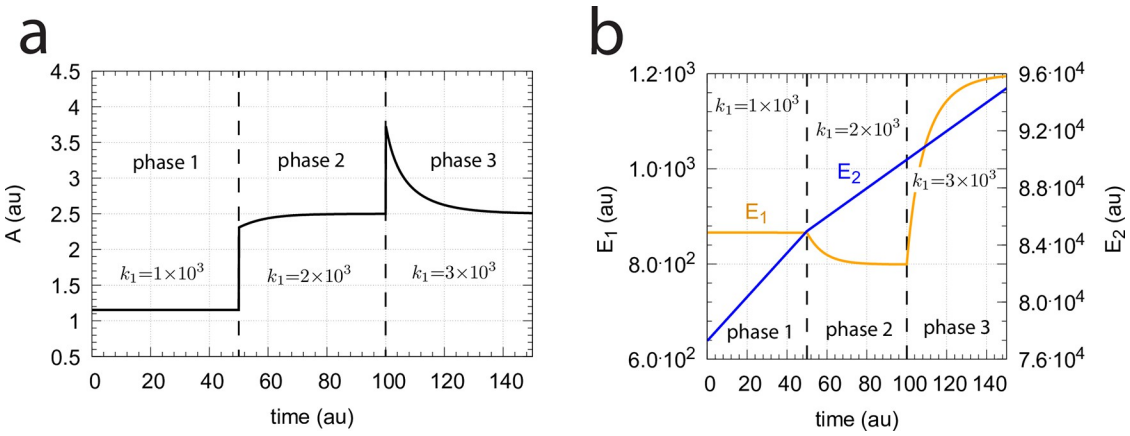

Fig 39. Under single-E control an increased perturbation k_1 moves A_{ss} in the m5 compulsory-order ternary-complex mechanisms (E_1 binding first to Ez) towards $A_{set}=k_7 \cdot Ez_{tot}/k_5$. (a) Phase 1: the system is that from Fig 38d with k_6=200 and k_1=1000.0. In phases 2 and 3 k_1 is stepwise increased to respectively 2000.0 and 3000.0. In phases 2 and 3 A is moved to $A_{set}=k_7 \cdot Ez_{tot}/k_5$=2.5. Rate constant values as in Fig 38d. (b) Corresponding changes in E_1 and E_2. Note the wind-up of E_2 and that only E_1 is the controller species. Initial concentrations: A_0=1.153, $E_{1,0}$=866.2, $E_{2,0}$=7.728 × 10^6, Ez_0=4.027 × 10^{-11}, $(E_1 \cdot Ez)_0$=5.999 × 10^{-7}, and $(E_1 \cdot Ez \cdot E_2)_0$=4.000 × 10^{-7}.

https://doi.org/10.1371/journal.pone.0262371.g039

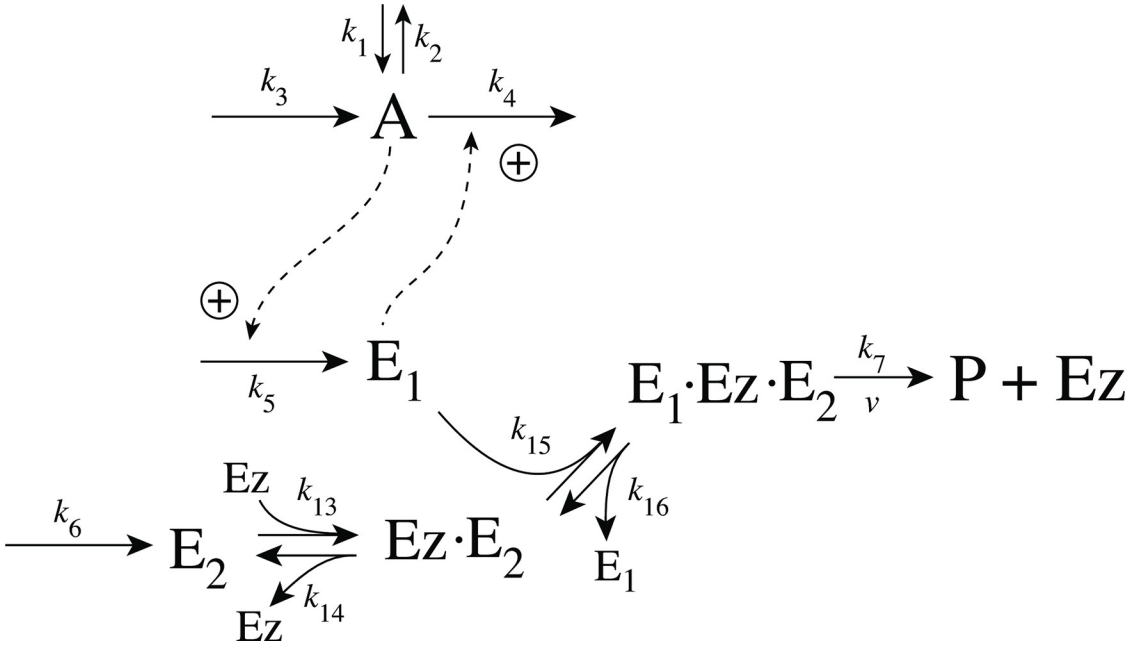

Fig 40. Scheme of the m5 controller when E_1 and E_2 are removed by a compulsory ternary-complex mechanism with E_2 binding first to Ez.

https://doi.org/10.1371/journal.pone.0262371.g040

expression of v (Eq 121) in this case is reduced to

$$v = \dot{P} = \frac{k_7 \cdot Ez_{tot}}{1 + \frac{k_7 + k_{16}}{k_{15} E_1}} = k_7 \cdot Ez_{tot} \left(\frac{E_1}{E_1 + \frac{k_7 + k_{16}}{k_{15}}} \right) \tag{122}$$

For a given perturbation k_1 the steady states in A and E_1 satisfy, under single-E control, the condition

$$v = k_7 \cdot Ez_{tot} \left(\frac{E_{1,ss}}{E_{1,ss} + \frac{k_7 + k_{16}}{k_{15}}} \right) = k_5 \cdot A_{ss} \; < \; k_6 \tag{123}$$

which results in the steady state for A:

$$A_{ss} = \frac{k_7 \cdot Ez_{tot}}{k_5} \cdot \left(\frac{E_{1,ss}}{E_{1,ss} + \frac{k_7 + k_{16}}{k_{15}}} \right) \tag{124}$$

The switch between single-E and dual-E control occurs at

$$k_6^{switch} = k_7 \cdot Ez_{tot} \left(\frac{E_{1,ss}}{E_{1,ss} + \frac{k_7 + k_{16}}{k_{15}}} \right) \tag{125}$$

where k_6^{switch} is the smallest k_6 value which is equal to v from Eq 123. In the case $k_6 < k_6^{switch}$ the controller is in dual-E control mode with $v{=}k_6{=}k_5 \cdot A_{set}^{dual-E}$.

As already addressed above in Fig 39, a typical property of m5 single-E control is that with increasing perturbation strength the controller species (E_1) increases and A_{ss} moves towards $A_{set}^{single-E}$. This is also observed for this controller, although higher k_1 values are needed here to reach $A_{set}^{single-E}$. Fig 43 shows the behavior when the Fig 42d parametrization is used with k_6=200.

Motif 5 dual-E controller removing E_1 and E_2 by a ping-pong mechanism with E_1 binding first to *Ez*. The scheme of this mechanism is shown in Fig 44.

We have included a first-order degradation term of E_2 with rate constant k_{17}. The reason for this is the observation that for this controller only E_1 acts as a control species while E_2 remains to be constant. To see the influence of E_2 on the set-point the first-order degradation of E_2 is included.

The rate equations are:

$$\dot{A} = k_1 + k_3 - k_2 \cdot A - k_4 \cdot E_1 \cdot A \tag{126}$$

$$\dot{E_1} = k_5 \cdot A - k_9(Ez)(E_1) + k_{10}(E_1 \cdot Ez) \tag{127}$$

$$\dot{E_2} = k_6 - k_{13}(Ez^*)(E_2) + k_{14}(Ez^* \cdot E_2) - k_{17} \cdot E_2 \tag{128}$$

$$\dot{Ez} = -k_9(Ez)(E_1) + k_{10}(E_1 \cdot Ez) + k_7(Ez^* \cdot E_2) \tag{129}$$

$$\frac{d(E_1 \cdot Ez)}{dt} = k_9(Ez)(E_1) - k_{10}(E_1 \cdot Ez) - k_{11}(E_1 \cdot Ez) + k_{12}Ez^* \tag{130}$$

$$\frac{d(Ez^* \cdot E_2)}{dt} = k_{13}(E_2)(Ez^*) - k_{14}(Ez^* \cdot E_2) - k_7(Ez^* \cdot E_2) \tag{131}$$

$$\dot{Ez^*} = k_{11}(E_1 \cdot Ez) - k_{12}Ez^* - k_{13}(E_2)(Ez^*) + k_{14}(Ez^* \cdot E_2) \tag{132}$$

The numerically calculated velocity v_{num} by which P is formed is calculated as

$$v_{num} = \dot{P} = k_7(Ez^* \cdot E_2) \tag{133}$$

v_{num} is in excellent agreement when $\dot{P}$ is calculated by using the steady-state approach with the help of the King-Altman method (see S1 Text).

In this case, v_{ss} is

$$v_{ss} = \frac{k_7 Ez_{tot}}{f_{ss}} \tag{134}$$

with

$$\begin{aligned} f_{ss} = {} & \frac{k_7}{k_9} \cdot \frac{1}{(E_1)} + \frac{k_7 k_{10}}{k_9 k_{11}} \cdot \frac{1}{(E_1)} + \frac{k_7 k_{10} k_{12}}{k_9 k_{11} k_{13}} \cdot \frac{1}{(E_1)(E_2)} + \frac{k_{10} k_{12} k_{14}}{k_9 k_{11} k_{13}} \cdot \frac{1}{(E_1)(E_2)} \\ & + \frac{k_7}{k_{11}} + \frac{k_7 k_{12}}{k_{11} k_{13}} \cdot \frac{1}{(E_2)} + \frac{k_{12} k_{14}}{k_{11} k_{13}} \cdot \frac{1}{(E_2)} + \frac{(k_7 + k_{14})}{k_{13}} \cdot \frac{1}{(E_2)} + 1 \end{aligned} \tag{135}$$

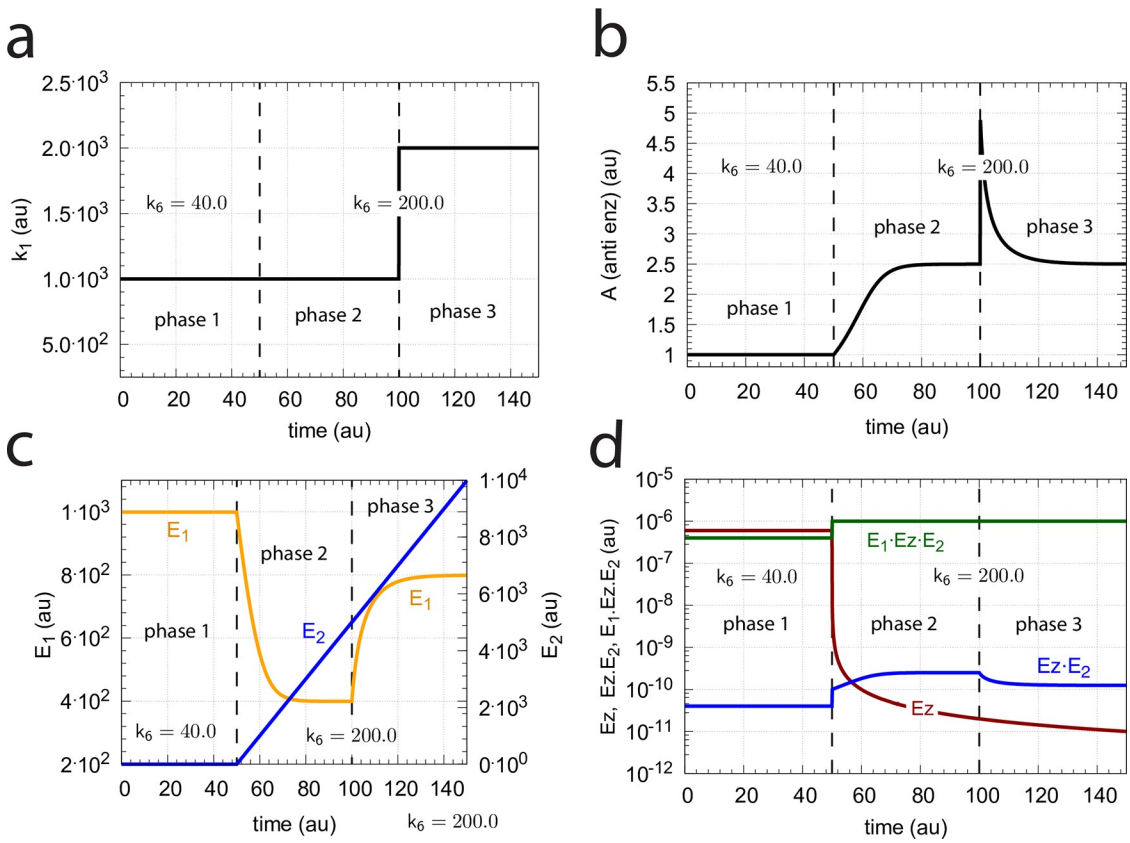

Fig 41. Switch from dual-E to single-E control by increase of k_6 in the compulsory ternary-complex mechanism of motif 5 when E_2 binds first to free Ez (Fig 40). An increase of k_1 in phase 3 shows that the set-point of A under single-E control is defended. (a) Perturbation k_1 as a function of time. (b) Change of the controlled variable A's concentration as a function of time. Phase 1: dual-E control; phases 2 and 3: single-E control. (c) Concentration of E_1 and E_2 as a function of time. (d) Concentration of the enzymatic species Ez, $Ez{\cdot}E_2$, and $E_1{\cdot}Ez{\cdot}E_2$ as a function of time. Rate constants: k_1=1000.0 (phases 1 and 2), k_1=2000.0 (phase 3), k_2=1.0, k_3=0.0, k_4=1.0, k_5=40.0, k_6=40.0 (phase 1), k_6=200.0 (phases 2 and 3) k_7=1 × 10^8, k_{13}=k_{15}=1 × 10^9, k_{14}=k_{16}=1 × 10^3. Initial concentrations: A_0=1.0, $E_{1,0}$=9.99 × 10^2, $E_{2,0}$=6.67 × 10^{-2}, Ez_0=5.999 × 10^{-7}, $(Ez{\cdot}E_2)_0$=4.004 × 10^{-11}, and $(E_1{\cdot}Ez{\cdot}E_2)_0$=4.00 × 10^{-7}.

https://doi.org/10.1371/journal.pone.0262371.g041

From the rate equation of E_2 (Eq 128) we see that the concentrations of E_2 are related to the concentrations of Ez^* and $Ez^*{\cdot}E_2$. Since Ez^* and $Ez^*{\cdot}E_2$ show constant steady-state values the concentration of E_2 is constant in time, but its value is dependent on the values of the other rate constants.

The relationship

$$k_5 \cdot A_{ss} = \dot{P} = \frac{k_7 Ez_{tot}}{f_{ss}} \tag{136}$$

determines the set-point for A, A_{set}, as

$$A_{set} = \frac{k_7 Ez_{tot}}{k_5 \cdot f_{ss}} \tag{137}$$

whenever $\dot{P}$ is constant and independent of the perturbation k_1. Independence of $\dot{P}$ from k_1 occurs when the terms $\alpha_i/(E_1)$ in the first line of Eq 135 become zero, either by sufficient large E_1 values or/and by the α_i's being close to zero (large k_9 and k_{11} values in comparison to k_7 and k_{10}). We found robust homeostasis in A for a large range of rate constant values. The rate

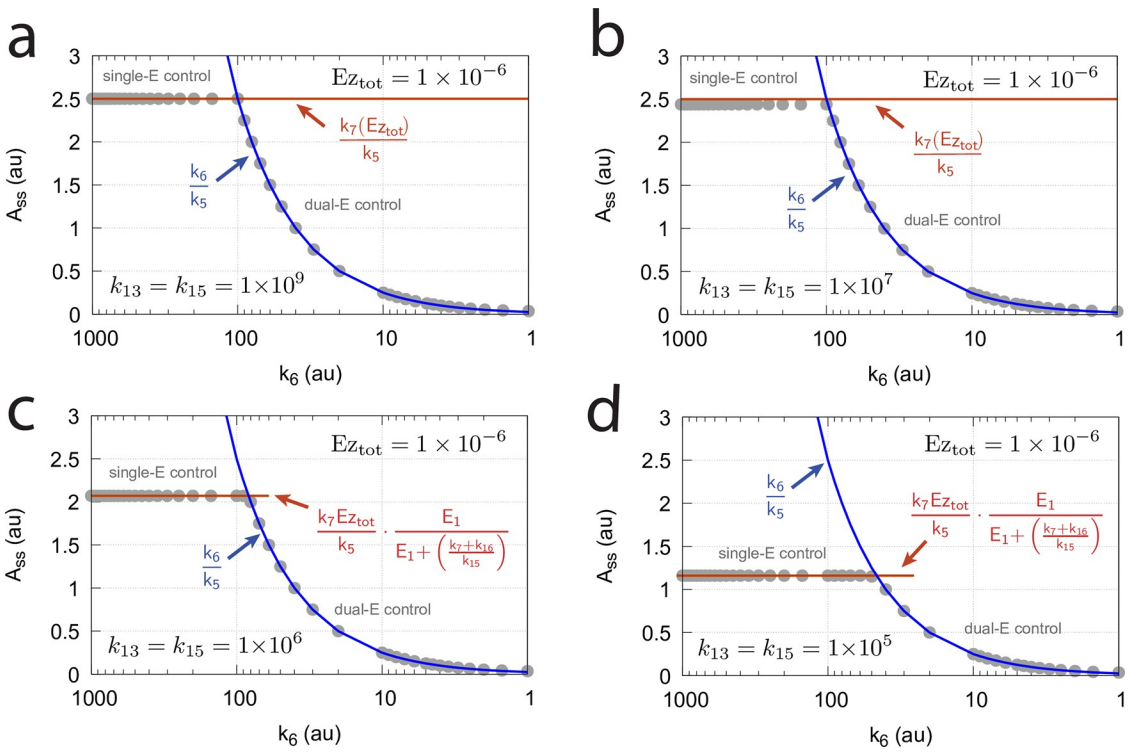

Fig 42. Switch between dual-E and single-E control in the m5 compulsory-order ternary-complex mechanisms (E_2 binding first to *Ez*, Fig 40) as a function of k_6, k_{13}, and k_{15}. The total enzyme concentration is 1×10^{-6} and constant. (a) k_{13}=k_{15}=1×10^{9}. A_{set} of the single-E controller is 2.5 (=$k_7 \cdot Ez_{tot}/k_5$, analogous to Eq 99. (b) k_{13}=k_{15}=1×10^{8}. Also in this case A_{set} of the single-E controller is still close to 2.5. (c) k_9=k_{11}=1×10^{6}. v ($\dot{P}$) is no longer zero-order with respect to E_1 and E_2, but is described by Eq 123, and A_{ss} of the single-E controller is described by Eq 124 with $E_{1,ss}$=4.82×10^{2} and $A_{ss}^{single-E}$=2.07. (d) k_9=k_{11}=1×10^{5}. At single-E control conditions we have $E_{1,ss}$=8.63×10^{2} and $A_{ss}^{single-E}$=1.16 (Eq 124). Other rate parameters as for Fig 37a.

https://doi.org/10.1371/journal.pone.0262371.g042

constant values used here have been chosen such that comparisons with the other controllers can be made and for getting controller response times which are not too large.

A striking observation in comparison with the m5-based controllers based on ternary-complex mechanisms is that E_2 has apparently no control function and that the ping-pong mechanism appears to be entirely controlled by E_1, even if $A_{ss} = A_{set} = k_6/k_5$, when k_{17}=0, described by the set-point condition

$$k_5 \cdot A_{set} = k_6 = k_7(Ez^* \cdot E_2)_{ss} \tag{138}$$

Fig 45 shows steady state values A_{ss} as a function of k_6 when k_{17}=100.0 and 0.0, at a total enzyme concentration of 1.0×10^{-6}. Each A_{ss} values represents an actual set-point of A, which is defended against step-wise perturbations by k_1.

Fig 46 shows the homeostatic behavior of A_{ss} in Fig 45 for k_6=10.0 when k_{17}=100.0 (panels a and b), or when k_{17}=0.0 (panels c and d). Note that only E_1 acts as the controller variable while E_2 is constant independent of the values of the perturbation k_1.

For k_6=100.0 the controller's behavior is shown in Fig 47. Also in this case robust homeostasis in A is observed due to the high values of E_1 and the constancy in E_2. Due to the large values

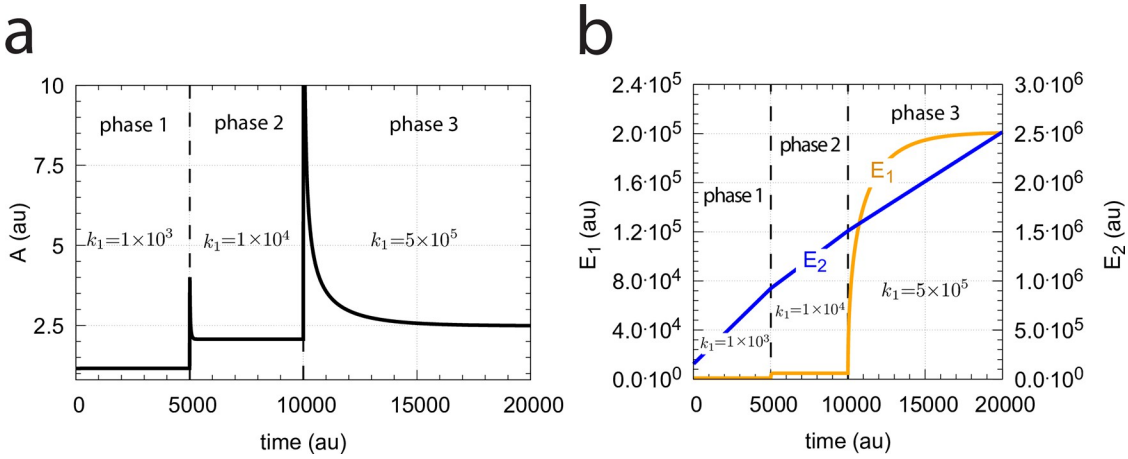

Fig 43. Under single-E control an increased perturbation k_1 moves A_{ss} in the m5 compulsory-order ternary-complex mechanisms (E_1 binding first to Ez) towards $A_{set}=k_7 \cdot Ez_{tot}/k_5$. (a) Phase 1: the system is that from Fig 42d with k_6=200 and k_1=1000.0. In phases 2 and 3 k_1 is stepwise increased to respectively 1×10^4 and 5×10^5. In phase 3 A is moved close to $A_{set}=k_7 \cdot Ez_{tot}/k_5$=2.5. Rate constant values as in Fig 42d. (b) Corresponding changes in E_1 and E_2. Note the wind-up of E_2 and that only E_1 is the active controller species. Initial concentrations: A_0=1.156, $E_{1,0}$=866.4, $E_{2,0}$=1.543 × 10^5, Ez_0=2.995 × 10^−9, $Ez \cdot (E_2)_0$=5.347 × 10^−7, and $(E_1 \cdot Ez \cdot E_2)_0$=4.622 × 10^−7.

https://doi.org/10.1371/journal.pone.0262371.g043

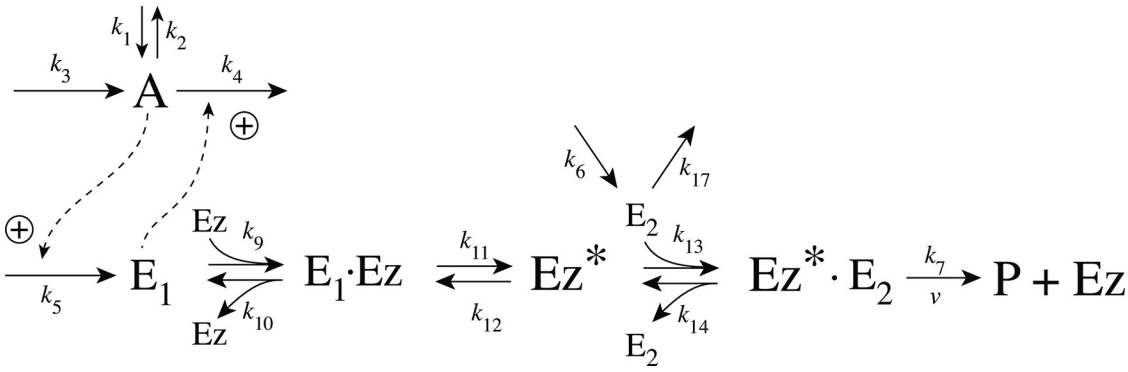

Fig 44. Scheme of the m5 controller when E_1 and E_2 are removed by a ping-pong mechanism with E_1 binding first to the free enzyme Ez.

https://doi.org/10.1371/journal.pone.0262371.g044

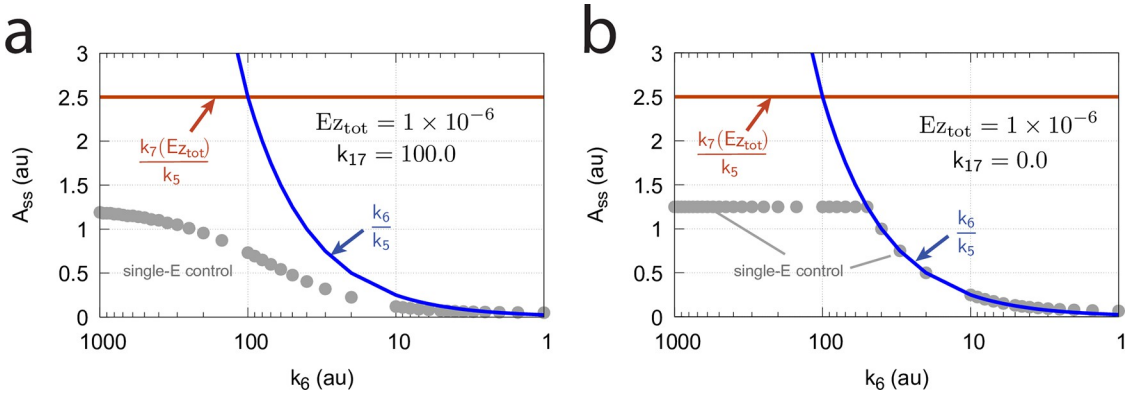

Fig 45. A_{ss} (=A_{set}) as a function of k_6 when (a) k_{17}=100.0 and (b) k_{17}=0.0. Gray solid points show the numerically calculated values of A_{ss}, while red and blue curves show the values of $k_7(Ez_{tot})/k_5$ and k_6/k_5, respectively. Other rate constant values: k_1=800.0, k_2=1.0, k_3=0.0, k_4=1.0, k_5=40.0, k_7=1 × 10^8, $k_9 = k_{11} = k_{13}$=1 × 10^8, and $k_{10} = k_{12} = k_{14}$=1 × 10^3. Initial concentrations: A_0=1.0, $E_{1,0}$=9.9 × 10^1, $E_{2,0}$=5.04 × 10^−1, Ez_0=6.03 × 10^−9, $(E_1 \cdot Ez)_0$=4.97 × 10^−7, $(Ez^* \cdot E_2)_0$=1.0 × 10^−7, and Ez^*_0=3.97 × 10^−7. Simulation time: 5000 time units, step-length: 0.01 time units.

https://doi.org/10.1371/journal.pone.0262371.g045

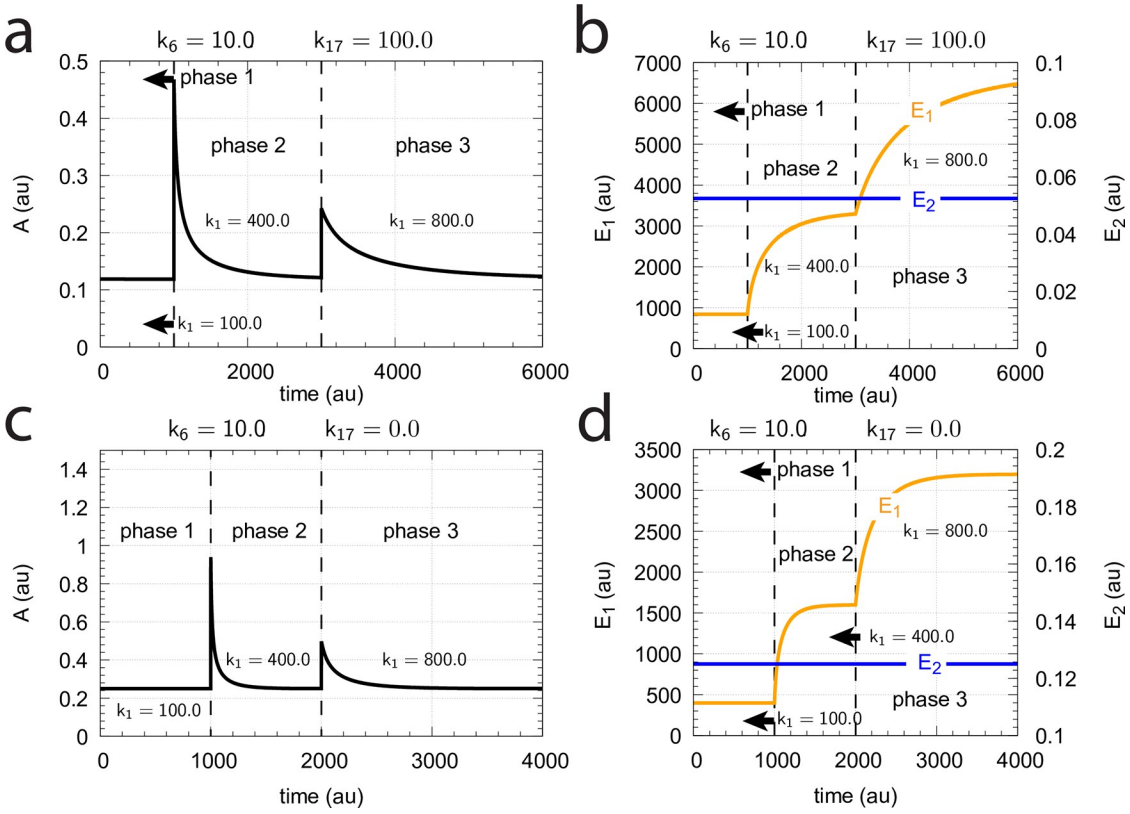

Fig 46. Demonstration of homeostatic behavior in A (Fig 45) when k_6=10.0 and k_{17}=100.0 (panels a and b) or k_{17}=0.0 (panel c and d). Step-wise perturbations are applied with values k_1=100 (phase 1), k_1=400 (phase 2), and k_1=800 (phase 3). Other rate constants as in Fig 45. Initial concentrations, (a) and (b): A_0=0.1189, $E_{1,0}$=8.40 × 10^2, $E_{2,0}$=5.25 × 10^{-2}, Ez_0=5.66 × 10^{-11}, $(E_1{\cdot}Ez)_0$=4.75 × 10^{-8}, $(Ez^*{\cdot}E_2)_0$=4.75 × 10^{-8}, and $f_{ss} = \frac{k_7}{k_{11}} + 1 = 2.0 \;\Rightarrow\; A_{set} = \frac{k_7 Ez_{tot}}{k_5 \cdot f_{ss}} = \frac{10^8 \times 10^{-6}}{2 \times 40.0} = 1.25 = 9.05 \times 10^{-7}$. Initial concentrations, (c) and (d): A_0=0.25, $E_{1,0}$=3.99 × 10^2, $E_{2,0}$=1.25 × 10^{-1}, Ez_0=2.51 × 10^{-10}, $(E_1{\cdot}Ez)_0$=1.00 × 10^{-7}, $(Ez^*{\cdot}E_2)_0$=1.00 × 10^{-7}, and Ez_0^*=9.76 × 10^{-7}.

https://doi.org/10.1371/journal.pone.0262371.g046

in both E_1 and E_2 the set-point of the controller is (k_{17}=0):

$$f_{ss} = \frac{k_7}{k_{11}} + 1 = 2.0 \;\Rightarrow\; A_{set} = \frac{k_7 Ez_{tot}}{k_5 \cdot f_{ss}} = \frac{10^8 \times 10^{-6}}{2 \times 40.0} = 1.25 \tag{139}$$

Motif 5 dual-E controller removing E_1 and E_2 by a ping-pong mechanism with E_2 binding first to *Ez*. Fig 48 shows the scheme of this mechanism.

The rate equations are:

$$\dot{A} = k_1 + k_3 - k_2 \cdot A - k_4 \cdot E_1 \cdot A \tag{140}$$

$$\dot{E_1} = k_5 \cdot A - k_9(Ez^*)(E_1) + k_{10}(Ez^* \cdot E_1) \tag{141}$$

$$\dot{E_2} = k_6 - k_{13}(Ez)(E_2) + k_{14}(E_2 \cdot Ez) - k_{17} \cdot E_2 \tag{142}$$

$$\dot{Ez} = -k_{13}(Ez)(E_2) + k_{14}(E_2 \cdot Ez) + k_7(Ez^* \cdot E_1) \tag{143}$$

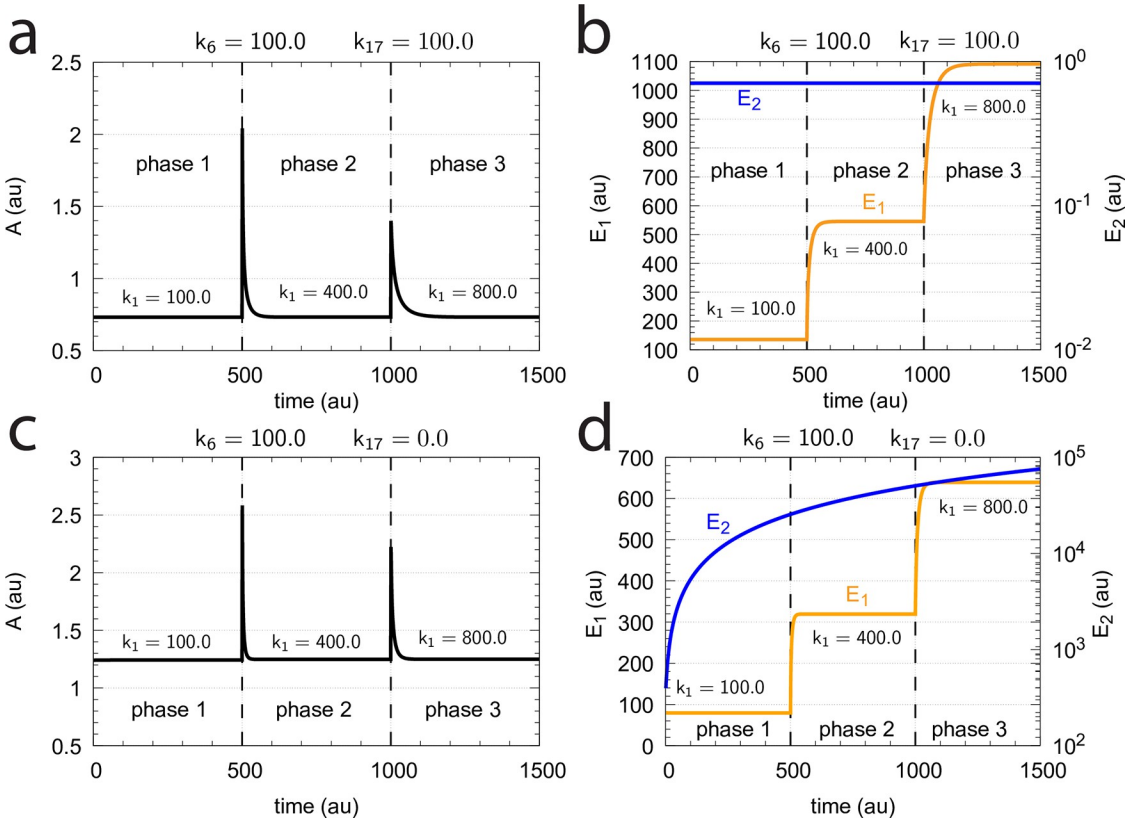

Fig 47. Demonstration of the homeostatic behavior of A_{ss} in Fig 45 when k_6=100.0 and k_{17}=100.0 (panels a and b) or k_{17}=0.0 (panel c and d). Step-wise perturbations are applied with values k_1=100 (phase 1), k_1=400 (phase 2), and k_1=800 (phase 3). Other rate constants as in Fig 45. The linear increase of E_2 is seen as a concave line due to the logarithmic scale of the E_2-axis. Initial concentrations, (a) and (b): A_0=0.7309, $E_{1,0}=1.36\times10^{2}$, $E_{2,0}=7.08\times10^{-1}$, $Ez_0=2.15\times10^{-9}$, $(E_1{\cdot}Ez)_0=2.95\times10^{-7}$, $(Ez^*{\cdot}E_2)_0=2.93\times10^{-7}$, and $Ez^*_0=4.13\times10^{-7}$. Initial concentrations, (c) and (d): A_0=1.24, $E_{1,0}=7.96\times10^{1}$, $E_{2,0}=3.50\times10^{-2}$, $Ez_0=6.23\times10^{-9}$, $(E_1{\cdot}Ez)_0=4.96\times10^{-7}$, $(Ez^*{\cdot}E_2)_0=4.96\times10^{-7}$, and $Ez^*_0=1.41\times10^{-9}$.

https://doi.org/10.1371/journal.pone.0262371.g047

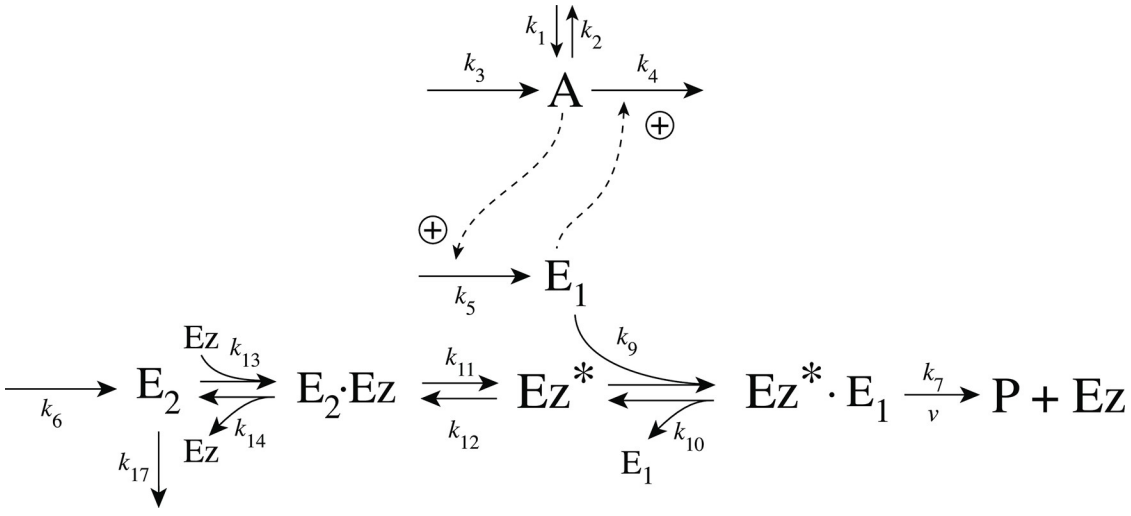

Fig 48. Scheme of the m5 controller when E_1 and E_2 are removed by a ping-pong mechanism with E_2 binding first to the free enzyme *Ez*.

https://doi.org/10.1371/journal.pone.0262371.g048

$$\frac{d(E_2 \cdot Ez)}{dt} = k_{13}(Ez)(E_2) - k_{14}(E_2 \cdot Ez) - k_{11}(E_2 \cdot Ez) + k_{12}Ez^* \tag{144}$$

$$\frac{d(Ez^* \cdot E_1)}{dt} = k_9(Ez^*)(E_1) - k_{10}(Ez^* \cdot E_1) - k_7(Ez^* \cdot E_1) \tag{145}$$

$$\dot{Ez^*} = k_{11}(E_2 \cdot Ez) - k_{12}Ez^* + k_{10}(Ez^* \cdot E_1) - k_9(Ez^*)(E_1) \tag{146}$$

The numerically calculated velocity is calculated as

$$v_{num} = \dot{P} = k_7(Ez^* \cdot E_1) \tag{147}$$

which has been found to be in excellent agreement with the steady-state expression

$$v_{ss} = \frac{k_7 Ez_{tot}}{\frac{D}{k_9 k_{11} k_{13}(E_1)(E_2)}} \tag{148}$$

with D being

$$\begin{aligned} D \quad &= k_7k_9k_{11}E_1 + k_7k_9k_{14}E_1 + k_7k_{12}k_{14} + k_{10}k_{12}k_{14} + k_7k_9k_{13}(E_1)(E_2) \\ &+ k_7k_{12}k_{13}(E_2) + k_{10}k_{12}k_{13}E_2 + k_7k_{11}k_{13}E_2 + k_{10}k_{11}k_{13}E_2 \\ &+ k_9k_{11}k_{13}(E_1)(E_2) \end{aligned} \tag{149}$$

Eq 148 is derived along the same lines as for Eq 134, i.e. by using the King-Altman method (S1 Text).

The set-point A_{set} for the controller is determined by its steady-state, A_{ss}, due to the condition

$$k_5A_{set} = k_5A_{ss} = k_7(Ez^* \cdot E_1)_{ss} = v_{ss} \tag{150}$$

where v_{ss} is independent of k_1. The maximum velocity is reached for zero-order conditions with respect to E_1 and E_2, and is given by

$$v_{max} = \frac{k_7 \cdot Ez_{tot}}{1 + \frac{k_7}{k_{11}}} \tag{151}$$

analogous to the condition by Eq 139.

The relationship between A_{set} and $(Ez^* \cdot E_1)_{ss}$ is also independent of k_6. Like for the m5 ping-pong based controller when E_1 binds first to Ez, E_2 has also here no control function and remains constant as long as the inflow of k_6 can be compensated by $v = \dot{P}$. However, when $k_6 > v_{max}$, and for example $k_{17} = 0$, E_2 will increase linearly. Fig 49 shows the controller's behavior for three different k_1 perturbation values analogous as in Fig 47 when k_6=100.0. For this high value of k_6 ($>v_{max}$ and $k_{17} = 0$) E_2 shows a (linear) increase.

Fig 50 shows how A_{ss} (which defines the set-point A_{set}) depends on k_6. Only when k_{17}=0 and $k_6 < v_{max}$ the set-point is defined by k_6/k_5. Despite the formal agreement with the set-point of a dual-E control when comparison is made to the above ternary-complex motif 5 mechanisms, the ping-pong mechanism shows robust single-E control conducted by E_1.

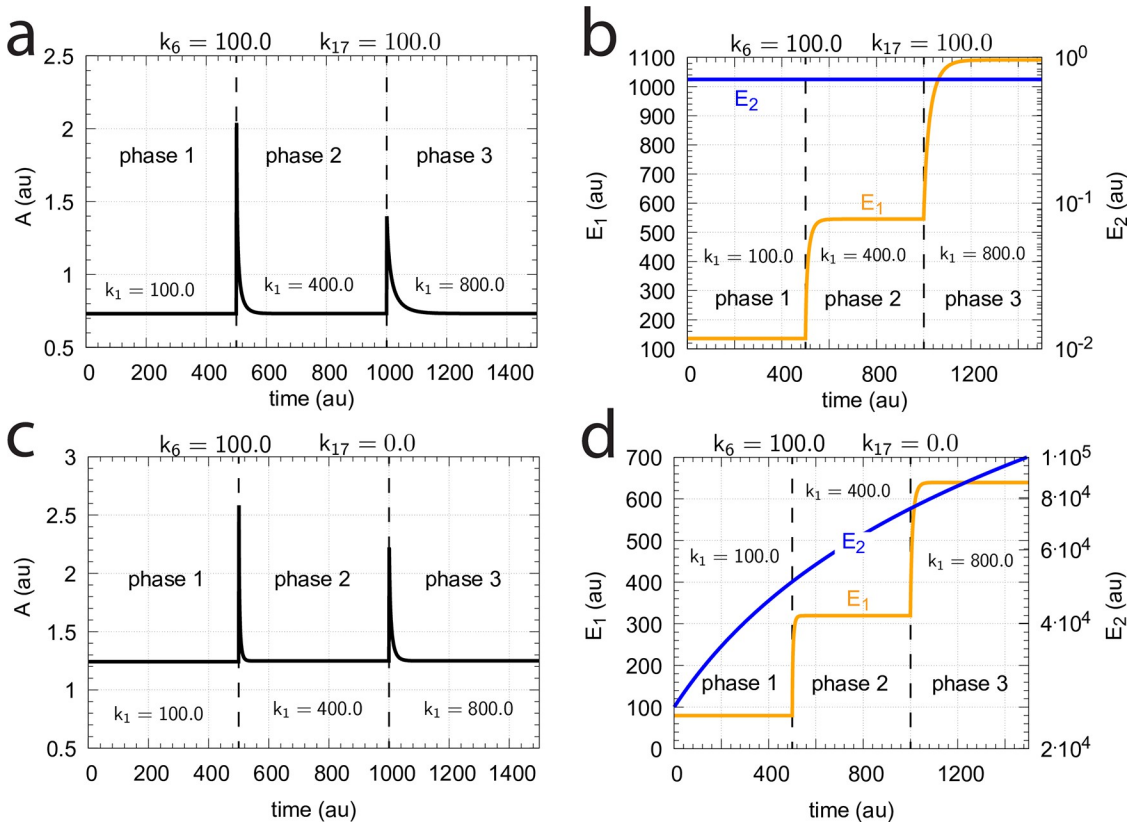

Fig 49. Demonstration of the homeostatic behavior of A_{ss} (scheme Fig 48) when k_6=100.0 and k_{17}=100.0 (panels a and b) or k_{17}=0.0 (panel c and d). The behavior is analogous to that shown in Fig 47. Step-wise perturbations are applied with values k_1=100 (phase 1), k_1=400 (phase 2), and k_1=800 (phase 3). Other rate constants as in Fig 45. The linear increase of E_2 is seen as a concave line due to the logarithmic scale of the E_2-axis. v_{max}=50 (Eq 151). Initial concentrations, (a) and (b): A_0=0.7309, $E_{1,0}=1.36\times10^{2}$, $E_{2,0}=7.08\times10^{-1}$, $Ez_0=2.15\times10^{-9}$, $(E_2{\cdot}Ez)_0=2.924\times10^{-7}$, $(Ez^*{\cdot}E_1)_0=2.924\times10^{-7}$, and $Ez_0^*=4.13\times10^{-7}$. Initial concentrations, (c) and (d): A_0=1.242, $E_{1,0}=7.95\times10^{1}$, $E_{2,0}=2.52\times10^{4}$, $Ez_0=1.97\times10^{-11}$, $(E_2{\cdot}Ez)_0=4.97\times10^{-7}$, $(Ez^*{\cdot}E_1)_0=4.97\times10^{-7}$, and $Ez_0^*=6.25\times10^{-9}$.

https://doi.org/10.1371/journal.pone.0262371.g049

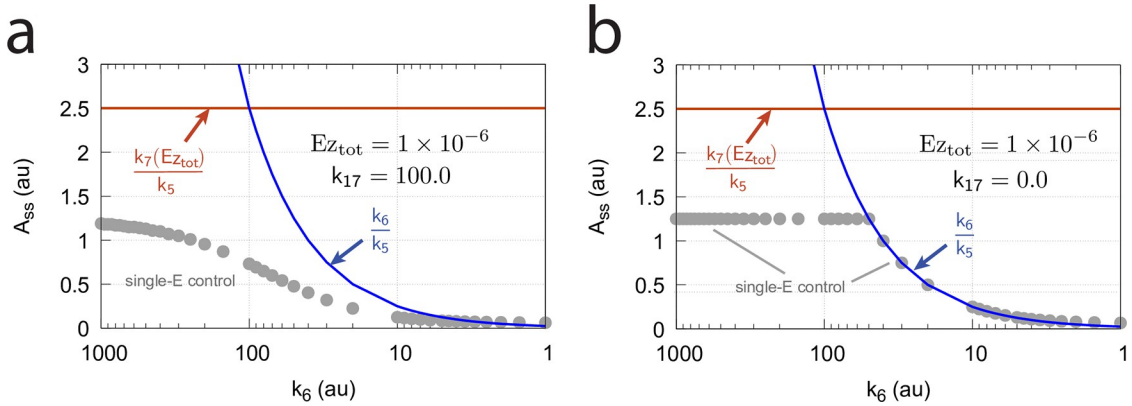

Fig 50. A_{ss} (=A_{set}) as a function of k_6 when (a) k_{17}=100.0 and (b) k_{17} = 0.0. Gray solid points show the numerically calculated values of A_{ss}, while red and blue curves show the values of $k_7(Ez_{tot})/k_5$ and k_6/k_5, respectively. Other rate constant values: k_1=800.0, k_2=1.0, k_3=0.0, k_4=1.0, k_5=40.0, $k_7=1\times10^{8}$, $k_9=k_{11}=k_{13}=1\times10^{8}$, and $k_{10}=k_{12}=k_{14}=1\times10^{3}$. Initial concentrations: A_0=1.0, $E_{1,0}=9.9\times10^{1}$, $E_{2,0}=5.04\times10^{-1}$, $Ez_0=6.03\times10^{-9}$, $(E_2{\cdot}Ez)_0=4.97\times10^{-7}$, $(Ez^*{\cdot}E_1)_0=1.0\times10^{-7}$, and $Ez_0^*=3.97\times10^{-7}$. Simulation time: 3000 time units, step-length: 0.01 time units.

https://doi.org/10.1371/journal.pone.0262371.g050

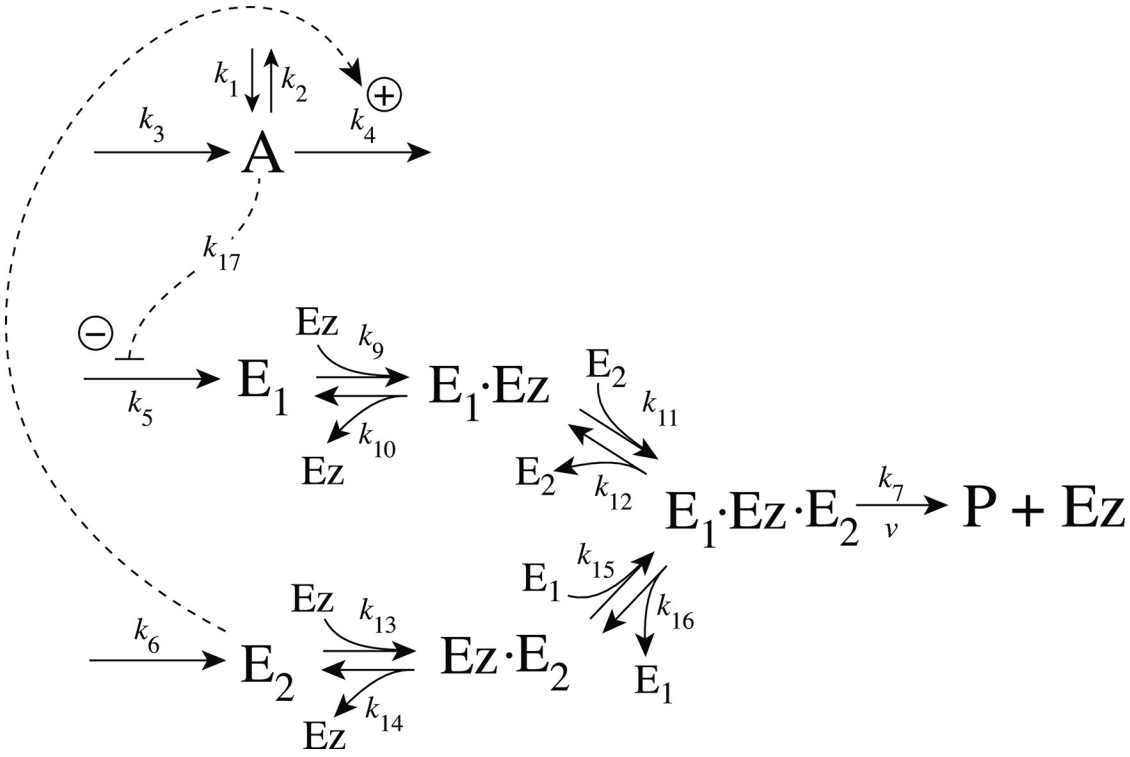

Fig 51. Reaction scheme of the m7-type of controller when E_1 and E_2 are removed by enzyme Ez with a random-order ternary-complex mechanism.

https://doi.org/10.1371/journal.pone.0262371.g051

Controllers based on motif 7

Motif 7 dual-E controller removing E_1 and E_2 by a random-order ternary-complex mechanism. Fig 51 shows the reaction scheme when in a m7 controller configuration E_1 and E_2 are removed by an enzymatic random-order ternary-complex mechanism.

The rate equations are:

$$\dot{A} = k_1 - k_2 \cdot A - k_4 \cdot (E_2)(A) + k_3 \tag{152}$$

$$\dot{E_1} = \frac{k_5 \cdot k_{17}}{k_{17} + A} - k_9(E_1)(Ez) + k_{10}(E_1 \cdot Ez) - k_{15}(Ez \cdot E_2)(E_1) + k_{16}(E_1 \cdot Ez \cdot E_2) \tag{153}$$

$$\dot{E_2} = k_6 - k_{11}(E_1 \cdot Ez)(E_2) + k_{12}(E_1 \cdot Ez \cdot E_2) - k_{13}(E_2)(Ez) + k_{14}(Ez \cdot E_2) \tag{154}$$

$$\dot{Ez} = -k_9(E_1)(Ez) + k_{10}(E_1 \cdot Ez) - k_{13}(E_2)(Ez) + k_{14}(Ez \cdot E_2) + k_7(E_1 \cdot Ez \cdot E_2) \tag{155}$$

$$\frac{d(E_1 \cdot Ez)}{dt} = k_9(E_1)(Ez) - k_{10}(E_1 \cdot Ez) - k_{11}(E_1 \cdot Ez)(E_2) + k_{12}(E_1 \cdot Ez \cdot E_2) \tag{156}$$

$$\frac{d(E_1 \cdot Ez \cdot E_2)}{dt} = k_{11}(E_1 \cdot Ez)(E_2) + k_{15}(Ez \cdot E_2)(E_1) - (k_7 + k_{12} + k_{16})(E_1 \cdot Ez \cdot E_2) \tag{157}$$

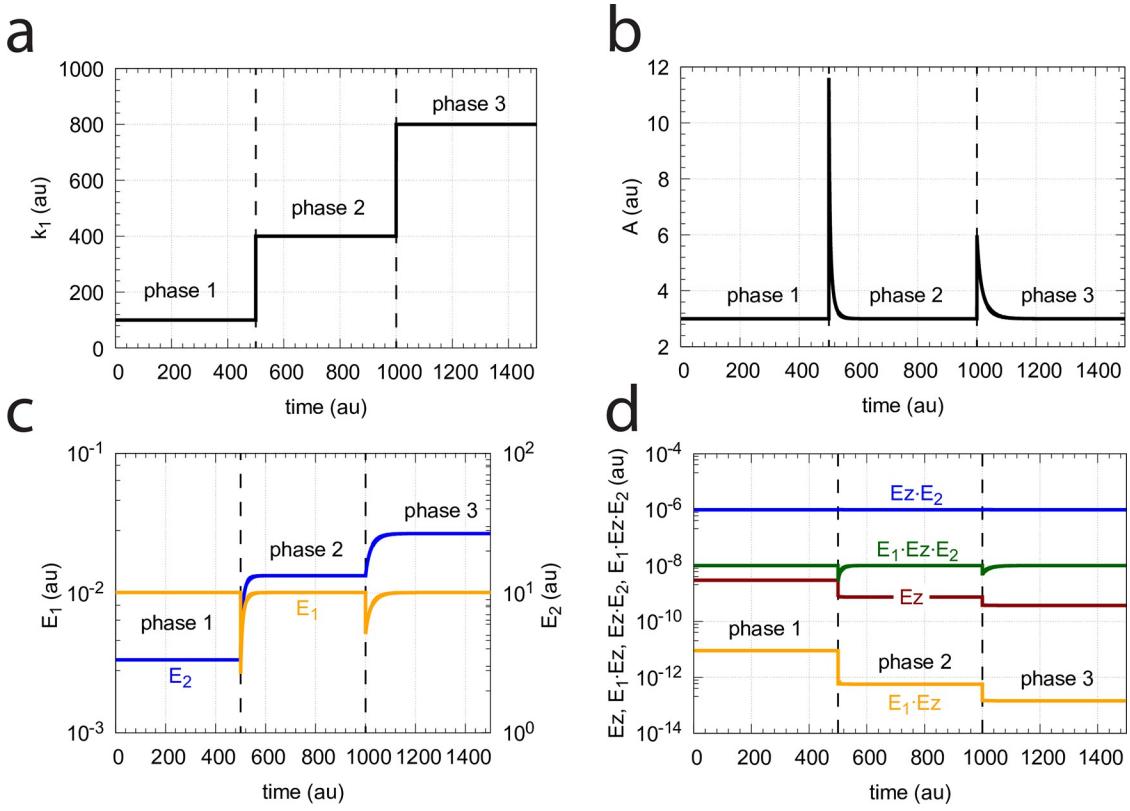

Fig 52. Homeostatic behavior towards step-wise perturbations of k_1 in the scheme of Fig 51. (a) stepwise changes of k_1, (b) homeostatic control of A, (c) Variation of controller variables E_1 and $E-2$, (d) changes in the enzymatic species Ez, $E_1{\cdot}Ez$, $Ez{\cdot}E_2$, and $E_1{\cdot}Ez{\cdot}E_2$. Rate constants: k_1=100.0 in phase 1, 400.0 in phase 2, and 800.0 in phase 3. k_2=k_3=0.0, k_4=1.01 × 10^1, k_5=31.0, k_6=1.0, k_7=1 × 10^8, k_8 not used, k_9=k_{11}=k_{13}=k_{15}=1 × 10^8, k_{10}=k_{12}=k_{14}=k_{16}=1 × 10^3, k_{17}=0.1. Initial concentrations: A_0=3.000, $E_{1,0}$=1.01 × 10^{-2}, $E_{2,0}$=3.333, Ez_0=2.994 × 10^{-9}, $(E_1{\cdot}Ez)_0$=9.102 × 10^{-12}, $(E_1{\cdot}Ez{\cdot}E_2)_0$=1.0 × 10^{-8}, $(EzE_2)_0$=9.871 × 10^{-7}, Ez_{tot}=1.0 × 10^{-6}.

https://doi.org/10.1371/journal.pone.0262371.g052

$$\frac{d(Ez\cdot E_2)}{dt} = k_{13}(E_2)(Ez) - k_{14}(Ez\cdot E_2) - k_{15}(Ez\cdot E_2)(E_1) + k_{16}(E_1\cdot Ez\cdot E_2) \tag{158}$$

Under dual-E conditions the steady state concentration of A is determined by setting inflow rates k_6 and $j_5 = k_5k_{17}/(k_{17} + A_{ss})$ equal to the outflow rate $v = k_7(E_1{\cdot}Ez{\cdot}E_2)$, i.e.,

$$v = k_7(E_1\cdot Ez\cdot E_2) = k_6 = \frac{k_5k_{17}}{k_{17} + A_{ss}} \tag{159}$$

Solving for A_{ss}, which is equal to A_{set}, gives

$$A_{ss} = A_{set} = \frac{k_{17}(k_5 - k_6)}{k_6} \tag{160}$$

Fig 52 illustrates the controller's homeostatic behavior, following Eq 160, for step-wise perturbations in k_1.The controller operates by increasing the controller variable E_2, which activates the compensatory flux $k_4{\cdot}(E_2)(A)$. Although E_1 undergoes an excursion during the perturbation, its steady-state value remains unchanged at the different k_1 values.

Operational range and irreversibility of the controller. Dual-E control is enabled as long as the condition by Eq 159 is obeyed, i.e., k_6 values need to be lower than k_5, together with $k_5 < k_7{\cdot}Ez_{tot}$. For these conditions the rates v, k_6, and $j_5 = k_5k_{17}/(k_{17} + A_{ss})$ are equal. However,

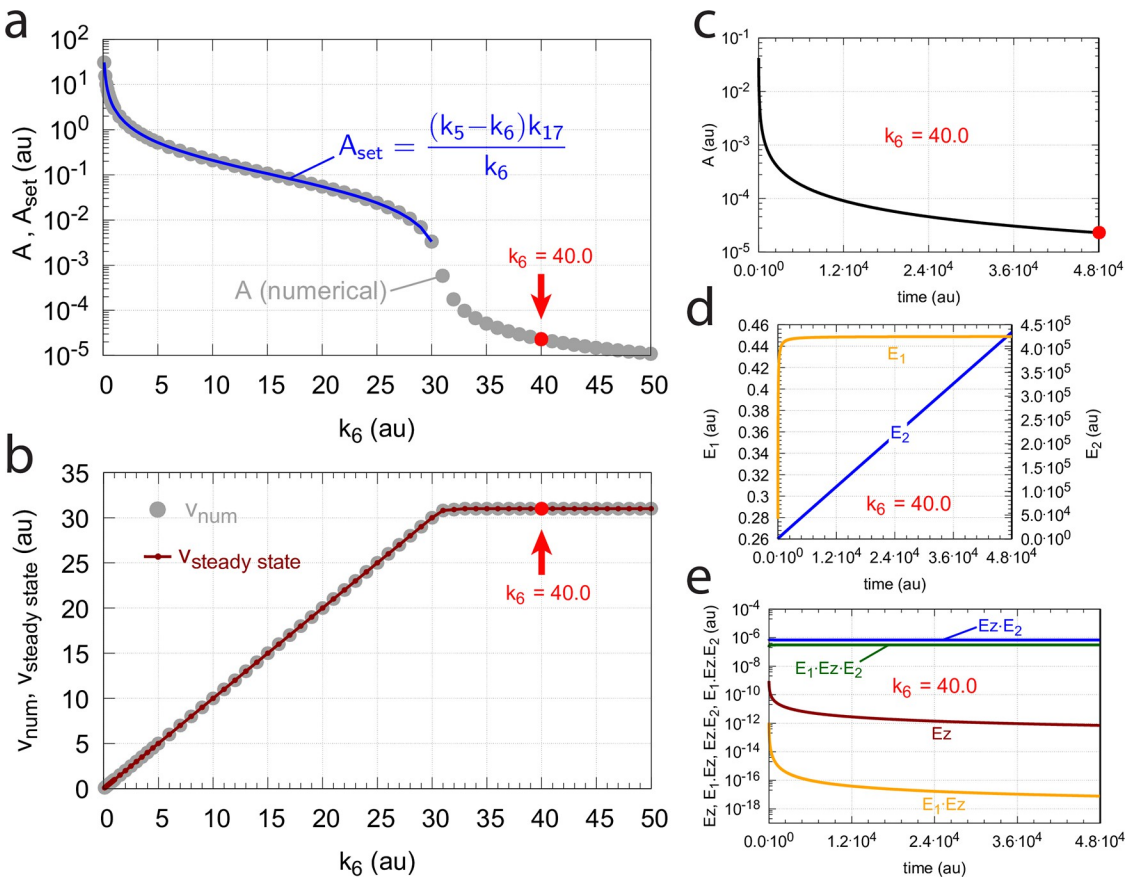

Fig 53. Loss of *A*-homeostasis in the m7 controller with a random-order ternary-complex mechanism (Fig 51) when $k_6 > k_5$. (a) A_{ss} as a function of k_6. (b) v_{num} (gray dots) and $v_{steady\ state}$ (King-Altman) (red line and small red dots) as a function of k_6. (c) Decrease of A as a function of time when k_6=40.0. (d) Steady state in E_1 and wind-up in E_2 when k_6=40.0. (e) Time profiles of the different enzyme species. Rate constants: k_1=100.0, k_2=1.0, k_3=0.0, k_4=1 × 10^1, k_5=31.0, k_7=1 × 10^8, k_8=0.1, k_9=k_{11}=k_{13}=k_{15}=1 × 10^8, k_{10}=k_{12}=k_{14}=k_{16}=1 × 10^3, k_{17}=0.1. Initial concentrations: A_0=2.5, $E_{1,0}$=5.5, $E_{2,0}$=52.1, Ez_0=1 × 10^{-6}, $(E_1{\cdot}Ez)_0$=0.0, $(E_1{\cdot}Ez{\cdot}E_2)_0$=0.0, $(EzE_2)_0$=0.0, Ez_{tot}=1.0 × 10^{-6}. Steady state values are determined after a simulation time of 48000 time units.

https://doi.org/10.1371/journal.pone.0262371.g053

when $k_6 \rightarrow k_5$, then $A_{ss} \rightarrow 0$, and $j_5 \rightarrow k_5$. In the limit, when $k_5 = k_6$, the feedback is broken and A does not exert inhibition on j_5.

In the case when $k_6 > k_5$, E_2 will continuously increase, because $v = k_7(E_1{\cdot}Ez{\cdot}E_2)$ balances with k_5, but not with k_6. Due to the continuous increase of E_2 the compensatory flux $k_4{\cdot}(E_2)(A)$ will also increase and drive A to zero.

The loss of homeostasis in A when $k_6 < k_5$ is described in Fig 53 where panels (a) and (b) show the numerically calculated A and v values (gray dots) as a function of k_6 after a simulation time of 48000 time units. In these calculations k_5=31.0 and k_{17}=0.1. The blue line in panel (a) shows the calculated A_{set} values by Eq 160. When $k_6 \geq 31.0$ A_{set} becomes (formally) negative. In this case A is found to decrease as a function of time due to the continuous increase of E_2 as a result of the negative feedback loss. The changes of A and E_2 concentrations are shown in panels (c) and (d) when k_6=40.0 (indicated by the red dot and red arrow). Panel (e) shows the concentrations of the different enzymatic species. Indicated in panel (b) is the loss of the negative feedback loop when $k_6 \geq 31.0$ leading to $A \rightarrow 0$ and a constant v_{num}=k_5=31.0.

As mentioned before a necessary condition to obtain robust control is the presence of a sufficient irreversible flux within the controller. This is indicated in Fig 54a–54c by using different

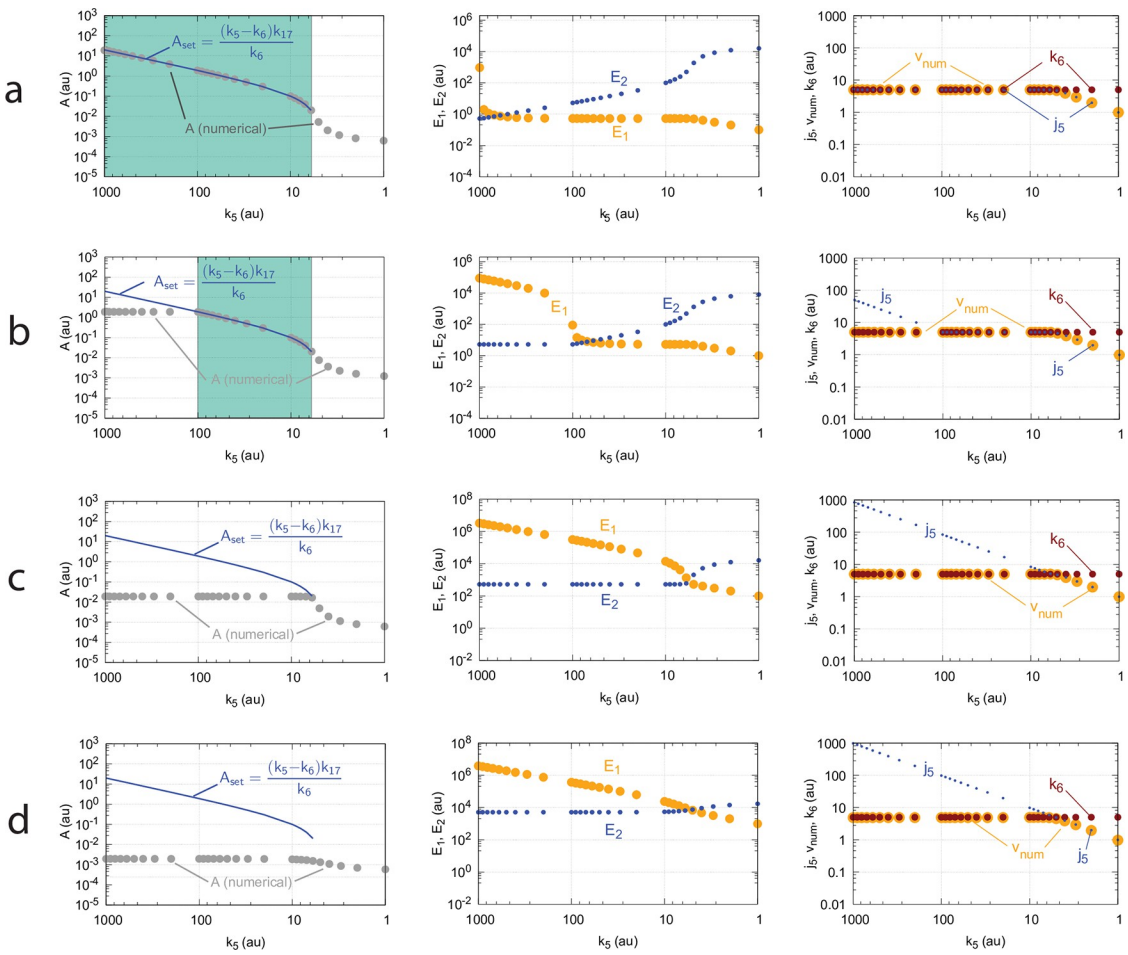

Fig 54. Decrease in the operational range of the enzymatic controller of Fig 51 (in dual-E control mode) as a function to decreased values of the forward enzymatic rate constants k_9, k_{11}, k_{13}, and k_{15}. The k_6 range for which homeostasis is observed is outlined as turquoise areas. (a) $k_9=k_{11}=k_{13}=k_{15}=1 \times 10^7$. (b) $k_9=k_{11}=k_{13}=k_{15}=1 \times 10^6$. (c) $k_9=k_{11}=k_{13}=k_{15}=1 \times 10^4$. The reverse rate constants k_{10}, k_{12}, k_{13}, k_{15} are in (a)-(c) kept constant at 1×10^3. (d) $k_9=k_{11}=k_{13}=k_{15}=1 \times 10^3$, while $k_{10}=k_{12}=k_{14}=k_{16}=0$. Despite the irreversibility of the system the k_9, k_{11}, k_{13}, and k_{15} values are too low to enable homeostasis. Other rate constants (a)-(d): $k_1=100$, $k_2=k_3=0$, $k_6=5.0$, $k_7=1 \times 10^8$, $k_{17}=0.1$. $Ez_{tot}=1 \times 10^{-6}$. Initial concentrations (a)-(d): $A_0=3.000$, $E_{1,0}=1.01 \times 10^{-2}$, $E_{2,0}=3.333$, $Ez_0=2.994 \times 10^{-9}$, $(E_1{\cdot}Ez)_0=9.102 \times 10^{-12}$, $(E_1{\cdot}Ez{\cdot}E_2)_0=1.0 \times 10^{-8}$, $(EzE_2)_0=9.871 \times 10^{-7}$, $Ez_{tot}=1.0 \times 10^{-6}$.

https://doi.org/10.1371/journal.pone.0262371.g054

values of the forward enzymatic rate constants k_9, k_{11}, k_{13}, and k_{15}, while the corresponding reverse rate constants k_{10}, k_{12}, k_{14}, and k_{16} are kept constant (1×10^3). In panel d the enzymatic process is entirely irreversible (k_{10}, k_{12}, k_{14}, and k_{16} are all zero), but due to the low value of the forward enzymatic rate constants k_{10}, k_{12}, k_{14}, and k_{16} (all 1×10^3), the controller does not show homeostasis at all, despite being completely irreversible.

The reason behind this failure to show homeostasis at high k_5 values is the incapability of the enzymatic system to absorb the high j_5 inflows. As a result the enzymatic system becomes saturated and E_1 increases continuously.

Effect of enzyme concentration. The above incapability of a saturated enzymatic system to maintain homeostatic behavior at large j_5 values can be counteracted by increasing the total enzyme concentration. This is shown in Fig 55, where total enzyme concentration changes from 1×10^{-6} to 1×10^{-3}. Clearly, the total amount of the enzyme plays an important role in the performance of catalyzed homeostatic controllers.

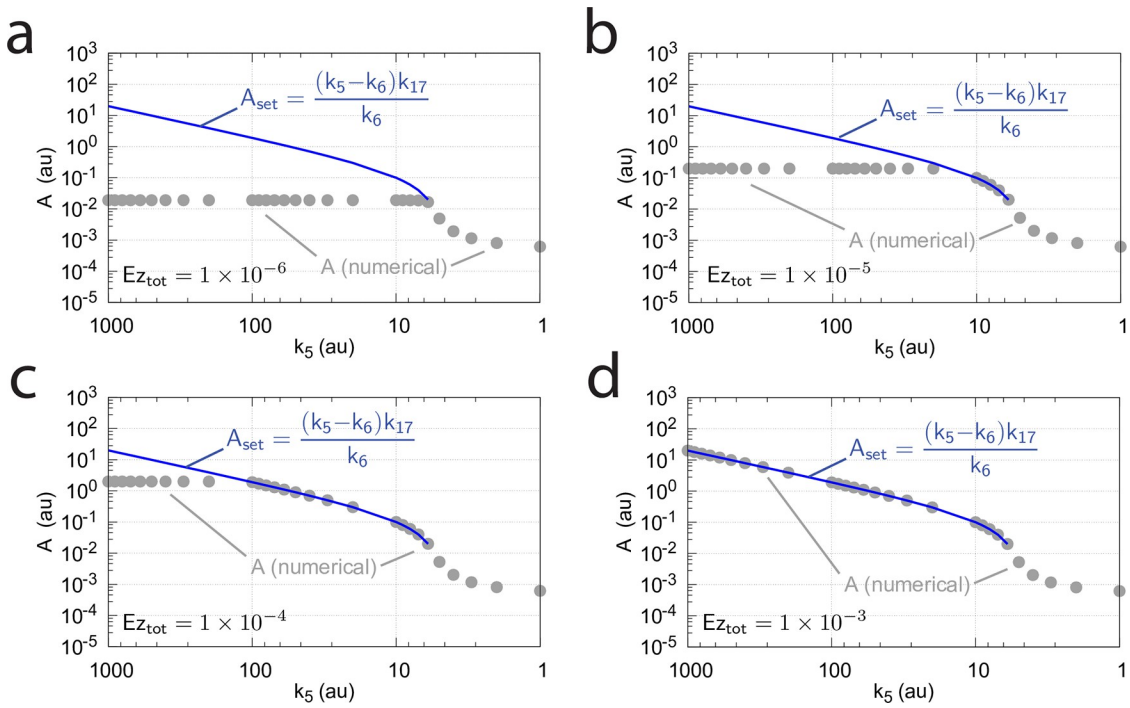

Fig 55. Influence of total enzyme concentration Ez_{tot} on the performance of the system in Fig 54c. (a) Ez_{tot}=1.0 × 10^{-6}; (b) Ez_{tot}=1.0 × 10^{-5}; (c) Ez_{tot}=1.0 × 10^{-4}; (d) Ez_{tot}=1.0 × 10^{-3}. Rate constant values as for Fig 54c. Initial concentrations: (a) A_0=3.000, $E_{1,0}$=1.01 × 10^{-2}, $E_{2,0}$=3.333, Ez_0=1 × 10^{-6}, $(E_1{\cdot}Ez)_0$=0.0, $(E_1{\cdot}Ez{\cdot}E_2)_0$=0.0, $(EzE_2)_0$=0.0. (b) A_0=3.000, $E_{1,0}$=1.01 × 10^{-2}, $E_{2,0}$=3.333, Ez_0=1 × 10^{-5}, $(E_1{\cdot}Ez)_0$=0.0, $(E_1{\cdot}Ez{\cdot}E_2)_0$=0.0, $(EzE_2)_0$=0.0. (c) A_0=3.000, $E_{1,0}$=1.01 × 10^{-2}, $E_{2,0}$=3.333, Ez_0=1 × 10^{-4}, $(E_1{\cdot}Ez)_0$=0.0, $(E_1{\cdot}Ez{\cdot}E_2)_0$=0.0, $(EzE_2)_0$=0.0. (d) A_0=3.000, $E_{1,0}$=1.01 × 10^{-2}, $E_{2,0}$=3.333, Ez_0=1 × 10^{-3}, $(E_1{\cdot}Ez)_0$=0.0, $(E_1{\cdot}Ez{\cdot}E_2)_0$=0.0, $(EzE_2)_0$=0.0.

https://doi.org/10.1371/journal.pone.0262371.g055

Motif 7 controller using compulsory-order ternary-complex mechanisms. As for the other ternary-complex controller motifs there are two compulsory-order mechanisms, one in which E_1 binds first to free Ez (Fig 56a), while in the other one (Fig 56b) E_2 binds first to Ez.

The two compulsory-order mechanisms behave quite similar compared with the random-order mechanism. In the case when E_1 is binding first to the free enzyme Ez (Fig 56a), the rate equations are:

$$\dot{A} = k_1 - k_2 \cdot A - k_4 \cdot (E_2)(A) + k_3 \tag{161}$$

$$\dot{E_1} = \frac{k_5 \cdot k_{17}}{k_{17} + A} - k_9(E_1)(Ez) + k_{10}(E_1 \cdot Ez) \tag{162}$$

$$\dot{E_2} = k_6 - k_{11}(E_1 \cdot Ez)(E_2) + k_{12}(E_1 \cdot Ez \cdot E_2) \tag{163}$$

$$\dot{Ez} = -k_9(E_1)(Ez) + k_{10}(E_1 \cdot Ez) + k_7(E_1 \cdot Ez \cdot E_2) \tag{164}$$

$$\frac{d(E_1 \cdot Ez)}{dt} = k_9(E_1)(Ez) - k_{10}(E_1 \cdot Ez) - k_{11}(E_1 \cdot Ez)(E_2) + k_{12}(E_1 \cdot Ez \cdot E_2) \tag{165}$$

$$\frac{d(E_1 \cdot Ez \cdot E_2)}{dt} = k_{11}(E_1 \cdot Ez)(E_2) - (k_7 + k_{12})(E_1 \cdot Ez \cdot E_2) \tag{166}$$

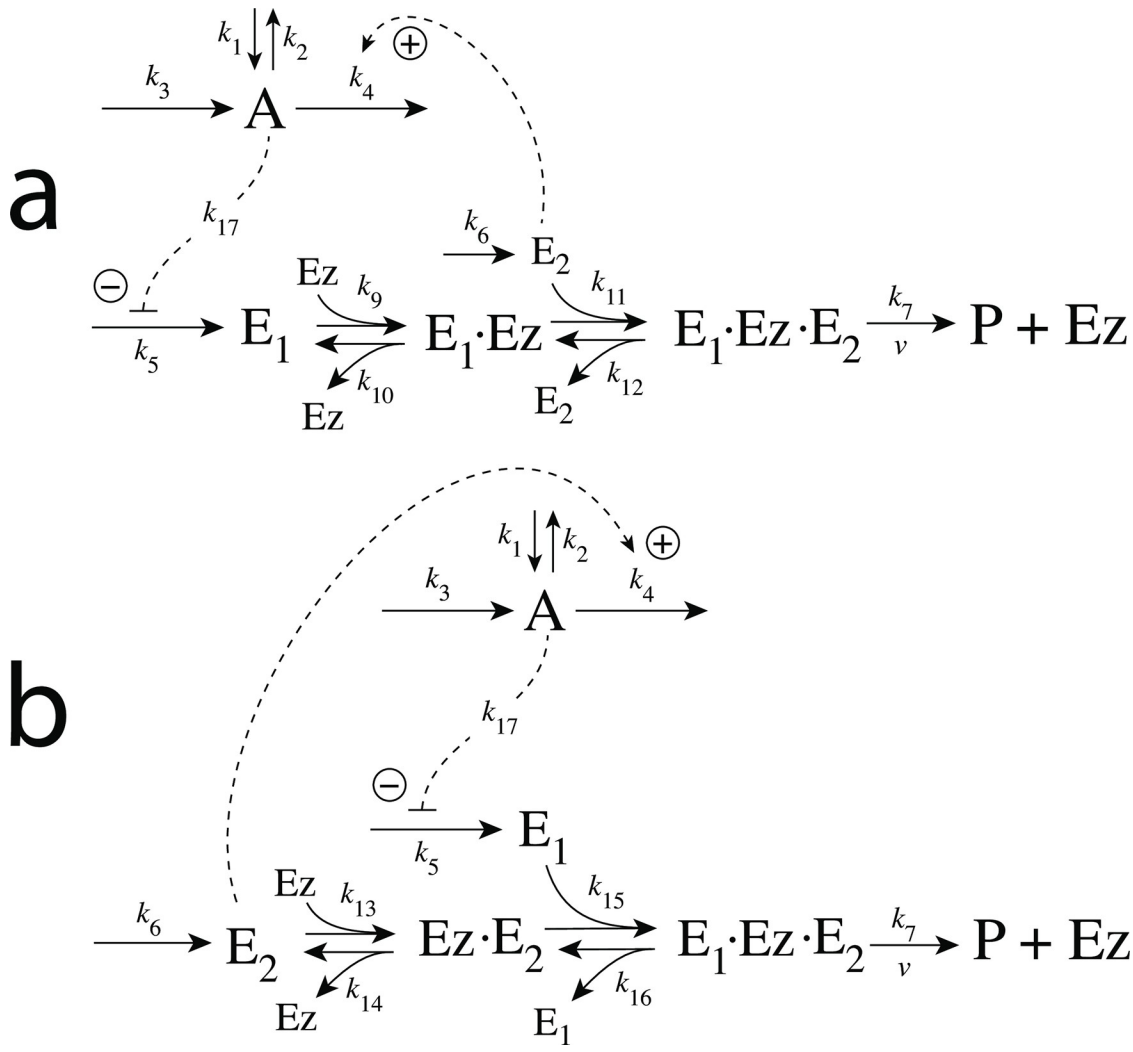

Fig 56. The two compulsory-order ternary-complex mechanisms with feedback motif m7. In (a) E_1 binds first to the free enzyme *Ez*, while in (b) E_2 binds first.

https://doi.org/10.1371/journal.pone.0262371.g056

The set-point for the controller in dual-E mode is derived in an analogous way as for the random-order mechanism, i.e. the condition for the operative controller is given by Eqs 159 and 160 for the set-point. Also here we have explored how the controller's performance changes in response to rate constant k_5 and find identical behaviors in response to the enzyme system's behavior to "absorb" the flux $j_5=k_5k_{17}/(k_{17}+A)$. High values of k_9 and k_{11}, as seen in Fig 57a, promote the functionality of the controller, while low k_9 and k_{11} values (Fig 57b) lead to a breakdown. As in the random-order case (Fig 55), an increase of the total enzyme concentration leads to an improvement of the controller's homeostatic behavior. In Fig 57c and 57d the total enzyme concentrations are increased from 1×10^{-6} to 1×10^{-4} and 1×10^{-3}. This allows the controller to maintain the homeostatic A_{set} for larger k_5 values.

In the case E_2 binds first to the free enzyme *Ez* (Fig 56b), the rate equations become:

$$\dot{A} = k_1 + k_3 - k_2 \cdot A - k_4 \cdot (E_2)(A) \tag{167}$$

$$\dot{E_1} = \frac{k_5 \cdot k_{17}}{k_{17} + A} - k_{15}(E_1)(Ez \cdot E_2) + k_{16}(E_1 \cdot Ez \cdot E_2) \tag{168}$$

$$\dot{E_2} = k_6 - k_{13}(E_2)(Ez) + k_{14}(Ez \cdot E_2) \tag{169}$$

$$\dot{Ez} = -k_{13}(E_2)(Ez) + k_{14}(Ez \cdot E_2) + k_7(E_1 \cdot Ez \cdot E_2) \tag{170}$$

$$\frac{d(Ez \cdot E_2)}{dt} = k_{13}(E_2)(Ez) - k_{14}(Ez \cdot E_2) - k_{15}(E_1)(Ez \cdot E_2) + k_{16}(E_1 \cdot Ez \cdot E_2) \tag{171}$$

$$\frac{d(E_1 \cdot Ez \cdot E_2)}{dt} = k_{15}(E_1)(Ez \cdot E_2) - (k_7 + k_{16})(E_1 \cdot Ez \cdot E_2) \tag{172}$$

As for the other m7 ternary-complex mechanisms the set-point of A is determined by the balance between reaction rates k_6, j_5=$k_5k_{17}/(k_{17} + A)$, and $v = k_7(E_1 \cdot Ez \cdot E_2)$ (see Eqs 159 and 160). With respect to varying values of k_1 and k_5 the controller's steady state values in A behave precisely as shown in Fig 57 for the other ternary-complex mechanisms, i.e., the loss of homeostasis by low forward rate constants k_{13} and k_{15} can be counteracted by an increase in the total enzyme concentration.

As we already saw from the previous controllers (see for example the m5 controller, Fig 38) an increase in the perturbation strength (here k_1) will drive the steady-state of the regulated variable A towards its theoretical set-point A_{set}. This is also observed for the m7-type of controllers for dual-E control. As seen in Fig 58, increasing k_1 values extend the homeostatic region of the controller. This same pattern of A as a function of k_5 for different k_1 values is also observed for the other ternary-complex mechanisms (Figs 51 and 56a).

Motif 7 dual-E controller removing E_1 and E_2 by ping-pong mechanisms. Fig 59 shows the reaction scheme when in a m7 controller configuration E_1 and E_2 are removed by the two enzymatic ping-pong mechanisms when E_1 binds first to Ez (Fig 59a) or when E_2 binds first to Ez (Fig 59b).

In the case E_1 binds first to Ez (Fig 59a) the rate equations are:

$$\dot{A} = k_1 + k_3 - k_2 \cdot A - k_4 \cdot (E_2)(A) \tag{173}$$

$$\dot{E_1} = \frac{k_5 \cdot k_{17}}{k_{17} + A} - k_9(E_1)(Ez) + k_{10}(E_1 \cdot Ez) \tag{174}$$

$$\dot{E_2} = k_6 - k_{13}(E_2)(Ez^*) + k_{14}(Ez^* \cdot E_2) \tag{175}$$

$$\dot{Ez} = -k_9(E_1)(Ez) + k_{10}(E_1 \cdot Ez) + k_7(Ez^* \cdot E_2) \tag{176}$$

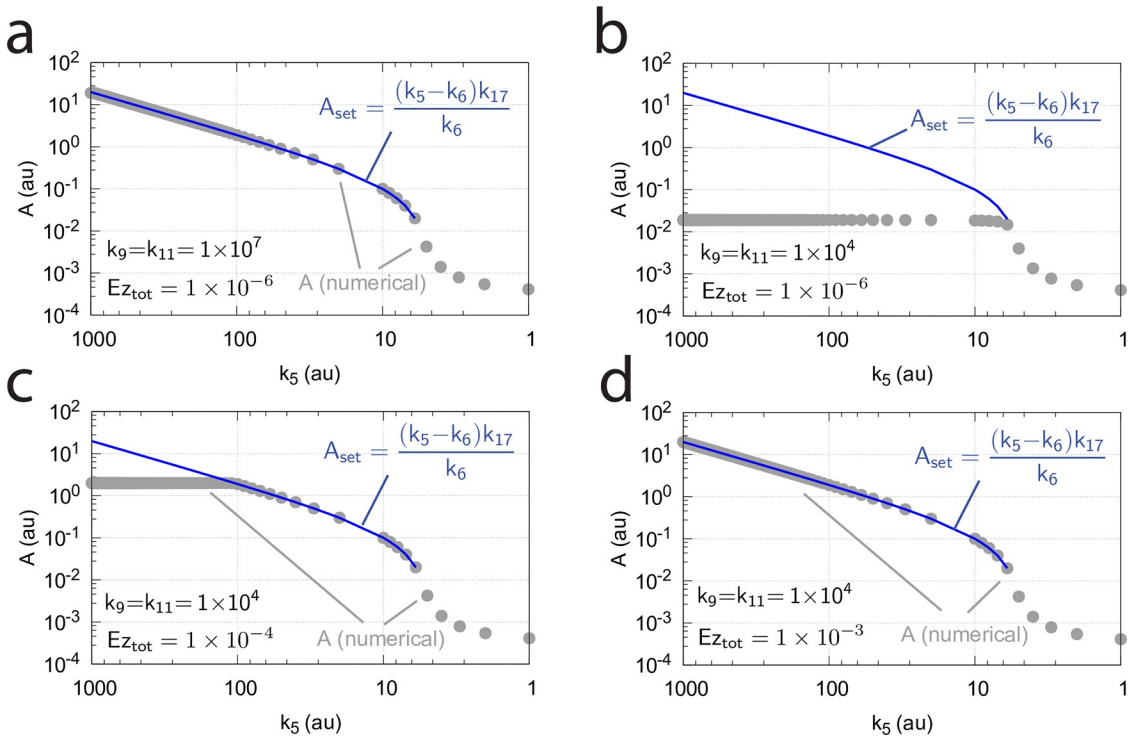

Fig 57. Influence of k_9, k_{11}, and Ez_{tot} on the operational range of the controller from Fig 56a. (a) Optimum controller behavior for large k_9 and k_{11} values (both 1×10^7) at $Ez_{tot}=1 \times 10^{-6}$. (b) Reducing k_9 and k_{11} to 1×10^4 leads to a complete loss of the controller's homeostatic behavior. Although the steady state values of A (gray circles) are independent and constant for $k_5 > k_6$, they depend on the perturbation k_1, which will be illustrated below for scheme Fig 56b. (c) Increasing the total enzyme concentration to 1×10^{-4} partially improves the controller's performance. (d) Increasing the total Ez concentration to 1×10^{-3} restores the homeostatic behavior as the increased k_9 and k_{11} values in (a) at low Ez_{tot}. Other rate constants (a)-(d): k_1=100, k_2=k_3=0, k_4=10.0, k_6=5.0, $k_7=1 \times 10^8$, k_9=k_{11}=k_{13}=$k_{15}=1 \times 10^8$, k_{10}=k_{12}=k_{14}=$k_{16}=1 \times 10^3$, k_{17}=0.1. Initial concentrations (a)-(d): A_0=0.08, $E_{1,0}=5.27 \times 10^{-2}$, $E_{2,0}$=125.0; (a)-(b) $Ez_0=1.0 \times 10^{-6}$, $(E_1{\cdot}Ez)_0$=$(E_1{\cdot}Ez{\cdot}E_2)_0$=0.0; (c) $Ez_0=1.0 \times 10^{-4}$, $(E_1{\cdot}Ez)_0$=$(E_1{\cdot}Ez{\cdot}E_2)_0$=0.0; (d) $Ez_0=1.0 \times 10^{-3}$, $(E_1{\cdot}Ez)_0$=$(E_1{\cdot}Ez{\cdot}E_2)_0$=0.0. The steady state values of A were determined after 6000 time units.

https://doi.org/10.1371/journal.pone.0262371.g057

$$\frac{d(E_1 \cdot Ez)}{dt} = k_9(E_1)(Ez) + k_{12}Ez^* - (k_{10} + k_{11})(E_1 \cdot Ez) \tag{177}$$

$$\frac{d(Ez^*)}{dt} = k_{11}(E_1 \cdot Ez) + k_{14}(Ez^* \cdot E_2) - k_{12}Ez^* - k_{13}(E_2)(Ez^*) \tag{178}$$

$$\frac{d(Ez^* \cdot E_2)}{dt} = k_{13}(E_2)(Ez^*) - (k_7 + k_{14})(Ez^* \cdot E_2) \tag{179}$$

Minor differences between the m7 ping-pong and ternary-complex mechanisms. The dynamic behaviors of the ping pong-mechanisms are very similar to the (m7) ternary-complex mechanisms. Also here A_{set} is determined by the balancing of the three fluxes j_5=$k_5k_{17}/(k_{17}$ + $A)$, the inflow described by k_6, and the rate v=$k_7(Ez^*{\cdot}E_2)$ making P. Accordingly, A_{set} is described by Eq 160. Also, an increase of total enzyme concentration and an increase of the forward enzymatic rate constants k_9, k_{11},. . . will improve the homeostatic performance of the ping-pong controllers.

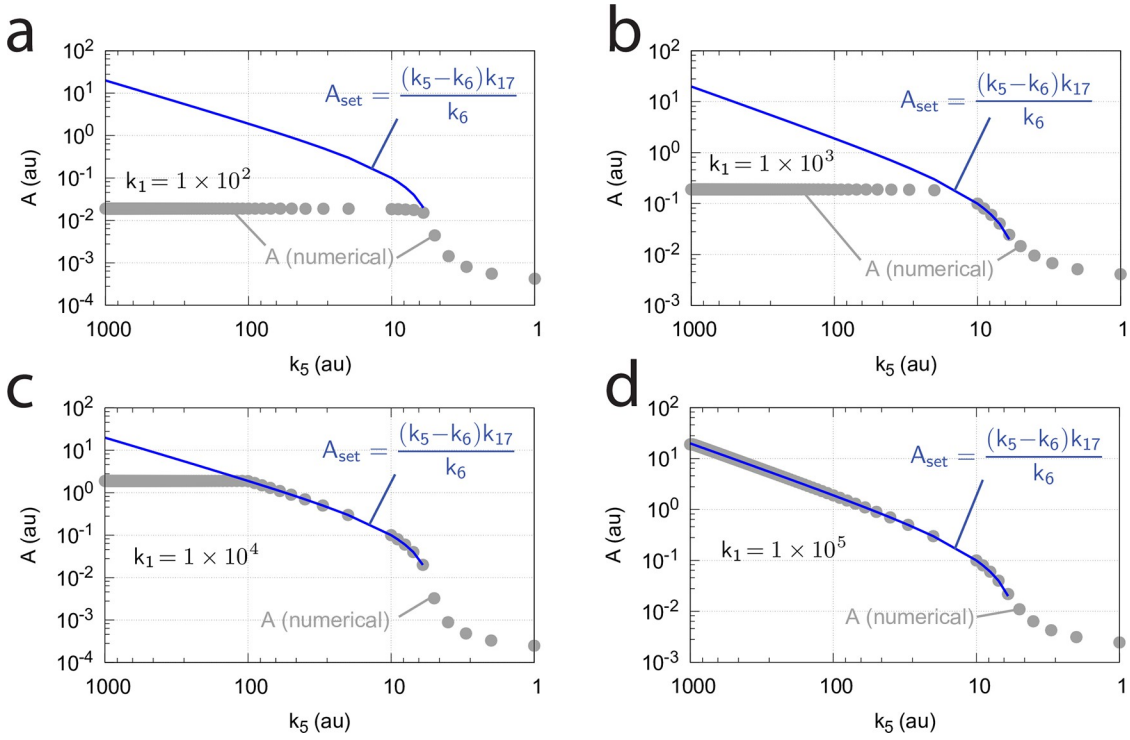

Fig 58. Influence of k_1 on the operational range of the m7 ternary-complex controllers. The results using the scheme of Fig 56b are shown. (a) k_1=1 × 10^2. (b) k_1=1 × 10^3. (c) k_1=1 × 10^4. (d) k_1=1 × 10^5. Other rate constants (a)-(d): k_2=k_3=0, k_4=10.0, k_6=5.0, k_7=1 × 10^8, k_{13}=k_{15}=1 × 10^4, k_{14}=k_{16}= k_{17}=1 × 10^3. Initial concentrations (a)-(d): A_0=1.88, $E_{1,0}$=5.39 × 10^2, $E_{2,0}$=5.315, Ez_0=1.0 × 10^{-6}, $(E_1{\cdot}Ez)_0$=$(E_1{\cdot}Ez{\cdot}E_2)_0$=0.0. Due to a slow response (large response time) of the controller at higher k_1, steady state values of A were determined after 1 × 10^6 time units.

https://doi.org/10.1371/journal.pone.0262371.g058

However, since the ping-pong mechanisms have a slightly longer enzymatic reaction chain in comparison with the ternary-complex mechanisms, in the ping-pong case larger forward enzymatic rate constants values are needed together with lower k_6 values to match the fluxes j_5, k_6, and v to achieve moving A_{ss} to its set-point. The influences of the forward enzymatic rate constants and the total Ez concentration are illustrated in Fig 60 where numerically calculated A values are compared with the theoretical set-point A_{set}. In comparison with the ternary-complex mechanism results from Figs 57a and 60a show the behavior of the ping-pong mechanism whenEz_{tot}=1 × 10^{-6}, and k_9=k_{11}=k_{13}=1 × 10^7. Unlike in the ternary-complex mechanism, in the ping-pong case deviations between the numerically calculated A values and A_{set} are observed at the higher ($k_5 > 460$) and lower $k_5 < 10$ ends of the k_5 scale. When in Fig 60a k_5 gets higher than 460 the enzymatic system cannot absorb the inflow flux j_5=k_5k_{17}/(k_{17}+ A). As a result, E_1 shows a linear increase in time, with a slope which is dependent on the value of k_5, but where A becomes constant and independent of k_5. At the lower end of the k_5 scale ($k_5 <$ 10) the value of k_6 is too high to get absorbed by $Ez^*{\cdot}E_2$. This has the result that E_2 shows a liner increase in time and an increasing compensatory flux $k_4{\cdot}A{\cdot}E_2$ with A decreasing continuously without reaching a steady state. The loss of homeostasis at high k_5 values can be overcome by either increasing the total amount of enzyme (Fig 60b) or by increasing the values of the forward rate constants k_9, k_{11}, and/or k_{13} (Fig 60c).

An increase of the perturbation k_1 leads also in the ping-pong controllers to an improvement in the homeostatic accuracy as for example observed in the m5 controllers, but not at low k_5 values. This is indicated in Fig 61. In panel a we have rate constant values for k_1, k_6,

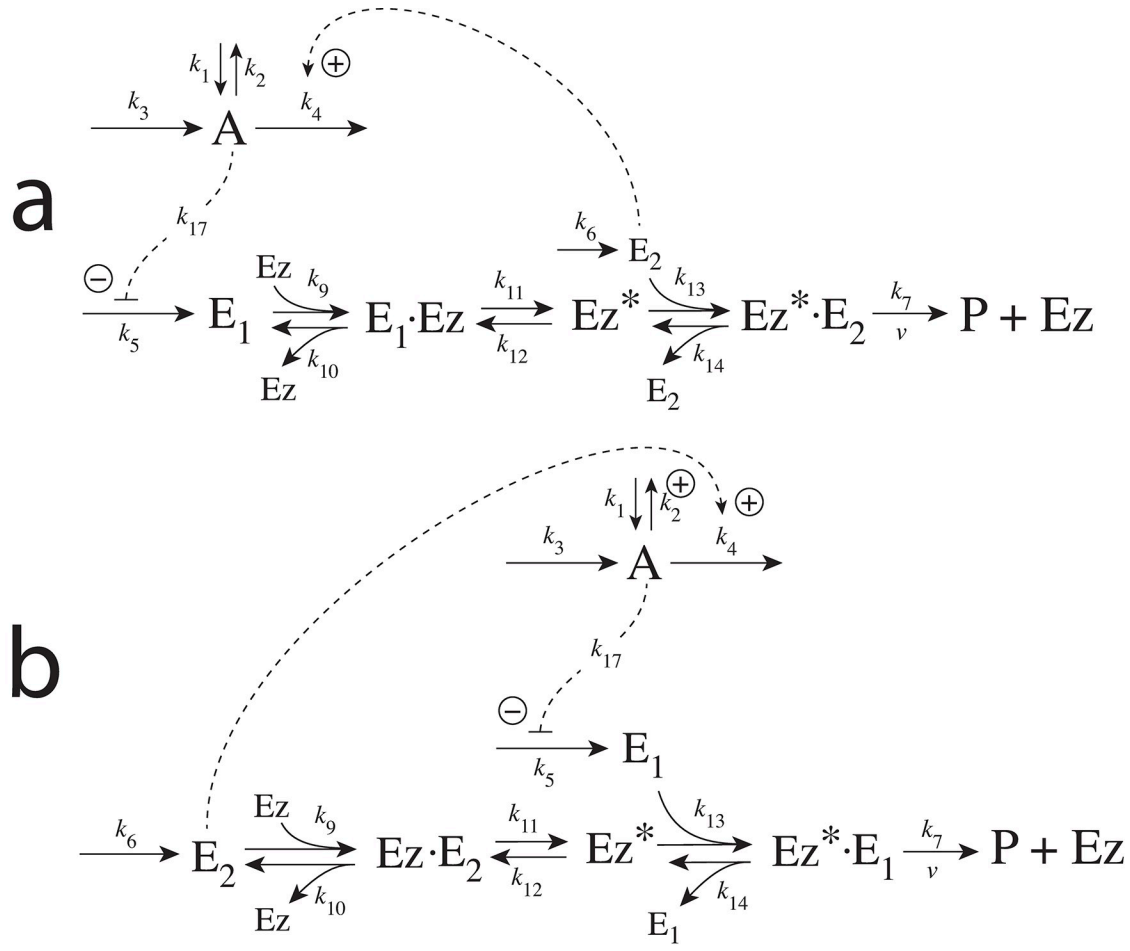

Fig 59. Reaction schemes of the two m7-type of controllers when E_1 and E_2 (Fig 3) are removed by enzyme *Ez* using ping-pong mechanisms with (a) E_1 binding first, or (b) when E_2 binds first.

https://doi.org/10.1371/journal.pone.0262371.g059

Ez_{tot}, and the forward enzymatic rate constants (k_9, k_{11}, and k_{13}) as in Fig 60a and as in the ternary-complex mechanisms of Fig 57a. An increase of k_1 from 1×10^2 to 1×10^4 in the ping-pong mechanism (Fig 61b) does improve the homeostatic response of the controller at high k_5 values, but not at low k_5, where the high inflow rate by k_6 cannot be absorbed. In fact, a decrease of k_6 from 5.0 to 1.0 leads to homeostasis for all k_5 values with $A_{set} > 0$ (Fig 61c).

An analysis of the two m7 ping-pong mechanisms in Fig 59 shows that their responses in A, E_1, and E_2 are, for different k_1 perturbation strengths, identical (see Fig 62a and 62b). Both use E_2 as the variable which controls the compensatory flux $j_{comp}=k_4 \cdot A \cdot E_2$. The roles of the enzymatic species Ez, Ez^*, $E_1 \cdot Ez$ and $Ez^* E_2$ in the mechanism of Fig 59a are in the mechanism of Fig 59b replaced by the respective species Ez^*, Ez, $Ez \cdot E_2$, and $Ez^* E_1$; see Fig 62c and 62d. While the concentrations in A, E_1, E_2, $E_1 \cdot Ez$, $Ez^* E_2$, $Ez \cdot E_2$, and $Ez^* E_1$ are identical as a function of k_5, the concentrations of Ez and Ez^* are different, but interchange in dependence whether E_1 or E_2 binds first to free Ez. The numerical results are shown in Fig 63 for the individual reaction species.

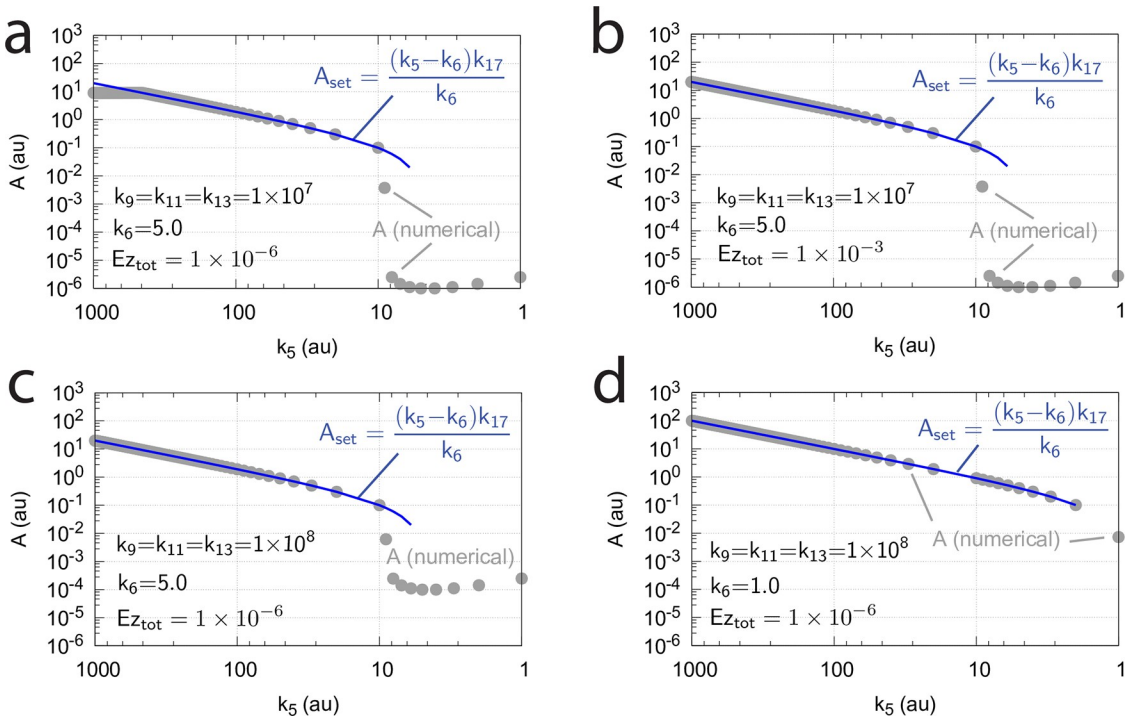

Fig 60. Influence of k_6, k_9, k_{11}, k_{13} and Ez_{tot} on the homeostatic behavior of the m7 ping-pong controller when E_1 binds first to free enzyme Ez. Numerical A values calculated after 10^4 time units are compared with corresponding analytical expressions of A_{set} as a function of k_5. (a) k_6=5.0, k_9=k_{11}=k_{13}=1 × 10^7, and Ez_{tot}=1 × 10^{-6}. (b) k_6=5.0, k_9=k_{11}=k_{13}=1 × 10^7, and Ez_{tot}=1 × 10^{-3}. (c) k_6=5.0, k_9=k_{11}=k_{13}=1 × 10^8, and Ez_{tot}=1 × 10^{-6}. (d) k_6=1.0, k_9=k_{11}=k_{13}=1 × 10^8, and Ez_{tot}=1 × 10^{-6}. Other rate constants (a)-(d): k_1=100.0, k_2=k_3=0, k_4=10.0, k_7=1 × 10^8, k_{12}=k_{14}=1 × 10^3. Initial concentrations (a), (c), and (d): A_0=3.0, $E_{1,0}$=1.0 × 10^{-2}, $E_{2,0}$=3.0 × 10^2, Ez_0=1.0 × 10^{-6}, $(E_1{\cdot}Ez)_0$=Ez^*_0=$(Ez^*{\cdot}E_2)_0$=0.0. Initial concentrations (b): A_0=3.0, $E_{1,0}$=1.0 × 10^{-2}, $E_{2,0}$=3.0 × 10^2, Ez_0=1.0 × 10^{-3}, $(E_1{\cdot}Ez)_0$=Ez^*_0=$(Ez^*{\cdot}E_2)_0$=0.0.

https://doi.org/10.1371/journal.pone.0262371.g060

Discussion

There are presently three kinetic approaches how error integration (Fig 1) can be achieved leading to perfect adaptation or homeostasis. One approach is the use of applying zero-order kinetics in the removal of the controller variable E [1, 2, 4–6, 18, 27]. A second approach [8, 28, 29] is based on a first-order autocatalytic production of E combined with its first-order removal. Finally, a third approach is based on antithetic control (described here also as dual-E control) [7, 8, 10, 11], where one of the controller variables (for example E_1) participates in a negative feedback and reacts with a second controller variable E_2, for example as described by Eq 3.

The advantage of the antithetic approach is that the removal of E_1 and E_2 does not necessarily need to be precisely a second-order process as formulated by Eq 3, but can in principle be of any type of kinetics. As practically all biochemical processes are catalyzed by enzymes, we have focussed here on mechanisms which remove E_1 and E_2 by classical two-substrate enzyme kinetics [12, 13]. In addition, taking a previously suggested basic set of negative feedback loops (controller motifs m1-m8) as a starting point, we have extended in Fig 3 this set for dual-E/antithetic control. Using enzyme kinetics with E_1 and E_2 as substrates allows for a large variety of processes as candidates for robust homeostasis.

Before we discuss a few examples where robust regulation appears to be associated with enzymatic dual-E controllers we would like to comment on cooperativity. Cooperativity by

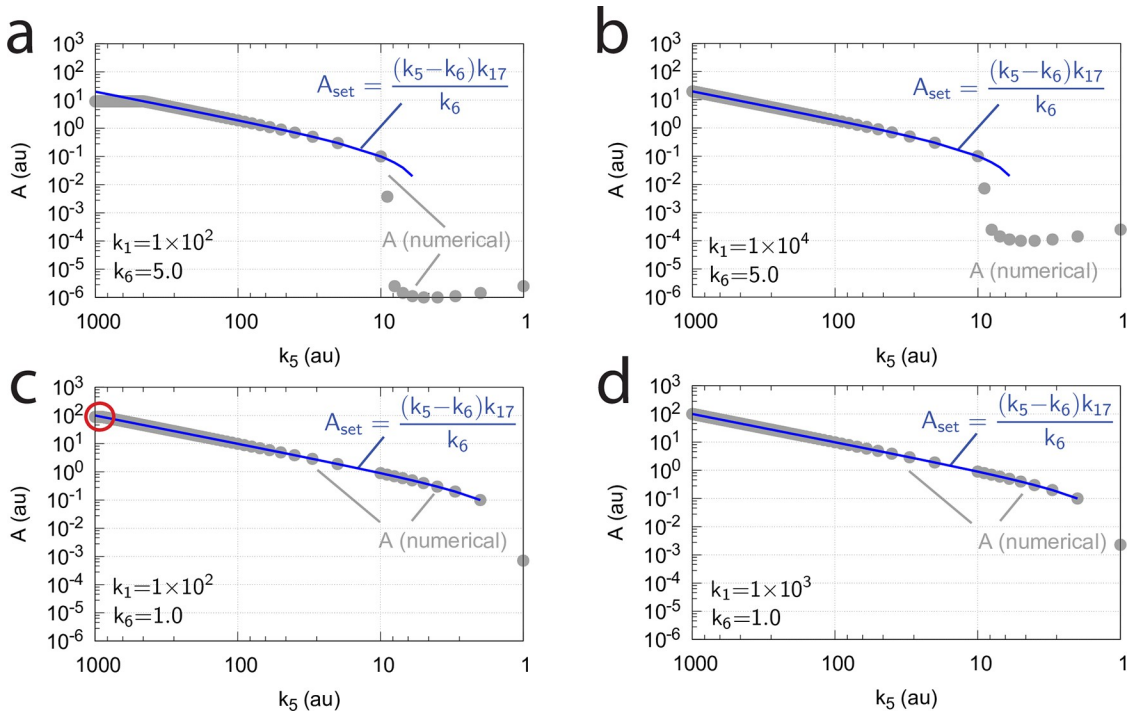

Fig 61. Influence of k_1 on the homeostatic behavior of the m7 ping-pong controller when E_1 binds first to free enzyme *Ez*. Since the response of the controller at higher k_1 values becomes significantly slower the numerical A values are calculated after 10^6 time units and compared with positive A_{set} (blue lines) as a function of k_5. (a) k_1=100.0, k_6=5.0. The controller looses homeostatic control in the k_5 range from 460–1000. (b) Increasing k_1 from 100.0 to 10000.0 moves A_{ss} to A_{set} for the higher k_5 values, but not for the lower k_5 values. (c) A decrease of k_6 from 5.0 to 1.0 while k_1 is kept at 100.0 gives a general improvement of the homeostatic performance of the ping-pong controller, except for the higher end k_5 range between 900–1000, where A_{ss} becomes constant (indicated by the red circle). (d) Low k_6 (1.0) and higher k_1 (1000.0) shows A_{ss} values that match A_{set}. Other rate constants (a)-(d): k_2=k_3=0, k_4=10.0, k_7=1 × 10^8, k_9=k_{11}=k_{13}=1 × 10^7, k_{12}=k_{14}=1 × 10^3, k_{17}=0.1. Initial concentrations (a)-(d): A_0=3.0, $E_{1,0}$=1.0 × 10^{-2}, $E_{2,0}$=3.0 × 10^2, Ez_0=1.0 × 10^{-6}, $(E_1{\cdot}Ez)_0$=Ez^*_0=$(Ez^*{\cdot}E_2)_0$=0.0.

https://doi.org/10.1371/journal.pone.0262371.g061

multisite binding or other mechanisms [30, 31], and conveniently described by a Hill function, is observed in many enzymatic systems [12, 13]. Although the influence of possible cooperative behaviors was not considered in this study, cooperativity may have significant effects on the controllers' resetting kinetics and set-points. For example, calculations by Drobac et al. [17] on multisite derepression controllers showed that a difference in cooperativity (Hill coefficients) in the inhibition mechanism had a significant effect on the speed how fast a set-point is approached, while in this case the set-point value itself was not affected. In general, one may expect that cooperativity in feedback signaling or in the enzymatic removal of the control species E_1 and E_2 will possibly lead to changed resetting kinetics. To what extent set-points of dual-E (or single-E controllers) are influenced by cooperativity seems to depend on how the controlled variable A's signaling will affect the manipulated variables E_1/E_2. These aspects, which are briefly mentioned here will need further and more systematic investigations.

Protein phosphorylation

Regulation by phosphorylating enzymes is observed in practically all aspects of life [32]. The enzymes, protein kinases, use as substrate a target protein and MgATP. A general feature of protein kinases is that they follow compulsory-order or random-order ternary-complex

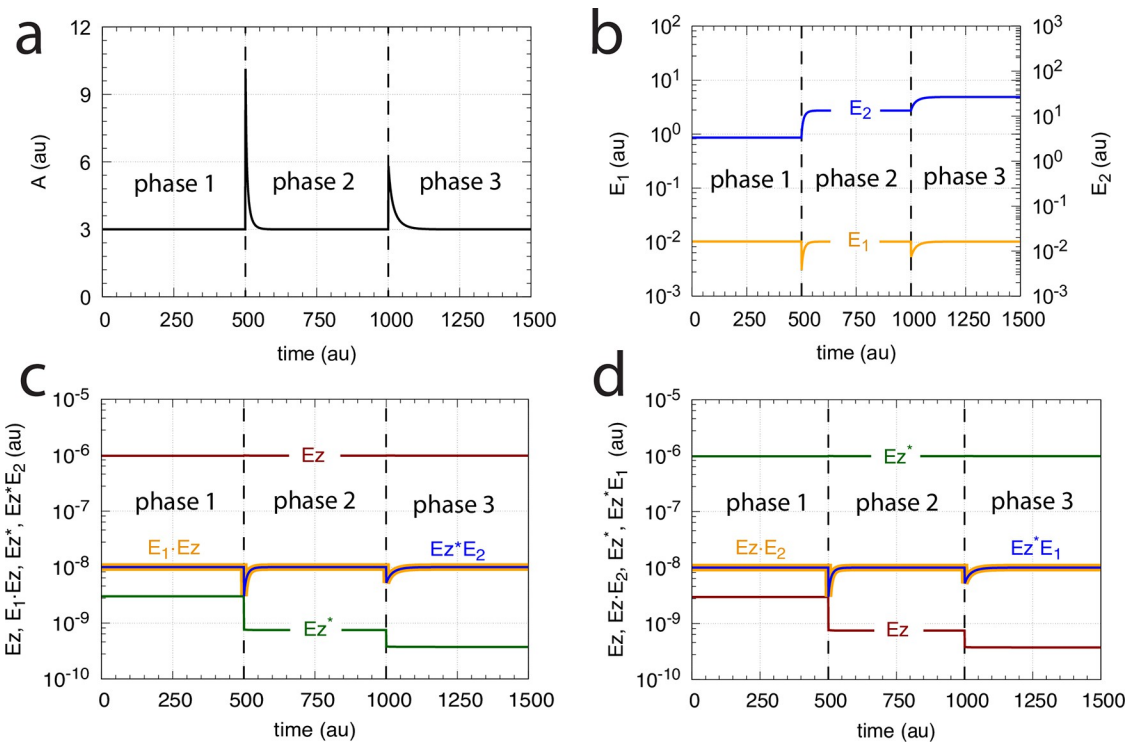

Fig 62. The m7 ping-pong mechanisms (Fig 59) show identical homeostatic responses for step-wise changes in k_1. Phase 1: k_1=100.0, phase 2: k_1=400.0, phase 3: k_1=800.0. (a) A as a function of the step-wise changes in k_1 for both controllers. (b) Concentration profiles of E_1 and E_2 for both controllers. (c) Concentration profiles of the enzyme species for the mechanism in Fig 59a. (d) Concentration profiles of the enzyme species for the mechanism in Fig 59b. Other rate constants: k_2=k_3=0, k_4=10.0, k_5=31.0, k_6=1.0, k_7=1 × 10^8, k_9=k_{11}=k_{13}=1 × 10^8, k_{12}=k_{14}=1 × 10^3, k_{17}=0.1. Initial concentrations for the controller of Fig 59a: A_0=3.0, $E_{1,0}$=1.0 × 10^{-2}, $E_{2,0}$=3.33, Ez_0=9.77 × 10^{-7}, $(E_1{\cdot}Ez)_0$=1.0 × 10^{-8}, Ez^*_0=3 × 10^{-9}, $(Ez^*{\cdot}E_2)_0$=1.0 × 10^{-8}. Initial concentrations for the controller of Fig 59b: A_0=3.0, $E_{1,0}$=1.0 × 10^{-2}, $E_{2,0}$=3.33, Ez_0=3 × 10^{-9}, $(Ez{\cdot}E_2)_0$=1.0 × 10^{-8}, Ez^*_0=9.77 × 10^{-7}, $(Ez^*{\cdot}E_1)_0$=1.0 × 10^{-8}.

https://doi.org/10.1371/journal.pone.0262371.g062

mechanisms [33]. In the following we give two examples that describe m2 control where ATP and the target protein are processed by a kinase using a ternary-complex mechanism.

Circadian rhythms. Circadian rhythms play an important part in the adaptation of organisms to their environment, in particular to the day/night and seasonal changes on earth. The molecular bases of circadian rhythms are transcriptional-translational negative feedback loops which oscillate with a period of circa 24 hours [34]. Using the model organism *Neurospora crassa* phosphorylation was found to serve two functions: firstly, to close the negative feedback loop by phosphorylating the transcription factor WCC (White Collar Complex). The WCC phosphorylation leads to its inhibition by its gene product, the protein FREQUENCY (FRQ) [35, 36], Secondly, FRQ, which is central to the *Neurospora* circadian pacemaker [37] is phosphorylated by CK1 with the result that phosphorylated FRQ is no longer able to inhibit WCC. Fig 64 indicates the central negative feedback loop in the *Neurospora* circadian clock describing the phosphorylation of FRQ by CK1 as a random-order ternary-complex mechanism, thereby moving FRQ out of the negative feedback loop. FRQ is phosphorylated at multiple sites [38] and hyper-phosphorylated FRQ is finally degraded. It should be noted that analogous feedback loops with post-translational phosphorylation have also been observed for the *Drosophila* circadian clock [39, 40].

In comparison with our m2 calculations above, Fig 64 predicts that *frq*-mRNA appears to be under homeostatic regulation with respect to its degradation. This prediction is indeed in

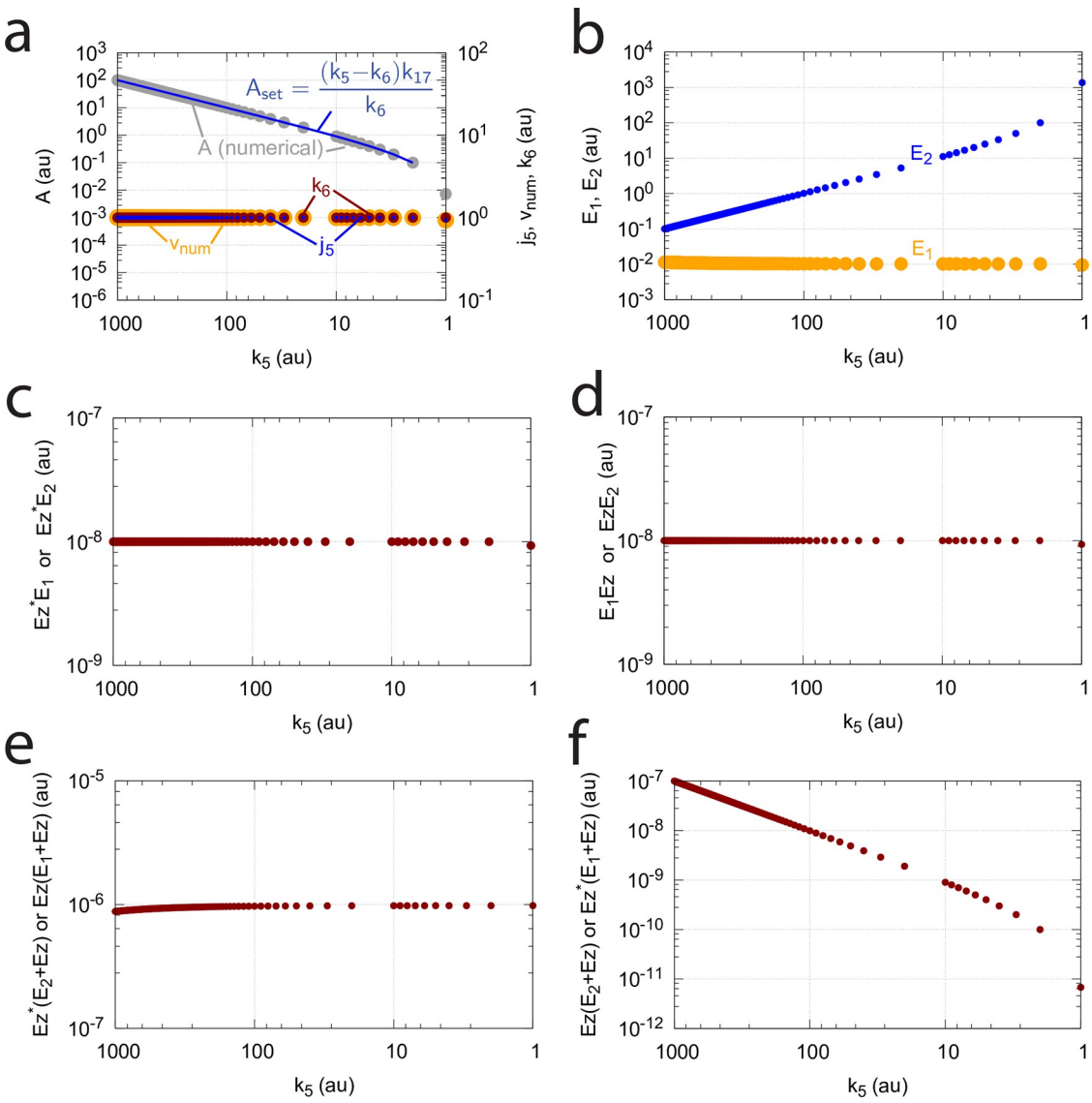

Fig 63. Concentration profiles of reaction species of the two m7 ping-pong mechanisms (Fig 59) as a function of k_5. (a) Left ordinate: Numerical steady state values of A (gray dots) in comparison with the theoretical set-point A_{set} (Eq 160, blue line). Ordinate to the right: k_6 (red dots), steady state values of $j_5=k_5k_{17}/(k_{17}+A)$ (blue dots), and numerically calculated reaction rate $v_{num}=dP/dt$ (orange dots). (b) Steady state values of E_1 (orange dots) and E_2 (blue dots). (c) Steady state profiles of Ez^*E_2 (Fig 59a) or Ez^*E_1 (Fig 59b). (d) Steady state profiles of E_1Ez (Fig 59a) or EzE_2 (Fig 59b). (e) Steady state profile of Ez when E_1 binds first to it (Fig 59a) or profile for Ez^* when E_2 binds first to Ez (Fig 59b). (f) Steady state profile of Ez when E_2 binds first to Ez (Fig 59b) or profile for Ez^* when E_1 binds first to Ez (Fig 59a). Rate constants: k_1=100.0, other rate constants as in Fig 62. Initial concentrations (a)-(f): A_0=3.0, $E_{1,0}=1.0\times10^{-2}$, $E_{2,0}=3.0\times10^{2}$, $Ez_0=1.0\times10^{-6}$, $(E_1{\cdot}Ez)_0=Ez^*_0=(Ez^*{\cdot}E_2)_0$=0.0.

https://doi.org/10.1371/journal.pone.0262371.g063

agreement with experimental findings by Liu et al. [41]. Their results indicate that the level of *frq*-mRNA, although changing on a circadian time scale, is on average not altered at different temperatures. Since, furthermore, the circadian period is compensated towards variations in temperature (temperature-compensation) [42–44], it will be interesting to investigate how FRQ phosphorylation by CK1, leading to putative *frq*-mRNA homeostasis, also contributes to temperature compensation in the *Neurospora* circadian clock as indicated by recent experiments [45].

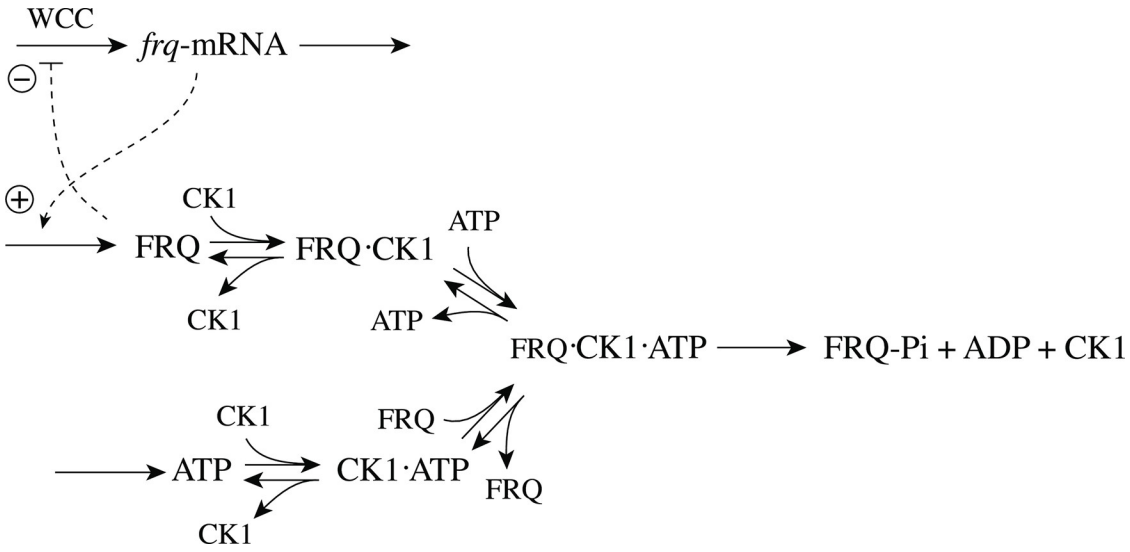

Fig 64. Central transcriptional-translational negative feedback loop of the *Neurospora* circadian clock. In the presence of FRQ the transcription factor White Collar Complex (WCC) is phosphorylated, which leads to its inhibition by FRQ and thereby suppressing FRQ synthesis. FRQ on its side is phosphorylated, which moves the inhibitory FRQ form out of the loop and leads to its eventually to its degradation. The dual-E controller suggests that *frq*-mRNA is under homeostatic control with respect to variable *frq*-mRNA degradation.

https://doi.org/10.1371/journal.pone.0262371.g064

Brassinosteroid homeostasis. Brassinosteroids (BRs) are plant hormones which have influence on plant growth and development, and adapt plants to environmental stresses. Plants lacking BRs show dwarf growth and abnormal organs [46]. BRs bound to their receptor BZR1 produce BZ1, which inhibits the transcription of the BR genes by binding to promoter regions of different genes in the BR synthesis pathway [47, 48]. The GSK3-like kinase BIN2 phosphorylates BZR1, which then leads to its proteasomal degradation [49]. Fig 65 shows the removal of BZR1 out of the negative feedback loop by BIN2 phosphorylation using a random-order ternary-complex mechanism [33].

Ubiquitination and proteasomal degradation

In metal-ion homeostasis many of the controller molecules are subject to proteasomal degradation in a metal-ion dependent fashion (for a summary, see the Supporting Material of Ref [6]). In proteasomal degradation, ubiquitin, a small protein, is moved through a cascade of three ligases (E1-E3; not to be confused with the controllers E_1 and E_2 above) and then added on to the target protein [50]. Repeated ubiquitin ligation of the target protein leads then finally to its degradation by the proteasome.

A relatively well understood example is mammalian iron homeostasis. At low iron levels IRP2 together with IRP1 promote the inflow of iron by stabilizing mRNAs which code for proteins that are necessary for iron supply. Results by Vashisht et al. [51] indicate that IRP2 is degraded in an iron-dependent manner where the F-box protein FBXL5 catalyzes IRP2 ligation with ubiquitin. While in this case three substrates are involved (iron, IRP2 and ubiquitin), dual-E control as described above cannot directly applied. However, the indication by Vashisht et al. [51] that iron stabilizes/activates FBXL5 leads to the following m1 dual-E mechanism (Fig 66) where iron activates FBXL5 from a pool of inactive enzyme. This allows the binding of IRP2 forming a SCF complex [51, 52]. For simplicity, the other components of the SCF complex are not shown and the pool of inactive enzyme ($FBXL5_i$) is considered to be constant.

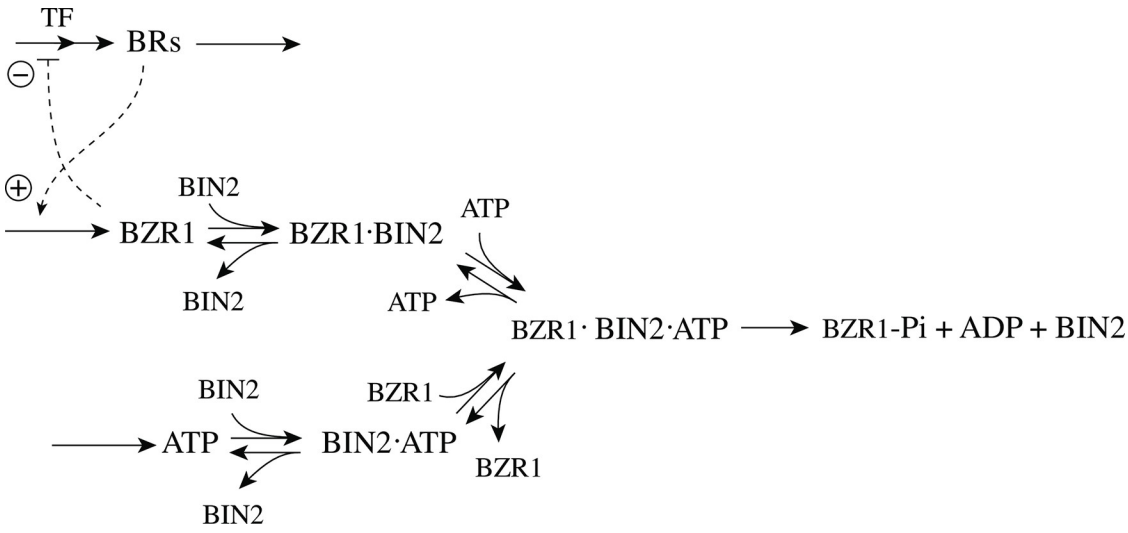

Fig 65. M2 dual-E control loop of Brassinosteroid homeostasis. Brassinosteroid genes are transcribed where TF indicate a set of transcription factors. When BRs bind to their receptors unphosphorylated BZ1 is produced which binds to the transcription factor and thereby inhibits Brassinosteroid transcription. The GSK3-like kinase BIN2 phosphorylates BZR1 and removes it from the negative feedback loop. Phosphorylated BZR1 is finally degraded by the proteasome.

https://doi.org/10.1371/journal.pone.0262371.g065

Under these assumptions iron is homeostatically controlled with set-point Fe_{set}, which is determined by the condition

$$v = k_7(FBXL5)(IRP2) = k_6 = k_5(Fe)(FBXL5_i) \tag{180}$$

resulting in

$$Fe_{set} = \frac{k_6}{k_5(FBXL5_i)} \tag{181}$$

Thus, the level of iron under iron-deficient conditions is given by the ratio between the rate of IRP2 generation and the rate of FBXL5 activation.

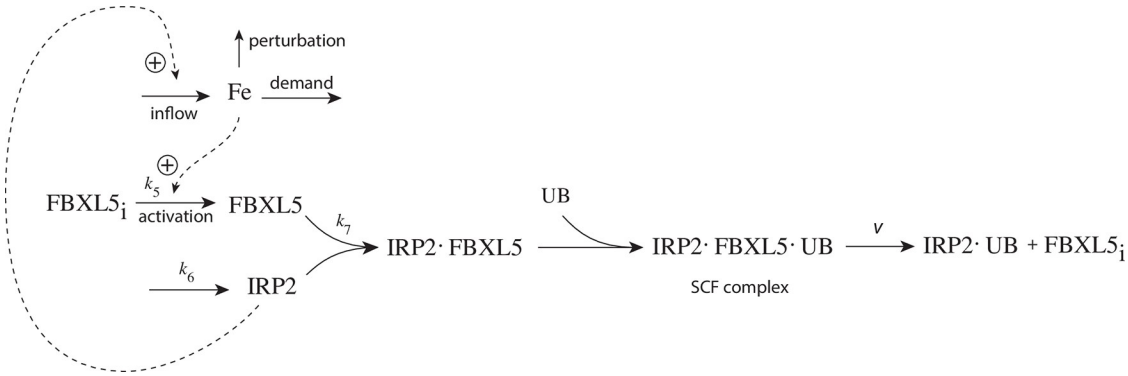

Fig 66. Suggested mechanism for the inflow control regulation of iron in mammalian cells. IRP2 activtes and stabilizes reactions promoting the inflow of iron into the cell. Iron activates the enzyme FBXL5 ($FBXL5_i$ is an inactive form) which enables the binding of IRP2 and UB leading to ubiquitinated IRP2. In this way IRP2 is moved out of the negative feedback loop.

https://doi.org/10.1371/journal.pone.0262371.g066

Iron and zinc homeostasis in yeast follow analogous strategies (see Supporting Material in Ref [6]).

Conclusion

We showed that antithetic/dual-E control can be incorporated into eight basic negative feedback motifs m1-m8. For four of them we have explicitly shown that robust antithetic control is possible when the removal of the two controller molecules E_1 and E_2 is catalyzed by an enzyme. Antithetic control has the advantage that it does not require specific kinetics, like zero-order kinetics is required for robust single-E control. Enzymatic dual-E control allows for the possibility that many enzymatic processes which take part in feedback regulations (like phosphorylation) may be better understood in terms of their contributions to obtain robust control. Although dual-E controllers based on ternary-complex or ping-pong mechanisms have similar (and often identical) dynamics with respect to the controlled variable, the kinetics of the participating enzymatic species are generally different for the different mechanisms. Low enzyme concentrations may limit robust homeostatic performance of catalyzed dual-E (and single-E) controllers. Transition between dual-E and single-E control may occur, but robust homeostasis for the resulting single-E controller is generally bound to zero-order kinetics. Single-E control within a dual-E network may show metastability, i.e. single-E control will switch spontaneously to dual-E control and "critical slowing down" may be observed.

Irreversibility of catalyzed (or uncatalyzed) controllers is one of the necessary conditions to obtain robust homeostasis. The work by Prigogine and coworkers [22] showed that organisms, as dissipative structures, exist as steady states far from chemical equilibrium [53]. In view of Cannon's definition [21, 54] homeostasis preserves these steady states and thereby contributes to the stability of organisms and cells.

Supporting information

S1 Text. Steady state (King-Altman) expressions for enzyme-catalyzed ternary-complex and ping-pong reactions using E_1 and E_2 as substrates.
(PDF)

Author Contributions

Conceptualization: Peter Ruoff.

Formal analysis: Huimin Zhou, Peter Ruoff.

Investigation: Qaiser Waheed, Huimin Zhou, Peter Ruoff.

Methodology: Huimin Zhou, Peter Ruoff.

Software: Peter Ruoff.

Supervision: Peter Ruoff.

Validation: Qaiser Waheed, Peter Ruoff.

Visualization: Peter Ruoff.

Writing – original draft: Peter Ruoff.

Writing – review & editing: Peter Ruoff.

References

1. Yi TM, Huang Y, Simon MI, Doyle J. Robust perfect adaptation in bacterial chemotaxis through integral feedback control. PNAS. 2000; 97(9):4649–53. https://doi.org/10.1073/pnas.97.9.4649 PMID: 10781070
2. El-Samad H, Goff JP, Khammash M. Calcium homeostasis and parturient hypocalcemia: an integral feedback perspective. J Theor Biol. 2002; 214(1):17–29. https://doi.org/10.1006/jtbi.2001.2422 PMID: 11786029
3. Wilkie J, Johnson M, Reza K. Control Engineering. An Introductory Course. New York: Palgrave; 2002.
4. Ni XY, Drengstig T, Ruoff P. The control of the controller: Molecular mechanisms for robust perfect adaptation and temperature compensation. Biophys J. 2009; 97(5):1244–53. https://doi.org/10.1016/j.bpj.2009.06.030 PMID: 19720012
5. Ang J, Bagh S, Ingalls BP, McMillen DR. Considerations for using integral feedback control to construct a perfectly adapting synthetic gene network. J Theor Biol. 2010; 266(4):723–738. https://doi.org/10.1016/j.jtbi.2010.07.034 PMID: 20688080
6. Drengstig T, Jolma I, Ni X, Thorsen K, Xu X, Ruoff P. A basic set of homeostatic controller motifs. Biophys J. 2012; 103(9):2000–2010. https://doi.org/10.1016/j.bpj.2012.09.033 PMID: 23199928
7. Briat C, Gupta A, Khammash M. Antithetic integral feedback ensures robust perfect adaptation in noisy biomolecular networks. Cell Systems. 2016; 2(1):15–26. https://doi.org/10.1016/j.cels.2016.01.004 PMID: 27136686
8. Briat C, Zechner C, Khammash M. Design of a Synthetic Integral Feedback Circuit: Dynamic Analysis and DNA Implementation. ACS Synth Biol. 2016; 5(10):1108–1116. https://doi.org/10.1021/acssynbio.6b00014 PMID: 27345033
9. Krishnan J, Floros I. Adaptive information processing of network modules to dynamic and spatial stimuli. BMC Systems Biology. 2019; 13(1):32. https://doi.org/10.1186/s12918-019-0703-1 PMID: 30866946
10. Aoki SK, Lillacci G, Gupta A, Baumschlager A, Schweingruber D, Khammash M. A universal biomolecular integral feedback controller for robust perfect adaptation. Nature. 2019; p. 1. PMID: 31217585
11. Khammash MH. Perfect adaptation in biology. Cell Systems. 2021; 12(6):509–521. https://doi.org/10.1016/j.cels.2021.05.020 PMID: 34139163
12. Segel IH. Enzyme Kinetics: Behavior and Analysis of Rapid Equilibrium and Steady State Enzyme Systems. New York: Wiley; 1975.
13. Cornish-Bowden A. Fundamentals of Enzyme Kinetics. Fourth Edition. John Wiley & Sons; 2012.
14. Radhakrishnan K, Hindmarsh AC. Description and Use of LSODE, the Livermore Solver for Ordinary Differential Equations. NASA Reference Publication 1327, Lawrence Livermore National Laboratory Report UCRL-ID-113855. Cleveland, OH 44135-3191: National Aeronautics and Space Administration, Lewis Research Center; 1993.
15. Fjeld G, Thorsen K, Drengstig T, Ruoff P. The performance of homeostatic controller motifs dealing with perturbations of rapid growth and depletion. J Phys Chem B. 2017; 121:6097–6107. https://doi.org/10.1021/acs.jpcb.7b01989 PMID: 28571313
16. Ruoff P, Agafonov O, Tveit DM, Thorsen K, Drengstig T. Homeostatic controllers compensating for growth and perturbations. PLoS One. 2019; 14(8):e0207831. https://doi.org/10.1371/journal.pone.0207831 PMID: 31404092
17. Drobac G, Waheed Q, Heidari B, Ruoff P. An amplified derepression controller with multisite inhibition and positive feedback. PloS One. 2021; 16(3):e0241654. https://doi.org/10.1371/journal.pone.0241654 PMID: 33690601
18. Ang J, McMillen DR. Physical constraints on biological integral control design for homeostasis and sensory adaptation. Biophys J. 2013; 104(2):505–515. https://doi.org/10.1016/j.bpj.2012.12.015 PMID: 23442873
19. Cleland WW. The kinetics of enzyme-catalyzed reactions with two or more substrates or products: I. Nomenclature and rate equations. Biochimica et Biophysica Acta (BBA)-Specialized Section on Enzymological Subjects. 1963; 67:104–137. https://doi.org/10.1016/0926-6569(63)90226-8
20. Lotka AJ. Elements of Physical Biology. Baltimore: Williams & Wilkins Company; 1925.
21. Langley LL, editor. Homeostasis. Origins of the Concept. Stroudsbourg, Pennsylvania: Dowden, Hutchinson & Ross, Inc.; 1973.
22. Nicolis G, Prigogine I. Self-organization in Nonequilibrium Systems. From Dissipative Structures to Order through Fluctuations. John Wiley & Sons; 1977.
23. Gánti T. The Principles of Life. Oxford University Press; 2003.

24. Capra F, Luisi PL. The Systems View of Life: A Unifying Vision. Cambridge: Cambridge University Press; 2014.

25. King EL, Altman C. A schematic method of deriving the rate laws for enzyme-catalyzed reactions. J Phys Chem. 1956; 60(10):1375–1378. https://doi.org/10.1021/j150544a010

26. Ganapathisubramanian N, Showalter K. Critical slowing down in the bistable iodate-arsenic (III) reaction. The Journal of Physical Chemistry. 1983; 87(7):1098–1099. https://doi.org/10.1021/j100230a004

27. Kleppe R, Waheed Q, Ruoff P. DOPA Homeostasis by Dopamine: A Control-Theoretic View. International Journal of Molecular Sciences. 2021; 22(23). https://doi.org/10.3390/ijms222312862 PMID: 34884667

28. Shoval O, Goentoro L, Hart Y, Mayo A, Sontag E, Alon U. Fold-change detection and scalar symmetry of sensory input fields. PNAS. 2010; p. 201002352. https://doi.org/10.1073/pnas.1002352107 PMID: 20729472

29. Drengstig T, Ni X, Thorsen K, Jolma I, Ruoff P. Robust adaptation and homeostasis by autocatalysis. J Phys Chem B. 2012; 116(18):5355–5363. https://doi.org/10.1021/jp3004568 PMID: 22506960

30. Gonze D, Ruoff P. The Goodwin oscillator and its legacy. Acta Biotheoretica. 2021; 69(4):857–874. https://doi.org/10.1007/s10441-020-09379-8 PMID: 32212037

31. Kim JK. Protein sequestration versus Hill-type repression in circadian clock models. IET Systems Biology. 2016; 10(4):125–135. https://doi.org/10.1049/iet-syb.2015.0090 PMID: 27444022

32. Cohen P. The origins of protein phosphorylation. Nature Cell Biology. 2002; 4(5):E127–E130. https://doi.org/10.1038/ncb0502-e127 PMID: 11988757

33. Wang Z, Cole PA. Catalytic mechanisms and regulation of protein kinases. Methods in Enzymology. 2014; 548:1–21. https://doi.org/10.1016/B978-0-12-397918-6.00001-X PMID: 25399640

34. Dunlap J. Molecular bases for circadian clocks. Cell. 1999; 96(2):271–290. https://doi.org/10.1016/S0092-8674(00)80566-8 PMID: 9988221

35. Huang G, Chen S, Li S, Cha J, Long C, Li L, et al. Protein kinase A and casein kinases mediate sequential phosphorylation events in the circadian negative feedback loop. Genes & Development. 2007; 21(24):3283–3295. https://doi.org/10.1101/gad.1610207 PMID: 18079175

36. Wang B, Kettenbach AN, Zhou X, Loros JJ, Dunlap JC. The phospho-code determining circadian feedback loop closure and output in *Neurospora*. Molecular cell. 2019; 74(4):771–784. https://doi.org/10.1016/j.molcel.2019.03.003 PMID: 30954403

37. Baker CL, Loros JJ, Dunlap JC. The circadian clock of *Neurospora crassa*. FEMS Microbiology Reviews. 2012; 36(1):95–110. https://doi.org/10.1111/j.1574-6976.2011.00288.x PMID: 21707668

38. Baker CL, Kettenbach AN, Loros JJ, Gerber SA, Dunlap JC. Quantitative proteomics reveals a dynamic interactome and phase-specific phosphorylation in the *Neurospora* circadian clock. Molecular Cell. 2009; 34(3):354–363. https://doi.org/10.1016/j.molcel.2009.04.023 PMID: 19450533

39. Edery I, Zwiebel LJ, Dembinska ME, Rosbash M. Temporal phosphorylation of the *Drosophila* period protein. Proceedings of the National Academy of Sciences.1994; 91(6):2260–2264. https://doi.org/10.1073/pnas.91.6.2260 PMID: 8134384

40. Rosbash M, Bradley S, Kadener S, Li Y, Luo W, Menet J, et al. Transcriptional feedback and definition of the circadian pacemaker in *Drosophila* and animals. In: Cold Spring Harbor Symposia on Quantitative Biology. vol. 72. Cold Spring Harbor Laboratory Press; 2007. p. 75–83.

41. Liu Y, Merrow M, Loros JJ, Dunlap JC. How temperature changes reset a circadian oscillator. Science. 1998; 281(5378):825–829. https://doi.org/10.1126/science.281.5378.825 PMID: 9694654

42. Rensing L, Mohsenzadeh S, Ruoff P, Meyer U. Temperature Compensation of the Circadian Period Length—A Special Case Among General Homeostatic Mechanisms of Gene Expression? Chronobiology International. 1997; 14(5):481–498. https://doi.org/10.3109/07420529709001470 PMID: 9298284

43. Rensing L, Ruoff P. Temperature effect on entrainment, phase shifting, and amplitude of circadian clocks and its molecular bases. Chronobiology International. 2002; 19(5):807–864. https://doi.org/10.1081/CBI-120014569 PMID: 12405549

44. Ruoff P, Loros JJ, Dunlap JC. The relationship between FRQ-protein stability and temperature compensation in the Neurospora circadian clock. Proceedings of the National Academy of Sciences.2005; 102(49):17681–17686. https://doi.org/10.1073/pnas.0505137102 PMID: 16314576

45. Hu Y, Liu X, Lu Q, Yang Y, He Q, Liu Y, et al. FRQ-CK1 Interaction Underlies Temperature Compensation of the Neurospora Circadian Clock. mBio. 2021; 12(3):e01425–21. https://doi.org/10.1128/mBio.01425-21 PMID: 34182774

46. Tanaka K, Asami T, Yoshida S, Nakamura Y, Matsuo T, Okamoto S. Brassinosteroid homeostasis in Arabidopsis is ensured by feedback expressions of multiple genes involved in its metabolism. Plant Physiology. 2005; 138(2):1117–1125. https://doi.org/10.1104/pp.104.058040 PMID: 15908602

47. He JX, Gendron JM, Sun Y, Gampala SS, Gendron N, Sun CQ, et al. BZR1 is a transcriptional repressor with dual roles in brassinosteroid homeostasis and growth responses. Science. 2005; 307(5715): 1634–1638. https://doi.org/10.1126/science.1107580 PMID: 15681342

48. Wei Z, Li J. Regulation of brassinosteroid homeostasis in higher plants. Frontiers in Plant Science. 2020; 11:1480. https://doi.org/10.3389/fpls.2020.583622 PMID: 33133120

49. He JX, Gendron JM, Yang Y, Li J, Wang ZY. The GSK3-like kinase BIN2 phosphorylates and destabilizes BZR1, a positive regulator of the brassinosteroid signaling pathway in Arabidopsis. Proceedings of the National Academy of Sciences.2002; 99(15):10185–10190. https://doi.org/10.1073/pnas.152342599 PMID: 12114546

50. Ciechanover A. The ubiquitin-proteasome proteolytic pathway. Cell. 1994; 79(1):13–21. https://doi.org/10.1016/0092-8674(94)90396-4 PMID: 7923371

51. Vashisht AA, Zumbrennen KB, Huang X, Powers DN, Durazo A, Sun D, et al. Control of iron homeostasis by an iron-regulated ubiquitin ligase. Science. 2009; 326(5953):718–721. https://doi.org/10.1126/science.1176333 PMID: 19762596

52. Zheng N, Schulman BA, Song L, Miller JJ, Jeffrey PD, Wang P, et al. Structure of the Cul1–Rbx1–Skp1–F box Skp2 SCF ubiquitin ligase complex. Nature. 2002; 416(6882):703–709. https://doi.org/10.1038/416703a PMID: 11961546

53. Karsenti E. Self-organization in cell biology: A brief history. Nature Reviews Molecular Cell Biology. 2008; 9(3):255–262. https://doi.org/10.1038/nrm2357 PMID: 18292780

54. Cannon W. Organization for physiological homeostatics. Physiol Rev. 1929; 9:399–431. https://doi.org/10.1152/physrev.1929.9.3.399